UNIVERSITÀ DI PARMA

DOTTORATO DI RICERCA IN

MEDICINA MOLECOLARE

XXXII CICLO

INNOVATIVE SOURCES OF NEURAL CREST – DERIVED ECTOMESENCHYMAL STEM CELLS FOR HEPATIC BIOENGINEERING

Coordinatore: Chiar.ma Prof.ssa Stefania Conti

Tutore: Chiar.mo Prof. Roberto Toni

Co-tutor: Chiar.mo Prof. Ivan Martin

Dottorando: ELIA CONSOLINI

ANNI 2016-2019

INDEX

SUMMARY

Liver disorders affect more than 100 million people worldwide and the therapeutic approaches for severe forms such as fulminant toxic hepatitis, cirrhosis, cancer and autoimmune liver disease remain palliative, awaiting for an organ transplant from a donor. An innovative approach involves intrahepatic transplantation of adult, multipotent stem cells of extrahepatic origin, whose up to now the mostly widely used have been mesenchymal stromal cells (MSC) from the bone marrow (bm-MSC). Specifically, MSC have been preliminarily *in vitro* or post-transplant *in vivo* induced to hepatocyte differentiation, and then associated with a biocompatible heterologous three-dimensional (3D) support like a decellularized or biostamped collagen matrix. Indeed, the 3D geometry of the matrix is believed to regulate the 3D self-assembly and differentiation of hepatic progenitors, as predicted by Gerald Edelman's Topobiological Theory.

Since MSC from bone marrow and other sources exhibit a number of limitations in hepatic differentiation, the aim of my study has been the identify and evaluate innovative sources of adult stem cells suitable for *in vitro* and *ex situ* (i.e. once used for a 3D matrix recellularization) hepatic differentiation. My interest has been focussed on the still poorly investigated differentiation potential of adult ectomesenchymal cells of neural crest origin (i.e. adult neuroectodermal stem cells), like those expected to be found in the adult thyroid gland and the cartilage of the nasal septum. In particular, recent evidence collected by the group of research leaded by Prof. Roberto Toni at the University of Parma, in Italy has shown that adult stem cells can *in vitro* be isolated and expanded using long-term (2-4 months) primary cultures from the male rat thyroid. Preliminary data obtained in collaboration with Prof. Stephen Pennington of the UCD – Ireland on their proteomic signature have shown a very high expression of

mesenchymal and, to a lesser extent endodermal protein markers. However, a minor fraction of these markers also includes proteins from a neuroectodermal lineage, in agreement with very recent evidence that the neural crest contribute to the development of the thyroid gland giving rise to its stromal matrix and, possibly to other still unknown progenitor cells. Since these cultures of adult rat stem cells can be *in vitro* differentiated to functional thyrocytes (that are classical endodermal cells like the hepatocytes), I reasoned that they could represent an innovative model source for hepatic differentiation.

To reach this goal, in the first year of my PhD program I preliminary widened the previously acquired data on the proteomic signature of our rat thyroid stem cells / progenitors (TSC/P) using an LC-MS/MS SRM technique based on in silico sequences of not previously investigated proteins of endodermal, mesodermal, and neuroectodermal lineage as well as markers of epithelial-mesenchymal transition. A semiquantitative evaluation based on score values depicted an increase in the number of markers of neuroectodermal lineage, and an evidence of some proteins of epithelial-mesenchymal transition. These results support the original assumption of our group that a large fraction of our rat TSC/P are ectomesenchymal cells of neural crest origin, although a minor effect on the induction of a mesenchymal phenotype was triggered by the monolayer culture *per se*, as suggested by the presence of few markers of epithelial-mesenchymal transition.

In addition, using light microscopic histochemistry, immunocytochemistry, and scanning electron microscopy I evaluated the hepatic differentiation of our rat TSC/P tested with two protocols of *in vitro* differentiation, both originally developed in our lab. at UNIPR. Of these, only one (n.1) was able to induce a satisfactory hepatocyte differentiation. A key role in this result was likely played by the use of Hepatocyte Growth Factor (HGF), whose Met receptor is expressed in neural crest and neural crest- derived cells like the ectomesenchyme, and also

in differentiated hepatocytes and thyrocytes suggesting a great affinity of our TSC/P for an hepatic lineage.

As a comparison, in the second year of my PhD program I studied a similar differentiation procedure using the currently believed, cellular gold standard for hepatic differentiation i.e. adult male rat bm-MSCs. Based on the same technologies as during the first year of work but in contrast to TSC/P, none of the two differentiation protocols used provided *in vitro* satisfactory development of bm-MSCs to hepatocytes. Since HGF may result in downregulation of MSC differentiation to hepatocytes when administered for long periods of times (as in our models), and use of Epidermal Growth Factor should be delivered at periods earlier than those chosen in our protocols, it is concluded that the weak differentiation results obtained depend on differentiation protocols for MSC not efficient enough when their multipotentiality is lowered by repeated culture passages from P3 ahead.

In the third year of my PhD program, I substantiated the results on the proteomic signature of TSC/P and bm-MSC following their hepatic differentiation using qualitative LC-LIT-Orbitrap XL. Remarkably, hepatic differentiation of TSC/P with the protocol that had shown the best immunocytochemical performances during the first year of work (n.1) confirmed upregulation of the hepatic marker albumin, and revealed presence of S100-A6, a protein associated with activated hepatic stellate cells. Since the latter are a normal component of the liver *in vivo*, and are of mesodermal origin, the present *in vitro* evidence supports the original assumption that the large majority of our TSC/P are cell from an ectomesenchymal, neural-crest derived lineage easily driven to hepatocytes once triggered with adequate differentiation factors. In contrast, MSC differentiated with both previous protocols exhibited a proteomic profile with numerous common markers, confirming their immaturity and resistance to hepatic differentiation in the experimental setting applied.

Finally, in search for a new source of neural crest-derived, ectomesenchymal cells potentially suitable for hepatic differentiation in humans (as those found in the rat and previously described), I engaged myself in the detailed lineage and molecular characterization of a very peculiar type of adult stem cells, obtained from the cartilage of the human nasal septum. This work has been developed between 2017 and 2018 under the tenure of my PhD Mobility Program, and in collaboration with the group of Prof. Ivan Martin at the Laboratory of Tissue Engineering / Department of Surgery and Biomedicine of the University Hospital in Basel, Switzerland. Prof. Martin and his group originally studied the gene expression of these cells, and used them as a new mean for repair of articular cartilage defects. They are adult nasal chondrocytes, taken following *in vivo* surgical sampling, and then *in vitro* de-differentiated. Recent collaborative studies between the groups of Prof. Toni and Prof. Martin have shown that a number of neuroectodermal markers of these cells can be found in the nasal septum of the human embryo, and can be recognized in the adult nasal chondrocytes by flow cytometry. During this last year of my PhD and using immunocytochemistry, I have evaluated the distribution of the majority of those embryonic markers also in primary cultures of adult nasal chondrocytes. In addition, using statistical analysis I have re-analyzed and re-calculated the quantitative results previously obtained by flow cytometry in nasal chondrocytes on the distribution of markers of mesodermal and neuroectodermal origin. Finally, using qualitative LC-LIT-Orbitrap XL I have obtained a preliminary profile of these adult stem cells showing a molecular setting based on downregulation of glycolytic enzymes and some DNA-associated histones as opposed to upregulation of a number of proteins involved in morphogenetic and developmental processes. Collectively, these data suggest that nasal chondrocytes are prone to a high plasticity of their phenotype, as expected for multipotent stem cells. Since flow cytometry showed that more than 80% of them express cytoplasmic and membrane markers

consistent with ectomesenchymal neural crest-derived cells, the current proteomic profile (although still incomplete) supports the original hypothesis that they might successfully be induced to differentiate to cell lineages similar to those observed with ectomesenchymal, neural crest-derived rat thyroid stem cells. As such, I expect that these adult human stem cells may represent a new source for differentiation to human hepatocytes, and become a very innovative tool for regenerative medicine and tissue engineering in disorders of the human liver.

INTRODUCTION

1. Organogenesis and anatomy of the rodent liver

Embryonic source of liver cells, their transcriptional control, and signalling pathways regulating hepatoblast formation

Liver parenchymal cells derive from the anterior portion of the definitive endoderm, which itself is established in the embryo during gastrulation [1]. There are three distinct domains of hepatic progenitor cells that are located in the medial and bilateral regions of the foregut [2]. As the foregut closes, the progenitor cells within these regions converge to lie adjacent to the developing heart and in close apposition to regions of the lateral plate mesoderm, that will ultimately generate the mesothelial cells of the pro-epicardium and the fibroblastic and muscular cells of the *septum transversum* [3] *[Figure 1]*.

The first molecular evidence of liver development is the expression of albumin (ALB), transthyretin, and α-fetoprotein in a region of the ventral endoderm located near the developing heart [4;5]. Hepatic specification occurs in mouse embryos at approximately the 7-somite stage, which corresponds to embryonic day (E) 8.25 (equivalent to E 22-23 in human).

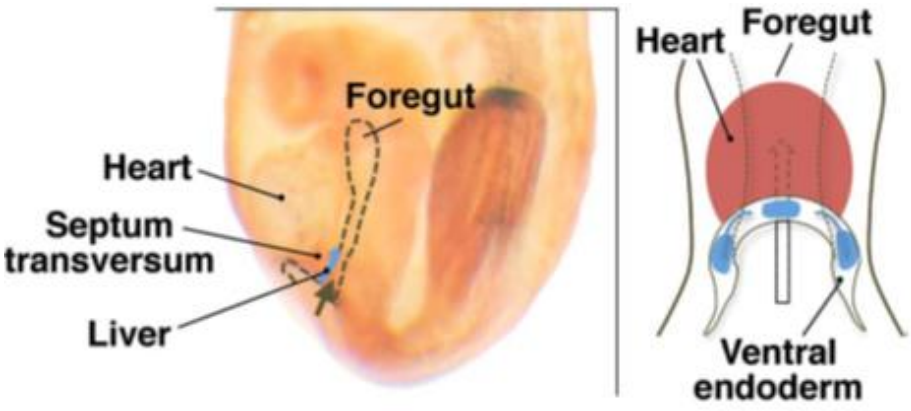

Figure 1: The left panel shows a mouse embryo at E8.25 (10 somites), while the right panel schematizes a slightly younger embryo with a ventral view on the anterior ventral opening. From Lemaigre F.P., Gastroenterology 2009;137:62–79.

In vivo DNA/protein analyses have shown that the albumin gene promoter is bound by Forkhead box (Fox A) and GATA-4 transcription factors, which decompact and open chromatin to provide access to additional transcription factors, such as nuclear factor-1 and C/EBPβ, eventually resulting in the transcriptional activation of albumin [6]. Because the hepatocyte nuclear factor HNF-1β stimulates expression of FoxA1 and FoxA2 in the pre-hepatic endoderm, it is clear that HNF-1β, FoxA1, FoxA2, and GATA-4 are critical initiators of liver development. Liver gene induction in mouse endoderm starts when FGF-1 and FGF-2 production is initiated by the cardiogenic mesoderm. At this point, the developing heart is adjacent to the pre-hepatic endoderm and produces low amounts of FGFs. Slightly later, the heart produces more FGFs but becomes separated from the pre-hepatic endoderm by the mesoderm of the *septum transversum*, a mesodermal tissue located caudally to the heart, and eventually giving rise to the muscle diaphragm.

These morphogenetic events, which move the endoderm away from the source of FGF-1 and FGF-2, ensure that hepatic cells are not exposed to excessive concentrations of FGFs [7].

Importantly, FGFs signaling is not sufficient for hepatic specification: in fact the mesoderm of the *septum transversum* produces bone morphogenetic proteins BMP-2 and BMP-4, which cooperate with FGF to induce hepatic gene expression, and which activity is mediated at least in part by the expression of the GATA-4 transcription factor. Wnt signalling is also shown to have a role in liver induction. When the primitive gut becomes patterned along its anteroposterior axis, Wnt signaling must be repressed anteriorly to maintain foregut identity, and to allow for subsequent liver development. This repression depends on the appropriate secretion by the endoderm of Wnt inhibitors [8;9]. Importantly, beyond the stage of patterning, Wnt signalling becomes necessary for liver development.

When endoderm cells have been specified, a diverticulum forms from the primitive gut at E9 in the mouse. The liver diverticulum is lined by endoderm cells, at this stage called hepatoblasts, that become columnar and undergo a transition to a pseudostratified epithelium [10]. The hepatoblasts proliferate and form a tissue bud delineated by a basement membrane that contains laminin, collagen IV, nidogen, fibronectin, and heparan sulphate proteoglycan [11]. Hepatoblasts then migrate through the basement membrane, and invade the mesoderm (which will give rise to septum transversum). This is reminiscent of an epithelial-mesenchymal transition, because the hepatoblasts transiently lose their epithelial morphology and reduce expression of E-cadherin when they move away from the endoderm.

Hepatoblast growth and proliferation, and role of the surrounding mesoderm

A network of transcription factors controls the onset of liver development. Hematopoietically expressed homeobox factor (Hex, also known as Prh) promotes interkinetic nuclear migration and hepatoblast proliferation [10;12;13]; GATA-6 is required to maintain the differentiation state of hepatoblasts [14]. There is a network of gene, which include Hex, GATA-6, HNF-6, Onecut

(OC-2), Tbx3, and Prox-1, involved in cell migration and adhesion. When the activity of metalloproteases (MMPs) produced by the hepatoblasts and mesenchymal cells is blocked, mainly MMP-14 and MMP-2, migration of hepatoblasts through the basement membrane is inhibited [15]. Since hepatoblasts continue to proliferate, a transition from an epithelium to a non-polarized cell type occurs into the hepatic bud, due to the loss of cell-cell interactions. At this point, mesoderm-derived cells (stromal and endothelial) arising from the mesenchyme of *septum transversum* invade the hepatic bud, and give rise to septa and blood vessels into the developing liver [16], a key event for the progress of the bud morphogenesis (see the "Liver morphogenetic changes during specification" paragraph) *[Figure 2]*. Several growth factors are involved in this process [17], as hepatocyte growth factor (HGF), which is expressed both by the surrounding mesoderm, by endothelial cells describe above and by hepatoblasts as well.

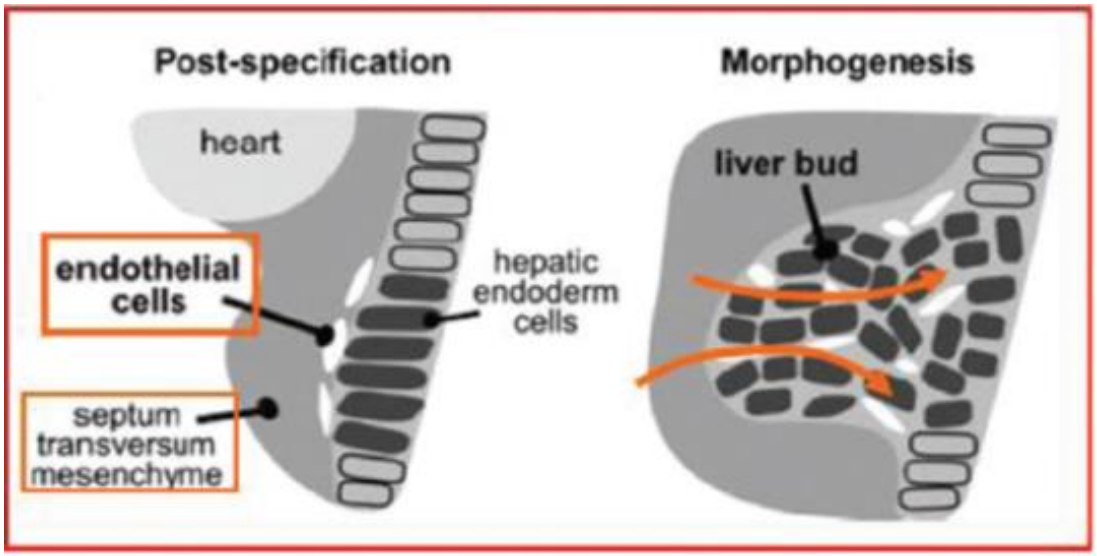

Figure 2: Early post-specification step of liver morphogenesis. Mesoderm-derived cells (stromal and endothelial) enter the multipotent endodermal cell groups of the liver, to laminate the future hepatic parenchyma. From Toni et al., Bio-Inspired Regenerative Medicine: Materials, Processes, and Clinical Applications, Pan Stanford 2016; Chapter 15: 357-388.

Transforming growth factor (TGF-β) pathway, together with its intracellular proteins Smad2/Smad3 involved in downstream activation of gene transcription, also stimulates

proliferation [18]. Interestingly, the HGF and TGF-β pathways functionally interact, because they converge on β1-integrin expression, which is necessary for proliferation. Hepatoma-derived growth factor (HDGF) is produced by foetal hepatoblasts and stimulates their proliferation *in vitro*. β-catenin is the best known mediator of the canonical Wnt signaling pathway, which not only promotes growth of the liver, but also controls the acquisition of global liver morphology [19]. In addition, β-catenin seems to represent a key node at the intersection of multiple signaling cascades (for example, it contributes to the growth stimulatory effects of FGF). Also retinoic acid have a role in hepatic development, but it stimulates proliferation of hepatoblasts by inducing the production of trophic factors by mesodermal cells rather than have a direct effect on the hepatoblasts.

A different perspective is taken when considering the Tumor Necrosis Factor-α (TNF-α): it, in fact, stimulates a signaling cascade that activates the transcription factor nuclear factor κB (NF-κB), which protects hepatoblasts against TNF-induced apoptosis [20]. In addition, several other transcription factors regulate hepatoblast proliferation. These include Prox-1 [21], which promotes proliferation according to a mechanism that is antagonized by the liver receptor homolog 1 (LRH-1), and FoxM1B which activates expression of regulators of the G2/M phase [22]. The X-box binding protein 1 (XBP-1), a transcription factor of the CREB/ATF family, is activated by endoplasmic reticulum (ER) stress, and controls the expansion of the ER surface [23]. Finally, the transcription factors N-Myc and Hlx are, unlike the previously discussed transcription factors, expressed in mesenchymal cells and both factors promote liver growth, most likely by regulating the expression of paracrine factors [24;25] *[Figure 3].*

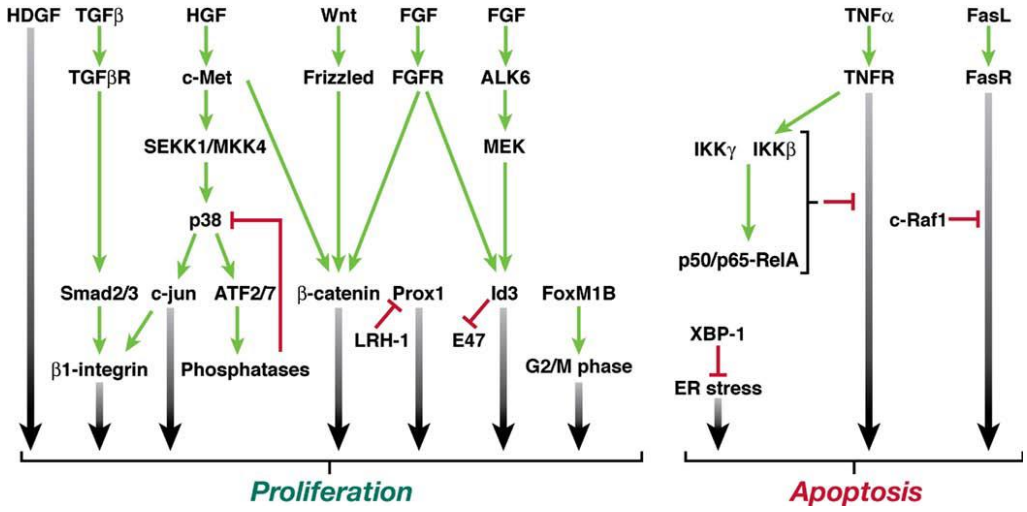

Figure 3: Molecular regulation of liver cell growth and apoptosis during development. From Lemaigre F.P., Gastroenterology 2009;137:62–79.

The lineage segregation stage: from hepatoblasts to hepatocytes and cholangiocytes

In rodent liver development, the concept of the cell fate decision seems to be reasonably applicable to hepatoblasts that have reached a stage at which they become committed either to the hepatocyte lineage or the cholangiocyte lineage *[Figure 4]*. Specifically, between E9.5 and E12.5 in mice, the hepatoblasts start to express genes that are active in mature hepatocytes, and in this sense HNF-4α is critical for hepatocyte fate determination [26]. Another way to determine the timing of lineage segregation is by the analysis of expression of biliary markers, such as cytokeratin 19 (CK-19) and CK-7, though it is preferable to use the different expression of the transcription factor SRY-related HMG box transcription factor 9 (SOX9) [27]. In fact, this factor is present in endodermal cells that line the hepatic diverticulum, but its expression disappears when the cells start to migrate throughout the mesoderm that will give rise to the *septum transversum*. SOX9 becomes re-expressed at E11.5 in liver epithelial cells

that are located a short distance from the branches of the portal vein, where the biliary cells differentiate; at later developmental stages, it is restricted to biliary cells.

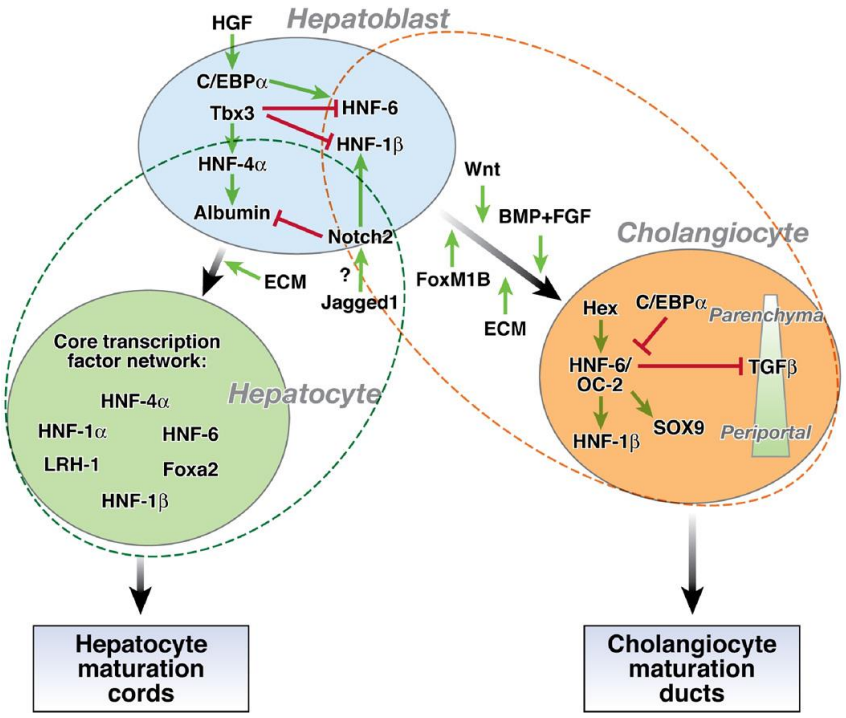

Figure 4: Mechanisms of cell fate determination in the liver.
From Lemaigre F.P., Gastroenterology 2009;137:62–79.

Biliary differentiation is promoted at the expense of hepatocyte differentiation, and at E9.5 the expression of HNF-6 and HNF-1β increases, whereas that of HNF-4α decreases, with Tbx3 that controls the timing of hepatoblast lineage decision and preventes a premature increase in HNF-6 and HNF-1β. Some transcription factors can influence hepatoblast cell fate determination by modulating extracellular signalling. In particular, TGF-β promotes differentiation of hepatoblasts to biliary cells and represses hepatocyte differentiation. HNF-6 and OC-2 are expressed in hepatoblasts, cholangiocytes, and hepatocytes, but the highest levels are found in cholangiocytes, and they control hepatoblast differentiation by modulating a

gradient of TGF-β signalling activity. Another issue that relates to the timing of hepatoblast differentiation pertains to the mechanisms of bile duct formation. Based on their SOX9 expression profile, biliary cells first differentiate at approximately E11.5 and then line the branches of the portal vein to form a ductal plate. Then, starting around E15.5, ducts initiate to form by apposition of hepatoblasts to the cholangiocytes of the ductal plate. These hepatoblasts delineate the lumen of the future ducts, and later differentiate to cholangiocytes, so the cell fate decision must be made at approximately E15.5, a time point much later than that of the appearance of the first signs of biliary differentiation. This indicates that at least a subset of hepatoblasts must remain bipotent to allow for this second wave of biliary differentiation. The involvement of key transcription factors and the TGF-β signalling pathway has been described previously, but other signalling mechanisms have been investigated. HGF stimulates expression of C/EBPα in isolated hepatoblasts, promoting differentiation toward the hepatocyte lineage [28]. The Jagged-Notch pathway controls biliary development, but arguments in favor of its involvement at the stage of cell fate decision are based on *in vitro* experiments [29]. Also Wnt signalling is implicated, by repressing hepatocyte differentiation and stimulating biliary development, although the mechanisms by which Wnt signalling controls hepatoblast fate decision are not clear [30]. Finally, many extracellular matrix components are implicated in cell fate determination, such as fibronectin, laminin and collagen types I and IV, but their role is very complex and still far to be defined [28].

Hepatocyte Maturation: Development of Function and Morphology

Following the lineage segregation stage, cells differentiated to the hepatocyte lineage undergo a process of maturation that consists in the progressive acquisition of peculiar morphology and physiologic functions. The transcription factors that control hepatocyte maturation nicely

illustrate the concept of a “dynamic transcriptional network”, and the number and complexity of interactions increases when hepatocyte maturation proceeds. There is a “core” of six factors (HNF-1α, HNF-1β, FoxA2, HNF-4α1, HNF-6, and LRH-1) that exert a mutual control each other; they also cooperate with cofactors to stimulate transcription of common targets, illustrating the concept of “synergistic interdependence” and delineating a model in which hepatocyte maturation depends on a network of factors that increase in concentration during maturation. These factors also have a metabolic role in the development of adult hepatocytes. It is well known that HNF-1β and HNF-4α control glucose metabolism as well as several other hepatic functions such as lipid and amino acid metabolism. HNF-1β is essential for bile acid sensing and fatty acid oxidation [31]. The three FoxA factors (FoxA-1, -2, and -3) regulate other numerous hepatic functions [32]. LRH-1 controls bile acid and cholesterol metabolism [33;34]. HNF-6 mediates some effects of growth hormone [35], inhibits glucocorticoid activity [36], and stimulates expression of genes in the gluconeogenic, glycolytic, and bile acid synthesis pathways [37;38;39], as well as hepatocyte proliferation [40]. C/EBPα, a member of C/EBP family, regulates glucose and glycogen metabolism as well as lipid homeostasis and hepatocyte proliferation. Another member of the family, C/EBPβ, is a regulator of gluconeogenesis and a potent stimulator of phosphoenolpyruvate carboxykinase.

Besides their role in the control of metabolic functions, liver-enriched factors are also important determinants of hepatocyte morphology. In particular, HNF-4α is required for expression of genes whose products regulate cell junction assembly and adhesion [41] and endoplasmic stress response [42]. Starting around E12 in the mouse embryo, differentiating hepatocytes are closely associated with hematopoietic precursor cells. The latter colonize the embryonic liver and, by the end of gestation and the early postnatal period, they leave the organ and migrate to the bone marrow. These hematopoietic cells are essential for hepatocyte maturation,

because they secrete oncostatin M (OSM), an interleukin-6 –related cytokine, that in turn stimulates expression of terminal hepatocyte differentiation markers such as the gluconeogenic enzymes glucose-6-phosphatase and phosphoenolpyruvate carboxykinase [43;44]. Wnt signaling controls hepatoblasts proliferation but is also involved in the maturation of hepatocytes, as a result of negative regulation of glucose-6-phosphatase, and positive regulation of glycogen synthase [45].

A key role is exerted by the endothelial sinusoidal cells, which can influence the apical-basal polarity of hepatocytes. Furthermore, hepatocyte maturation is not complete at birth: in fact, the production of HGF is greater in the postnatal than in the prenatal period, to complete the hepatocytes maturation. In the first weeks after birth the so-called “metabolic zonation” occurs, in which hepatocytes constitute a heterogeneous cell population that expresses different gene sets and exerts different metabolic functions, depending on their location in the hepatic lobule [46;47]. HNF-4α and Wnt signalling contribute to the establishment of lobular and metabolic zonation [48] *[Figure 5].* The final morphology of mature hepatocyte is characterized by polygonal shape with round and central nucleus, and they may be binucleated; they have also numerous microvilli and grumous cytoplasm, with high nucleus to cytoplasm ratio.

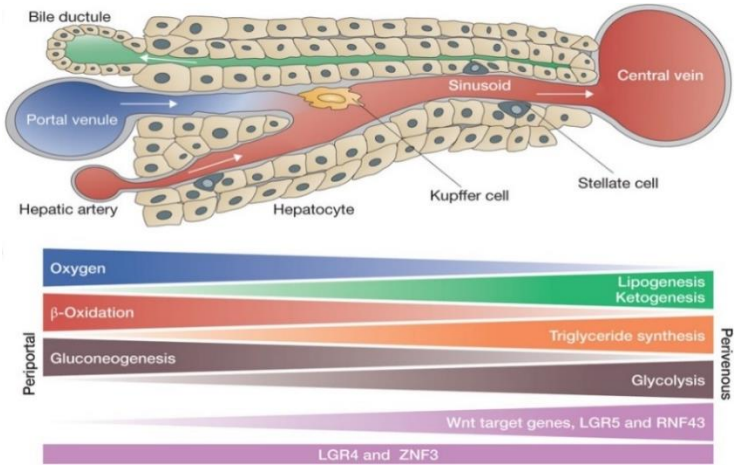

Figure 5: Metabolic zonation of the liver.
From Birchmeier W., Nature Cell Biology 2016 Apr 27;18:463-5.

Cholangiocyte maturation: development of function and morphology

Cholangiocyte cells line the extrahepatic and intrahepatic bile ducts but have a dual origin. The extrahepatic biliary tract develops from an outpocket of the endoderm, located caudally to the liver, and closely associated with the ventral pancreatic bud. The extrahepatic biliary tract morphogenesis depends on the appropriate development of both the cholangiocyte epithelium and the surrounding mesenchyme [49]. Loss of expression of epithelial transcription factors such as HNF-6 or HNF-1β or FoxF1 was associated with dysmorphogenesis of the gallbladder and common bile duct [31;50;51]. The extrahepatic biliary tract develops before the intrahepatic bile duct, but the mechanism by which they anastomose is not known.

Intrahepatic bile duct cholangiocytes derive from hepatoblasts. Intrahepatic bile duct morphogenesis starts with the alignment of the cholangiocytes around the periportal mesenchyme to form a single-layer ring of cells called the ductal plate. The formation of ducts relies on a unique tubulogenic process in which hepatoblasts become affixed to specific areas of the ductal plate to generate ducts, that are considered to be asymmetrical [27]. The latter

differentiate to cholangiocytes between E15.5 and E18.5, thereby allowing for the development of ducts entirely lined by cholangiocytes. During this period, the expression of cell adhesion molecules such as E-cadherin [27] and spermatogenic immunoglobulin superfamily (nectin-like molecule-2) [52] increases, and that of neural cell adhesion molecule decreases [53]. Furthermore, the ductal plate areas not involved in tubulogenesis regress, whereas the ducts grow in length following a hilum-periphery axis, and become surrounded by periportal mesenchyme. Few factors were shown to impact tubulogenesis, such as HNF-6, HNF-1β, and SOX9, which is downstream of HNF-6 and upstream of C/EBPα [27;54]. Important at this stage is Jagged-1, expressed in the periportal mesenchyme; it interacts with Notch-2 in cholangiocytes to stimulate expression of Hes-1, an effector of Notch signalling, to induce ductal morphogenesis [55;56], also with the help of angiogenic factors which stimulate cholangiocyte proliferation [57], and activation of the epidermal growth factor/mitogen-activated protein kinase pathway, as a positive regulator of cholangiocyte proliferation [58;59] *[Figure 6]*.

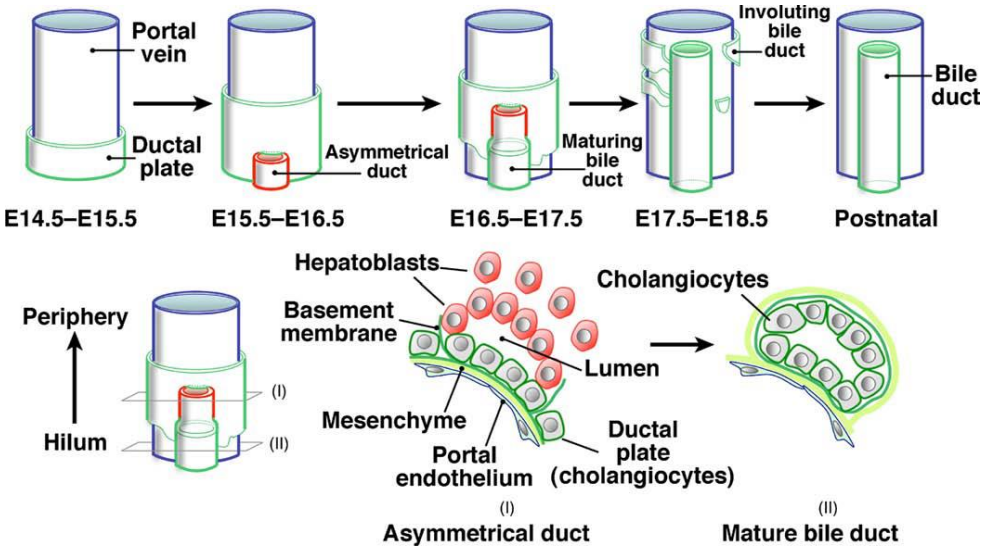

Figure 6: Morphogenesis of the intrahepatic bile ducts.
From Lemaigre F.P., Gastroenterology 2009;137:62–79.

Liver morphogenetic changes during specification and post-specification

During the embryonic specification, liver endodermal epithelial cells receive stimuli from surrounding mesodermal cells, able to regulate gene expression and cell division. In this context, the mesoderm that will give rise to the *septum transversum* has an essential role, by surrounding the embryonic midgut endoderm, and eliciting a secondary morphogenetic induction within the nascent liver bud [1;60;61]. In this sense, liver bud morphogenesis is marked by: 1) the formation of the rostral diverticulum of the gut, 2) remodelling of the extracellular matrix around the hepatoblasts, and 3) reassembly of E-cadherin-based connections between the cells. Furthermore, liver bud requires the transitions from a columnar epithelium to cells dividing more rapidly and migrating into the surrounding mesoderm (E9.5), the latter providing precursors of the endothelial cells that begin to form intrahepatic vascular structures. In this phase, it is important to consider also the fundamental role of the liver transcription factors, Hex [12] and Prox1 [62] allowing for a transition from an epithelium to a non-polarized cell type. Primitive endothelial cells, or angioblasts, appear near the hepatoblasts and promote the growth of the latter into the perihepatic mesenchyme, later giving rise to the *septum transversum* [63;64]. Then, during the outgrowth of the hepatic bud, the mesoderm-derived endothelial cells enter spaces within the hepatic bud, and give rise to vesicles that fuse to form blood vessels into the developing liver.

Local hematopoietic cells differentiate inside the growing liver and the organ becomes distinct from the gut epithelium. Interesting, the cell interactions that we have found to occur during organogenesis may be recapitulated in adult tissue during liver regeneration, due to the signalling between endothelial cells and hepatocytes, which is critical to establish a sinusoidal liver architecture [65;66;67].

Anatomy of the mature rodent liver

In Mammals and man, the liver is the largest gland in the body exhibiting both endocrine and exocrine properties. Endocrine functions include the secretion of several hormones such as insulin-like growth factors, angiotensinogen, and thrombopoietin, while the major exocrine secretion is in the form of bile. The liver is also essential for glycogen storage, drug detoxification, control of metabolism, regulation of cholesterol synthesis and transport, urea metabolism, and secretion of an extensive array of plasma proteins including albumin and apolipoproteins. Liver histological sections show a rather homogeneous landscape of hepatocytes periodically infiltrated with vascular tissue and bile ducts. The basic architectural unit of the mammalian liver is the liver lobule *[Figure 7]*. The lobule consists of plates of hepatocytes lined by sinusoidal capillaries that radiate toward a central efferent vein. In many Mammals, primarily the pig and rat (although not in humans), the three-dimensional (3D) structure of the liver lobule corresponds to a gross hexagonal polyhedron with each of the six corners demarcated by the presence of a portal triad of vessels consisting of a portal vein, bile duct, and hepatic artery. Both the portal vein and hepatic artery supply blood to the lobule, which flows through a network of sinusoidal capillaries before leaving the lobule through the central vein.

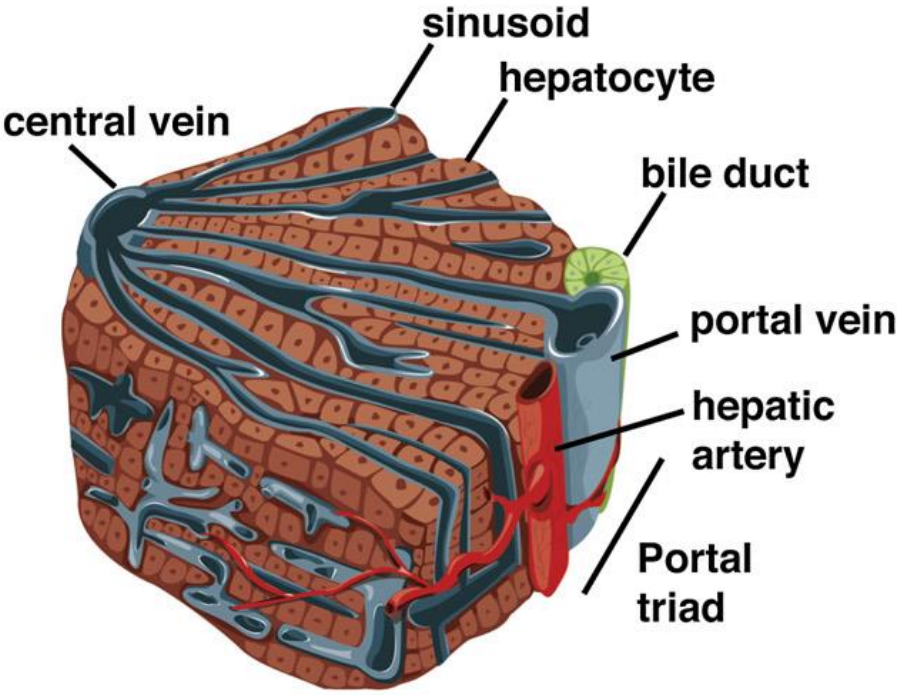

Figure 7: Structure of a portion of a rodent liver lobule.
From Karim Si-Tayeb et al., Developmental Cell 2010 Feb 16;18:175-89.

The macroscopic lobulation of the rat and human liver is similar, with an equivalence between the left lobe of the rat with the segment II of the humans, the middle lobe to segments III, IV, V, and VIII, and the right lobe to segments VI and VII. The hepatocytes are polarized epithelial cells arranged as cords with the basolateral surfaces fenestrated, which facilitates the endocrine secretions transfer from them to the blood stream. Tight junctions between neighbouring hepatocytes generate a canaliculus surrounding each hepatocyte and responsible for collection of bile acids and bile salts that are transported across the hepatocyte's apical surface. Bile collected by the canaliculi is carried to the bile ducts within the portal triad and subsequently transported for storage in the gall bladder [3].

2. Lessons from organogenesis for *ex-situ* developmental bio-engineering of the liver

Over the past decade, research has shown that the extracellular matrix (ECM) plays a fundamental role in determination, differentiation, proliferation, survival, polarity, migration, and behaviour of mammalian cells [68]. As such, it regulates morphogenesis of tissues and organs. In particular, the ECM exerts a mechanical support to self-assembling cells, and provides a 3D architecture to the developing organs, influencing stromal molecular composition, cell adhesion molecules, mechano-chemical signalling from the cell surface to the nucleus, and binding of morphogens (gradient growth factors) to developing cells.

All these functions make the ECM an excellent model of biocompatible scaffold for 3D organ reconstruction in the tissue engineering and regenerative medicine field. Then, the 3D organ reconstruction “on the laboratory bench” requires a 3D substrate for seeded cells, which is the reflection of a general biological property of embryonic development. In fact, during the *in vivo* organogenesis, stem cells and precursor elements acquire different phenotypes, depending upon the geometry of their environment or “niche” [69], a phenomenon proved to occur also in bioengineered contexts [70;71]. Therefore, the 3D architecture of cell assembly and its inherent physical-chemical properties are fundamental to regulate expansion and functional differentiation of the resident cells. As predicted by the morphoregulatory theory of Topobiology, the tissue environmental geometry provides a mechano-chemical regulation on cell growth and differentiation [72]. Specifically, the morphoregulatory input induces histodifferentiation and, thus, brings about organ functional activity. As a result, organ physical topology becomes coincidental with organ signal topology [73]. In this way, in endoderm-derived endocrine organs, like the liver, the inner stromal/vascular scaffold (SVS), i.e. the natural organomorphic matrix, may act as a pivotal mechano-chemical information for growth and differentiation of stem cells

and progenitors during morphogenesis. As a result, endocrine *ex situ* engineered bioconstructs are expected to become biologically similar to the native endocrine organ as much as accurate provision of structural and functional factors involved in the natural development and physiological maturation come into play. The presence of a 3D context reproducing *ex situ* the geometrical, physical and biochemical properties of the inner SVS seems to be a key factor to elicit the morphogenetic potential of cultured cells, and establish a reconstruction procedure retracing their developmental steps. Then, a generic 3D architecture of the scaffold/matrix seems not sufficient to *ex situ* bioengineer an entire and functional 3D organ, because the 3D growing architecture dictates the functional differentiation of the resident cells. Consequently, only a 3D geometry of the scaffold recapitulating that of the supporting and trophic system in the parent organ may fulfil the scale requirements necessary to guide *ex situ* cell auto-assembly up to the formation of a viable and physiologically competent, macroscopic endocrine organ [74].

3. Models of liver differentiation using different sources of rodent stem cells/progenitors

Currently, many different cell types have been induced to differentiate to liver cells, using specific differentiation protocols.

Oval cells, hypothesized to be the progeny of intrahepatic stem cells and referred as adult liver stem cells [75], have been pushed to differentiate to hepatocyte using BMP-4 [76]. Specifically, WB-F344 rat hepatocytic epithelial stem-cell-like cell line (oval cells) were cultured for 2 months, and analysed for different parameters including growth, morphology and hepatocyte function.

The results demonstrated that the amount of urea secreted from these cells treated with BMP-4 increased gradually, and the level of ALB secretion was also significantly stimulated. In addition, glycogen storage and Idocyanine Green (ICG) uptake were found enhanced, whereas the level of connexin-43, an endodermal marker, was found to progressively decrease. Finally, BMP-4 induced a characteristic hepatic morphology, by increasing the cell volume, and inducing a classical polygonal shape with microvilli.

Similar, LE/2 and LE/6 oval cell lines, non-parenchymal liver epithelial (oval) cell lines derived from rats maintained on a choline-deficient carcinogenic diet, were induced to hepatic differentiation in 3D [77]. Cells were suspended in a collagen gel layered either below or above a hydrated cell-free collagen gel layer. Then, bone marrow-derived mesenchymal stromal cells (BM-MSCs) were added to this culture system, suspended in a feeding medium covering the upper collagen gel layer where they grew in a monolayer without invading the collagen gel underneath. DMSO and hrHGF were used for hepatocyte differentiation, whereas hrHGF combined with KGF (keratinocyte-grow factor) were administered for ductal differentiation. The collagen gel is believed useful for both promoting hepatocytic differentiation of precursor cells, and preserving their differentiated state [78]. Additionally, the MSCs feeder layer is considered essential for inducing hepatocytic differentiation. Indeed, with this system oval cells differentiated along the hepatocytic lineage, showing markers as ALB, CK-8, and CK-18 although were unable to acquire a full adult phenotype. Oval cells also showed morphological evidence of bile duct lineage differentiation, although they did not show expression of typical bile duct markers, such as gamma-glutamyl transpeptidase (GGT) and CK 19.

However, the most widely used cells to induce hepatic differentiation are the MSCs. Lin et colleagues [79] used BM-MSCs of 2- to 3-month-old, Sprague–Dawley male rats cultured on alginate scaffolds, in the presence of specific growth factors including HGF, epidermal growth

factor (EGF) and FGF-4. They found that cells attached to the scaffold formed multicellular spheroids and proliferated, and these cells expressed a subset of hepatocyte genes including α-fetoprotein (AFP), ALB, connexin 32 (Cox 32) and CYP7A1. AFP was seen after 14 days of differentiation, but was not detected after 28 days. ALB, a marker of mature hepatocytes, appeared after 14 days of culture, and its expression increased after 28 days in culture. Cox 32, a cell–cell communication factor, and CYP7A1 a cytochrome p450 (CYP) enzyme, were detected in cells that had undergone differentiation for 28 days. The differentiated cells also showed CK-18, a marker of mature hepatocytes, and the capacity to store glycogen.

Similar, Ouyang et al. [80] used BM-MSCs from six-week-old, Sprague–Dawley female rats. They use 2-(4-bromophenyl)-N-(4-fluorophenyl)-3-propyl-3H-imidazo[4,5-b]pyridin-5-amine (SJA710-6), a small molecule able to selectively differentiate MSCs toward hepatocyte-like cells. The differentiation protocol had a pre-induction step of 24 hours, an induction step of 2 days, a differentiation step of 7 days, and a maturation step of 14 days. After four weeks, 14% of cells treated with SJA710-6 exhibited hepatic differentiation, which is comparable with the positive control group (growth factor-treated). The resultant hepatocyte-like cells exhibited a polygonal shape with grumous cytoplasm and retractile cell borders, which are characteristic of hepatocytes. In addition, these cells were able to synthesize urea, uptake LDL, and secrete ALB, whereas the mRNA levels of hepatocyte-specific genes such as ALB, AFP, CK18, c-Met, CYP1A1, CYP2B1, and HNF3β were all found significantly increased.

Sgodda et collegues [81] used rAT-MSC isolated from rat peritoneal adipose tissue obtained from wildtype Fischer 344 rats. These cells, treated with HGF and EGF and cultured on plastic dishes for 28 days, differentiated into hepatocyte- like cells with expression of specific markers for epithelial cells (CK18), cell–cell interaction (CX32, CD26), hepatocyte secretory function (ALB) and relevant metabolic capacities such as detoxification (CYP1A1) and gluconeogenesis

(PCK1). The differentiated MSC also produced urea, stored glycogen, and presented a polygonal shape typical of hepatocytes.

Also Sarvandi et al. [82] used MSC for hepatic differentiation. These MSCs were derived from the omental tissue (rOT-MSCs) of neonatal Wistar rats (age 12 days/weight 15–16 g), and were treated with liver extract (6 μg/ml) in 25 cm^2 flasks for 21 days. At the end of the differentiation protocol, the cells acquired a cuboidal morphology typical of hepatocyte-like cells, and were binucleated; in addition, the nucleus to cytoplasm volume ratio increased. Differentiation of cells to the hepatic phenotype was confirmed with expression of ALB, CK18 and AFP. For ALB, the immunocytochemistry results showed significantly greater levels of ALB after 18 days of differentiation as compared to the control. The majority of rOT-MSC-derived hepatocytes were also strongly positive for PAS staining at day 19, and urea production and secretion was detected at various time points throughout the differentiation protocol (best levels at 16-21 days).

rMSC, derived from plastic-adherent mononuclear bone marrow cells after expansion in culture, were used by Lange et colleagues [83] in fibronectin-coated vessels, co-cultured with freshly isolated rat liver cells. After 2 weeks, co-cultured MSCs expressed ALB and CK-18 mRNA, whereas MSCs cultured without liver cells (but in presence of HGF, EGF, SCF, and FGF-4) did not express any. This showed that cultivation of rMSCs with only some hepatocye-specific growth factors on fibronectin-coated surfaces is not sufficient to induce full hepatic differentiation.

In 2002, Schwartz [84] derived primitive multipotent adult progenitor cells (MAPCs) from normal human, mouse, and rat postnatal bone marrow. Human, mouse, and rat MAPCs cultured on Matrigel with FGF-4 and HGF, differentiated into epithelioid cells, expressing HNF-3β, GATA4, CK19, transthyretin, and AFP at day 7, and CK18, HNF-4, ALB and HNF-1α at days 14–28.

These cells also secreted urea and ALB, had phenobarbital-inducible cytochrome p450, could take up LDL, and stored glycogen. Very interesting, in this study many different growth factors were tested including aFGF, bFGF, FGF-4, HGF, FGF-7, and OSM, but only FGF-4 and HGF promoted hepatocyte differentiation. FGF-4 alone induced hepatocyte differentiation, but the degree of differentiation measured by absence of immature markers such as AFP and CK19 was higher when cells were also treated with HGF. This is consistent with the observation that FGF-4 is important in initial endoderm patterning and may play a role in endoderm specification [85], and that HGF induces differentiation of hepatocytes that are not actively proliferating [86;87;88;89].

Wang et colleagues [90] also used fetal liver stem/progenitor cells (FLSPCs) from adult F344 rats. The authors hypotesized that Notch inhibition obtained with N-[N-(3,5-difluorophenacetyl)-L-alanyl]-Sphenylglycine t-butyl ester (also called DAPT), might directly up-regulate hepatocyte differentiation via HGF and HNF-4α or might impair cholangiocyte differentiation thereby. However, the results demonstrated that Notch inhibition does not induce significant upregulation of HGF or HNF-4α in FLSPCs. This suggests that Notch inhibition induces hepatocyte differentiation without the influence of HGF or HNF-4α. Moreover, significant down-regulation of HNF-1β was observed, presumably dependent on an impairment of cholangiocyte differentiation. Then, data demonstrated that the inhibition of cholangiocyte differentiation spontaneously induces hepatocyte differentiation. In fact, the differentiated cells expressed markers of hepatocyte such as HNF-4α and low HNF-1β, low CK-19, high CYP450 and G6P, high ALB and urea production, Claudin-1, glycogen production and ICG uptake, and also the ability to process LDL.

In order to obtain adult hepatocyte, Block [91] used hepatocytes from male Fischer 344 rats that, after population expansion and clonal growth, returned to a mature hepatocyte phenotype.

The authors showed that HGF/SF, EGF and TGF-α induced a significant cell proliferation, while KGF, SCF and aFGF had not effects; in addition, Matrigel was very important for polarity induction and canalicular differentiation, possibly as a result of its high laminin content [92]. Cells in Matrigel formed bile canaliculi and acinar/ductular structures, expressed ALB and mRNA for AFP, CK-14, CK-18, and CK19, and exhibited increased production of HNF-4, HNF-1, HNF-3, and C/EBPβ. These cells also showed cytochrome IIB1 expression and presence of glycogen. Very interestingly, the removal of DEX from the culture medium strikingly reduced DNA synthesis in the culture, indicating a primary growing effect of this steroid. Similar effects were seen with NTA. Moreover, it was also showed that HGF/SF with EGF had the strongest proliferative effect.

Others cell type have equally been tested for their ability to differentiate to hepatic-like cells. Nishiofuku et al. [93], and Ruhnke et al. [94] used rat embryonic stem cells, whereas Marongiu and colleagues [95] rat amniotic epithelial cells, and Sun et colleagues [96] rat induced pluripotent stem (iPS) cells. All obtained efficient hepatic differentiation.

4. Rodent thyroid stem cells/progenitors

Although thyroid and liver have the same endodermal origin, the cells of the two organs are different in functional terms, due to their differentiation process. Specifically, both human and rodent thyroid gland have a low cell turnover rate, of approximately five times over the course of a lifetime [97;98]. In addition, in the mouse thyroid it is possible to cytometrically distinguish two different side populations (SP), i.e. two subpopulations of cells having specific markers of pluripotency: a CD45(-)/c-kit(-)/Sca1(+), known as SP1, and CD45(-)/c-kit(-)/Sca1(-), named SP2 [99]. These thyroid SP cells show a round shape of the nucleus and are, on average very

small in size, with high nucleus to cytoplasm ratio [100;101]. They are characterized by the expression of the Abcg2 gene, other genes associated with thyroid differentiation such as Titf1, Pax 8, TPO, Tg, and TSHr, and also genes characteristic of embryonic cell lineages, e.g. nucleostemin and Oct4, the latter known for its essential role in maintaining pluripotency of cells of the inner cell mass and embryonic stem cells, and recently found in in several human adult stem cells [102;103;104;105;106].

The Abcg2 gene is mainly expressed at similar levels both in SP1 and SP2 cells, but not in main population (MP) cells: the cells expressing Abcg2 reside in the interfollicular space of the thyroid gland [99]. Nucleostemin is in general highly expressed in SP1, followed by SP2 cells as compared with MP cells, whereas Oct4 expression is found at similar levels in both SP fractions. TPO and Tg, the genes directly involved in thyroid hormone synthesis, are not significantly expressed in either SP1 or SP2 cells, as compared with MP cells. Expression of Ttf1 and TSHr is detected in the SP2 fraction, suggesting a possible role for these two genes in commitment and/or maintenance of thyroid lineage. Altogether, these results suggest that thyroid SP cells, in particular SP1 cells, are less differentiated or not terminally differentiated as compared with MP cells, and have characteristics of a stem/progenitor cell when judged by gene expression patterns [99].

During the early time of mouse thyroid formation, precursor cells start to express the transcription factors TTF1, TTF2, and Pax8, whereas expression of thyroid-specific genes as Tg, TSH receptor, thyroperoxidase, and sodium iodide symporter first occurs after completion of migration [107]. In culture, these thyroid SP cells grow slowly compared with MP cells, and stay undifferentiated. After one week of culture, SP1 cells show polygonal or multipolar shape, which by three weeks of culture become well connected to each other by their cytoplasmic projections. MP cells also demonstrate polygonal or multipolar morphologies at the beginning

of the culture period, however, after one week they expand rapidly and organize continuous pavement with occasional tubular structure. MP cells with hyperchromatic oval nuclei form epithelial arrangement and follicle-like structures, which are immunoreactive for Ttf1 and Tg; finally, SP2 cells show an intermediate character between SP1 and MP cells regarding growth rate and morphology. These results suggest that mouse thyroid SP cells are less differentiated compared to MP cells, and are likely to have some properties of stem/progenitor cells, as judged from limited expression of thyroid differentiation marker genes (i.e. Tpo and Tg), and exclusive expression of genes related to stem cell proliferation and self-renewal (i.e. nucleostemin and Oct4). On the other hand, thyroid SP2 cells appeared to be slightly more differentiated, or closer to mature thyrocytes than SP1 cells, as demonstrated by the weak expression of Ttf1 and TSHr. The frequency of stem cells in mouse thyroid would have been estimated at most to be 1 out of 1000 [97].

Similar results were obtained by our group in the thyroid of adult male rats. We identified a side population expressing Abcg2 and THE epithelial markers CK, although occasionally we detected also the mesenchymal filament, vimentin [108]. Using 50% Matrigel, cells from primary thyroid cultures exhibited rapid differentiation (days 4-8) up to formation of polarized follicles [109]. In addition, starting from the same primary monolayers, we developed long-term (2-4 months) cultures under starvation protocol, giving rise to CFU-like cultures [110]. These CFU-like cultures were shown to be multipotent: indeed, using TSH we were able to differentiate them to thyrocyte-like cells containing TG and NIS, whereas using an adipogenic medium to adipocytes [110;111]. In contrast, none osteogenic differentiation was achieved. These cells had numerous markers of multipotency and endodermal progenitor lineage including ABCG2-, Oct-3/4-, HNF4a-, GATA-4, and Sca-1; CFU-like cultures resulted also diffusely positive for vimentin, suggesting a possible contribution to the multipotency from resident MSCs [110].

5. Proteome characterization of rodent thyroid stem cells/progenitors

The understanding of when and where the proteins were expressed became the major challenge after the completion of the Human Genome project in 2003 [112]. In order to reach this objective, a new branch of study called proteomics was developed, aimed at the complete detection of the protein expression (i.e. the proteome) of a cell, tissue, organ or organism [112;113]. The importance of studying protein expression lay on the fact that proteins essentially catalyse and control all cellular process and the proteome define the cell's functional state (i.e. the functional phenotype). Remarkably, proteomics stands at a different level with respect to genomics because the true size of a proteome cannot be derived from the number of cell genes and, conversely the same genome can express proteome profiles very different in relation to the overall functional state of the cell *[Figure 8]*.

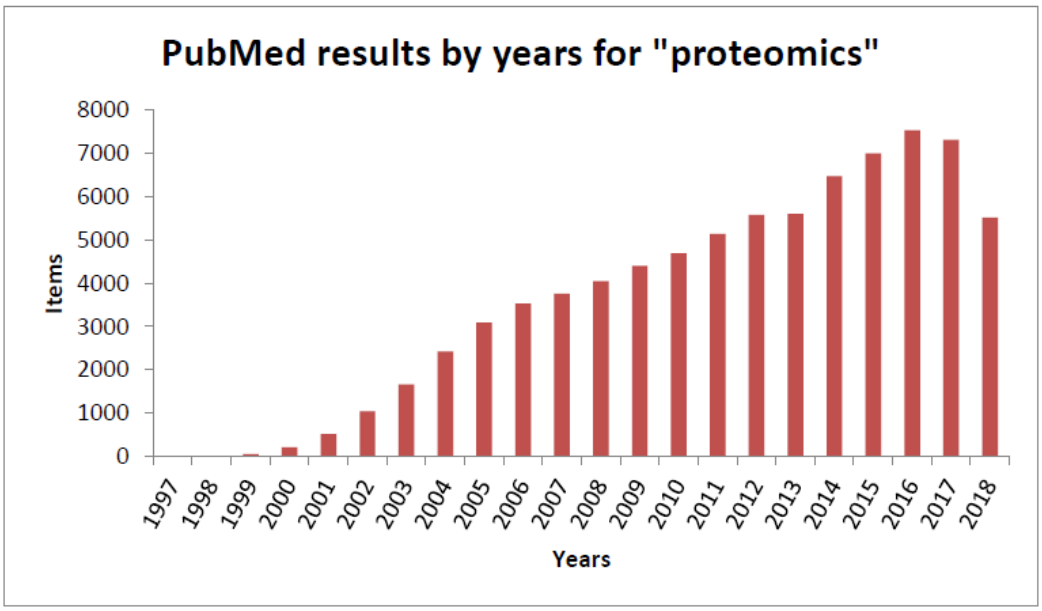

Figure 8: The number of items for "proteomics" in PubMed during years update to September 2018.

The main way to investigate the proteome is the use of mass spectrometry (MS). A mass spectrometer consists of an ion source (common ion source are the electrospray source ionization (ESI) and matrix-assisted laser desorption/ionization (MALDI)), a mass analyser that measures the mass-to-charge ratio (m/z) of the ionized analytes, and a detector that registers the number of ions at each m/z value [114]. The main approach used in proteomics is the “bottom-up” method, i.e. the identification of a protein starting from its proteolyzed peptides [115]. Specifically, proteins are digested by sequence-specific enzymes such as trypsin, and ensuing peptides are separated by reverse-phase chromatography, following by their ionization, and channelling to a mass spectrometer for analysis.

In this sense, a mass spectrometry analysis was carried out in collaboration with Dr. Marco Alfieri, RE.MO.BIO.S Lab (Director Prof. Roberto Toni), University of Parma (Italy) and the Conway Institute of Biomolecular and Biomedical Research (Director Prof. Stephen R. Pennington), University College of Dublin - UCD (Ireland), to analyze the different proteome profiles between adult rat thyroid cells from primary culture (THY) and adult rat thyroid stem cells / progenitors (TSC/P) and identify a specific proteomic signature for TSC/P.

Statistical analysis revealed that 16% (721 proteins) of identified proteins in TSC/P and THY proteomes were differently expressed *[Figure 9]*, and, of those, the 52% (375 proteins) were up-regulated in TSC/P *[Figure 10]*.

Figure 9: Venn diagram of total proteins identification and overlap between rat THY and TSC/P.

These proteins belonged to the cellular pathways controlling cell proliferation, as expected by the fact that TSC/P replicates at least three times faster than THY.

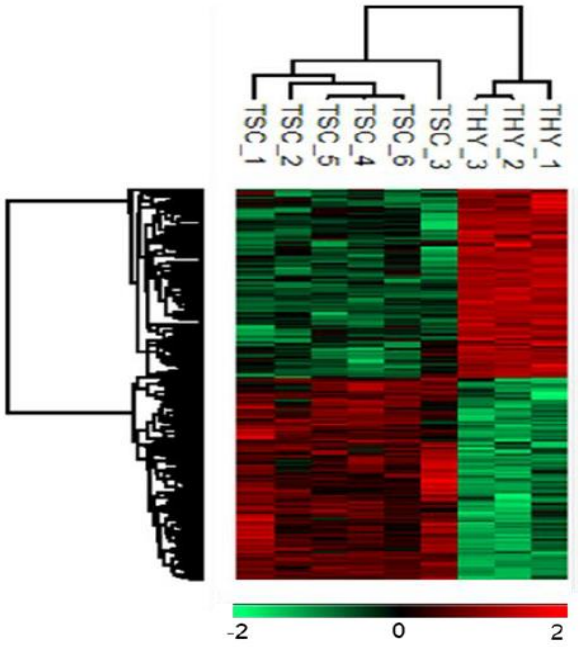

Figure 10: The heat map of 721 proteins differentially expressed based on clustering. Each column represents a different sample, plotted as a three biological replicates for THY and six for TSC. Red color indicates proteins that were up-regulated and green color indicates proteins that were down-regulated. Black spot evidence proteins whose expression unchanged between samples.

Orbitrap Fusion analysis allowed to obtain an exhaustive panel of CD molecules. Of 50 identified CD proteins, 36 appeared to be expressed without any statistical differences in the analysed samples while 9 CD were up-regulated in TSC/P, and 5 were down-regulated. Remarkably, we identified eleven typical MSC markers (identified: CD13, CD29, CD44, CD49a, CD54, CD71, CD73, CD90, CD105, CD106, CD166) [116;117] but only two of those were differently expressed in TSC/P (CD71 and CD90) with respect to THY. Specifically, CD90 was 1.89 times more expressed in THY than TSC/P *[Table 1]*.

Protein IDs	Protein names	Gene names	Log2 fold change TSC/THY	t-Test p-value
D3ZQM3	Integrin alpha 3 (CD49c)	Itga3	4.02	0.0024
G3V667	Integrin alpha 6 (CD49f)	Itga6	6.91	0.0001
A0A0G2JWK0	Integrin beta 3 (CD61)	Itgb3	2.56	0.0006
Q99376	Transferrin receptor protein 1 (CD71)	Tfrc	1.76	0.0005
Q5U334	Poliovirus receptor (CD155)	PVR	1.20	0.0004
P97710	Signal regulatory protein alpha (CD172a)	Sirpa	1.96	0.0012
G3V824	Insulin-like growth factor 2 receptor (CD222)	Igf2r	0.84	0.0010
F1LMA7	C-type mannose receptor 2 (CD280)	Mrc2	0.80	0.0032
Q62786	Prostaglandin F2 receptor negative regulator (CD315)	Ptgfrn	0.91	0.0009

Table 1: Up-regulated CD proteins in rat TSC/P. Protein ID, protein name, gene name, log2 fold change, and p-value are listed for each protein.

In addition to CD markers, the analysis showed that TSC/P express different types of annexins and integrins that could represent suitable candidate markers of these cells. Annexins are implicated in several biochemical processes, including cell proliferation, immune tolerance, ion-channel activation, cell-cell interactions and cell differentiation, while integrins are involved in many cellular functions ranging from cell-substrate adhesion, cytoskeleton organisation, cell motility and response to stimuli. In particular, four types of integrins are normally expressed in

mesenchyme-derived cells (Itga3, Itga8, Itga11 and Itgb1) and another one (Itga6) was used as a marker of several progenitor cells.

The analysis of phenotypic markers showed that TSC/P tend to primarily express proteins of the mesodermal / mesenchymal lineage, although some endodermal markers and few neuroectodermal markers (Nestin and Tubulin β3) were detected *[Figure 11]*. Nestin (Nes) is used as a marker for neural stem cells, and its expression is inversely correlated with cellular differentiation [118]. Nevertheless, in recent publications, nestin expression has also been described in several MSCs, progenitor cells [119;120] and cancer stem cells [121].

Protein IDs	Protein names	Gene names	Log2 fold change TSC/THY	t-Test p-value
Q99376	Transferrin receptor protein 1 (CD71)	Tfrc	1.76	0.0006
Q8K3R4	Adiponectin	Adipoq	1.45	0.0001
P01830	Thy-1 membrane glycoprotein (CD90)	Thy1	-1.12	0.0012
P04937	Fibronectin	Fn1	-1.89	0.0047
P43245	Multidrug resistance protein 1 (CD243)	Abcb1	-0.63	0.0044
P49134	Integrin beta 1 (CD29)	Itgb1		
G3V928	LDL receptor-related protein 1 (CD91)	Lrp1		
P21588	5-nucleotidase (CD73)	Nt5e		
P47853	Biglycan	Bgn		
Q05030	Platelet derived growth factor receptor beta (CD140b)	Pdgfrb		
P31000	Vimentin	Vim		
Q00238	Intercellular adhesion molecule 1 (CD54)	Icam1		
P26051	Cd44 antigen	Cd44		
M0RBA8	Endoglin (CD105)	Eng		
A0A0G2JVZ6	Integrin alpha V (CD51)	Itgav		
B5DEG1	Integrin subunit alpha 8	Itga8		
M0RBA8	Endoglin (CD105)	Eng		
P18614	Integrin alpha 1 (CD49a)	Itga1		
O35112	Cd166 antigen	Alcam		

Protein IDs	Protein names	Gene names	Log2 fold change TSC/THY	t-Test p-value
Q4QRB4	Tubulin beta-3	Tubb3	-1.34	0.0005
P21263	Nestin	Nes	Identified only in TSC/P samples	

t-Test p-value	Log2 fold change TSC/THY	Gene names	Protein names	Protein IDs
7.90E-05	-7.86	Cd81	Cd81 antigen	Q62745
0.0071	-1.72	Rab13	Ras-related protein Rab-13	P35286
9.23E-06	1.05	Ezr	Ezrin	P31977
Identified only in THY samples		Cdh2	Cadherin-2 (CD325)	G3V803
		Cd59	Cd59 antigen	P27274
		Cd63	Cd63 antigen	P28648
		Krt14	Keratin type I, 14	Q6IFV1
		Anpep	Aminopeptidase N (CD13)	P15684
		Ctnnb1	Catenin beta 1	Q9WU82
		Cd38	ADP-rybosyl cyclase 1	Q64244
		Cd151	Cd151 antigen	Q9QZA6
		Lamp1	Lysosome-associated membrane glycoprotein 1 (CD107a)	P14652

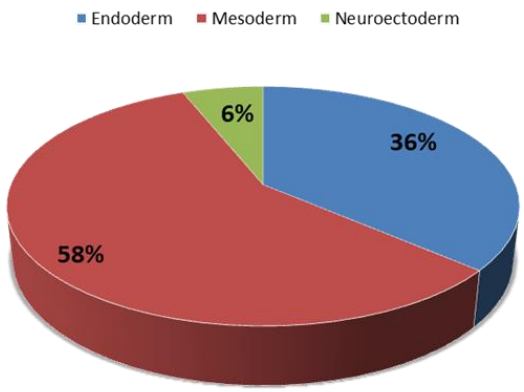

Figure 11: Proteins identified as markers of mesenchyme, endoderm and ectoderm phenotypes. Table highlighted in red shows proteins used as markers of mesenchyme, table highlighted in green shows markers of neuroectoderm and table highlighted in blue shows markers of endoderm.

Based on this evidence, we can assume that adult male rat TSC/P tend to express both endoderm/epithelial and mesenchyme markers, with a slightly predominance of the latter. Moreover, a small percentage is represented by neuroectodermal markers, implying a heterogeneity of this cell population (58% Mesoderm – 36% Endoderm – 6% Neuroectoderm), probably due to both the tissue source used for the primary culture and the starvation process to isolate the staminal counterpart.

Lastly, blotting analysis and immunocytochemistry have previously shown that these cells also express markers of the endodermal lineage such as Hnf4α, Gata-4, and Sca-1 (data not shown).

As summarized in *Table 2*, analysis of CD molecules allowed the identification of 4 putative markers that could be used for TSC/P isolation: Itga6 (CD49f), Sirpa (CD172a), Tfrc (CD71) and Igf2r (CD222). All these CD proteins have been previously used as a markers of stemness for MSCs and progenitor cells of different origins and represent the main candidates for the TSC/P molecular signature. Of particular interest is the high expression of CD49f, which has been extensively characterized as a marker of a wide range of stem and progenitor cells of both mesodermal and endodermal origin [122].

Protein IDs	Protein names	Gene names	Log2 fold change TSC/THY	t-Test p-value
G3V667	Integrin alpha 6 (CD49f)	Itga6	6.91	0.0001
P97710	Signal regulatory protein alpha (CD172a)	Sirpa	1.96	0.0012
Q99376	Transferrin receptor protein 1 (CD71)	Tfrc	1.76	0.0006
G3V824	Insulin-like growth factor 2 receptor (CD222)	Igf2r	0.84	0.0016

Table 2: Putative markers for TSC/P molecular signature

6. Bone marrow - derived mesenchymal stromal cells

Research in mesenchymal stromal cells (MSCs) evolved into several application fields in the last years. Mesenchymal stromal cells (MSCs) are multipotent spindle shaped cells with an apparent degree of plasticity that could be isolated from several tissues, characterized by possessing self-renewal capacity, long term viability and capacity to differentiate into all elements of the mesodermal lineage, including osteoblasts, chondrocytes, adipocytes, myoblasts and stromal cells *[Figure 12]*. Furthermore, in the past few years, several studies have reported that in addition to their mesenchymal-related multipotency, MSCs were also able to give rise to ectodermal neural cells [123] and endodermal hepatic elements [124].

This flexibility is termed “plasticity.” A widely accepted definition of plasticity has yet to be established, but, in general, this term refers to the newly discovered ability of adult stem cells to cross lineage barriers and to adopt the expression profiles and functional phenotypes of a different tissue – specific cells.

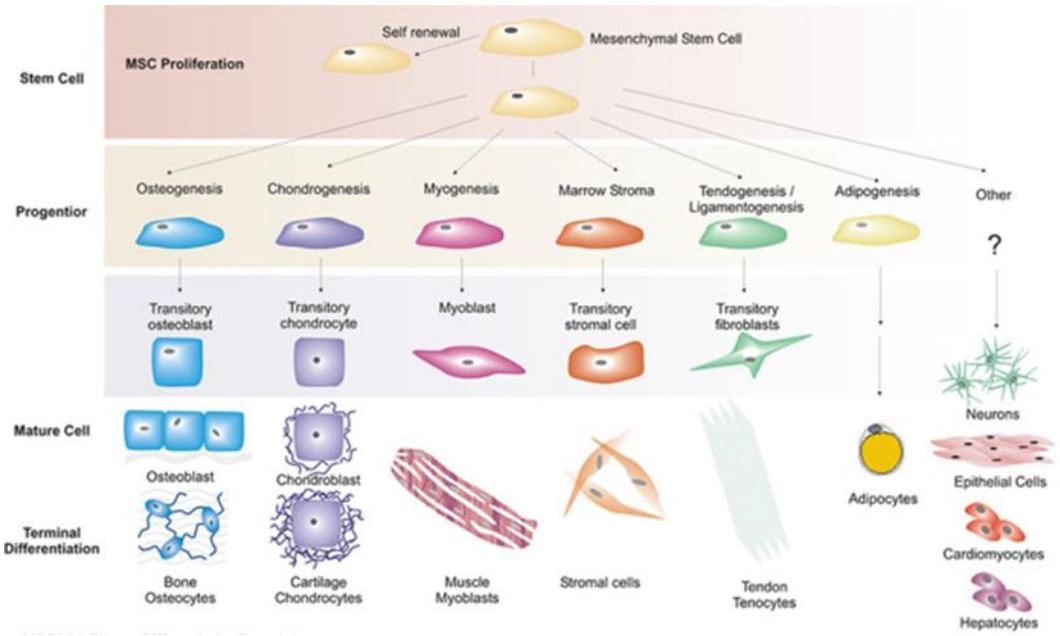

Figure 12: MSCs multipotency. MSCs can differentiate into bone osteoblasts, cartilagine chondrocytes, muscle myoblasts, stromal cells, adipocytes. and other cells types.
From Caplan AI and Bruder SP., Trends Mol Med 2001 Jun;7:259-64)

MSCs were initially identified as a subpopulation of bone marrow (BM) cells with osteogenic potential, as shown by heterotopic transplantation, to subsequently improve this evidence with studies that confirmed their content of clonal, plastic adherent bone-marrow derived nonhematopoietic cells in the mouse and guinea pig. These cells have been defined as colony-forming units–fibroblastic (CFU-Fs) [125;126;127]. Successive studies focused on the role of a similar population of bone marrow stromal cells derived from the adherent layers of long-term bone marrow cultures in supporting haematopoiesis [128]. Anatomically, BM stroma includes all nonhematopoietic cells types found in the BM microenvironment, namely osteoblasts, endothelial cells, fibroblasts and reticular cells, each of which, in principle, may play a critical role in haematopoiesis [129]. In bone marrow there are two “niches”, a sinusoidal niche and an endosteal niche [130]. The cells within the sinusoidal niche have been defined reticular cells

and they correspond to CFU-Fs with self-renewal and clonogenic capability [131]. In this way, a specialized microenvironment was defined, which precisely maintains a long-term storage of quiescent, slowly dividing HSCs by preventing their proliferation, differentiation or apoptosis. Despite originally these MSCs had been defined mesenchymal “stem” cells [132] because not governed by a limited or a fixed number of mitotic divisions, later they were more appropriately considered mesenchymal stromal cells, due to the fact that not all the cells in the population exhibited stemness characteristics [133].

Minimum criteria for MSCs identification included [134]:

- plastic adherence
- in vitro differentiation to adipogenic, chondrogenic, and osteogenic cells
- cell surface expression of CD105 (endoglin, SH2), CD73 (ecto-50-nucleotidase), and CD90 (Thy1) and the absence of the hematopoietic markers, namely CD45, CD19, CD19 or CD79, CD14 or CD11b, and HLA-DR.

However, for the characterization of mesenchymal stromal marrow cells there is no univocal antigenic profile. It is universally accepted that adult human bone marrow – derived MSCs do not express neither hematopoietic markers CD45, CD34, CD14, or CD11 nor costimulatory molecules CD80,CD86,or CD40, as well as adhesion molecules CD31 (platelet/endothelial cell adhesion molecule), CD18 (leukocyte function-associated antigen-1), or CD56 (neuronal cell adhesion molecule-1). In contrast, they can express CD105 (SH2),CD73, CD44, CD90 (Thy-1), CD71, and Stro-1 as well as the adhesion molecules CD106 (vascular cell adhesion molecule-1), CD166 (activated leukocyte cell adhesion molecule), intercellular adhesion molecule (ICAM)-1, and CD29 [135;136]. It is well known that MSCs lack expression of hematopoietic markers, although there are differences in molecular expression between human and other species MSCs [137]. The BM-MSCs isolated from rats [138] were found to be

negative for CD11b, CD45 and positive for CD29, CD49e, CD73, CD90, CD105 and Stro-1. Differences in cell surface expression of several markers may be influenced by factors from accessory cells, and the *in vitro* expression of some markers by MSCs does not correlate with their expression pattern *in vivo* [139].

Although the bone marrow has always been the main source of MSCs, they represent approximately 0.01% of mononuclear cells in this tissue. Mesenchymal stromal cells have also been isolated from other tissues, including adipose tissue [140], umbilical cord Wharton's jelly [141], dental pulp [142], umbilical cord blood [143].

MSC plasticity is clinically attractive as starting point for tissue engineering and regenerative medicine. To recreate functional tissues, the key ingredients are extracellular scaffolds (to anchor, deliver and orient cells), bioactive factors (to provide the instructional and molecular cues), and cells capable of responding to their environment by synthesizing the new tissue of interest. Given the multi-lineage potential of MSCs, their exquisite sensitivity to specific signalling molecules, and their relative ease of handling *in vitro*, they are a potentially powerful tool in tissue engineering. This approach has been employed for bone, cartilage, muscle, marrow stroma and liver repair and regeneration [144;145;146;147].

Similar to these evidences, our research group leaded by Prof. Roberto Toni isolated and characterized adult rat bone marrow – mesenchymal stromal cells. Specifically, the femur bone marrow was collected by inserting a 18-gauge needle into the bone diaphysis and bone marrow mononuclear cells were isolated by gradient centrifugation on Histopaque-1077 (Sigma-Aldrich), and washed twice in culture medium, counted, and plated on a standard plastic, T25 flasks (Corning, USA) at a density of 2x105/cm2. After 72 h, non-adherent cells were removed, the adherent ones (passage 0 or P0) re-seeded in a T25, and the medium replaced every 2–3

days. At 80 % confluence (i.e. subconfluence) cells were detached using trypsin 0.02 % EDTA for 1 min, splitted 1:2 (passage 1 or P1), and re-seeded.

Afterwards, the expression of typical mesenchymal markers (CD73, CD90) and the proliferative ability in our cell population were evaluated. In this sense, the cytofluorimetric positivity to CD73 and CD90 markers, as well as the absence of CD45 expression, confirmed the mesenchymal origin of our cells. Moreover, TEM analysis revealed numerous intra-cytoplasmatic vesicles, abundant rough endoplasmic reticulum (RER), and elongated mitochondria, numerous lysosomes and dense filaments, typical ultrastructural features of mesenchymal stromal cells [148;149]. Regarding proliferative capacity of our cells, there has been an increase of cells' number at each split, with very active cells that constantly replicated. In fact, there was not a substantial difference in the number of days to reach subconfluence at each culture split. Moreover, our bone marrow cell population express desmin. This protein, important for structural integrity and function of smooth muscle [150], was found by our group using western blot analysis (band of 53 kDa). In fact, recent studies demonstrated that this intermediate filament protein is constitutively expressed also under basal condition in mesenchymal stromal cells [151;152].

Importantly, bm - MSCs were maintained in culture medium until passage 4 (P4), and used for hepatic differentiation.

7. The cranial neural crest with particular emphasis on the nasal neural crest and its relevance to the formation of the nasal septum in humans

In humans, O'Rahilly and Müller have morphologically studied the development of the human neural crest between the 4th and 7th week of embryonic development [153]. During 4th week

of embryonic development, the neural folds begin to fuse, and the optic sulcus appears. A longitudinal groove, sulcus cristae, is found on the medial aspect of each neural fold. A careful reconstruction of the Corner embryo gave a distinct impression that the crest cells are extensively dispersed, and the mesencephalic, trigeminal, and facial components form a continuous mass, thereby occupying the future sites of rhombomeres 1 and 3.

Between the mesencephalon and the otic placode, crest cells develop at sites where the neural folds have not yet fused, thus clearly deriving from the ectoderm of the neural tube. At the same time, the optical crest derived from the optical primordial becomes visible. Mesencephalic crest mixes with the optic crest and contributes to the sheath of the optic vesicle. Some mesencephalic crest cells migrate towards the future frontonasal region. Crest cells clearly derived from the ectoderm of the neural tube continue to emerge at sites where the neural folds have become fused.

At this time, pharyngeal arches 1 to 3 have developed and mesencephalic and trigeminal cells migrate into the pharyngeal arches. In the middle of 4th week of embryonic development, optic crest becomes particularly evident. Neural crest cells eventually developing into pia mater cells surrounds the surface of the mesencephalon. Formation of the neural crest proceeds at the levels of rhombomeres 2, 4, 6, and 7. The trigeminal ganglion contains some short nerve fibres, and it continues to receive neural crest cells from the roof of rhombomere 2. Trigeminal and facial neural crest cells continue to migrate into pharyngeal arches 1 and 2, respectively.

The facial ganglion receives neural crest cells from the roof of rhombomeres 4, and also from its lateral walls. The otic vesicle is now related to rhombomere 5. Some of its migrating cells (that, however, are not neural crest cells) begin to form the vestibular ganglion. Glossopharyngeal and vagal ganglia are discernible, and migration of neural crest cells

continues from rhombomeres 6 and 7. A characteristically horizontal arrangement of the crest of the accessory nerve is observed in this developmental step.

Some crest cells derived from rhombomeres 6 and 7 are in continuity ventrally with the hypoglossal crest, and at this developmental step it probably gives rise also to the cardiac neural crest. The spinal crest has migrated caudally, and in a cross-section, it can be seen to extend between the surface of the alar lamina of the neural tube and the dermatomyotomes of the somites.

At the end of 4th week of embryonic development, the terminalis-vomeronasal crest develops from the pluri-stratified epithelium of the nasal placodes. The ectoderm located above the trigeminal ganglion gives rise to cells that are added to the ganglion. At this step, epipharyngeal placodes are clearly present and contribute to the facial ganglion, the inferior glossopharyngeal ganglion, and the inferior vagal ganglion. The neural crest of the accessory nerve uninterruptedly continues from the vagal crest to the spinal crest. The hypoglossal cell cord migrates to pharyngeal arch 2 and in the same time cells of the spinal crest migrate medial to the somites and occupy an extensive surface [153].

During 5th week of embryonic development, nasal crest cells migrates ahead from the nasal placodes but without reaching the telencephalon. The vestibular ganglion is clearly identifiable by its passage through efferent nerve fibres to the future utricle. At the end of the 5th week of embryonic development, a nasal pit has appeared and the crest cells from its epithelium adhere to each other and form fascicles. The nasal crest reaches the telencephalon while the hypoglossal cord penetrates the region of pharyngeal arch 1. The cervical ganglia reach their typical ventral position. Pia mater is identifiable as a single layer of neural crest cells.

In the 6th week of embryonic development, between the nasal pit and the telencephalic wall a relatively extensive mesenchymal zone is formed, crossed by neural crest cells and nerve

fibres. In particular, the latter are axons of crest-derived olfactory nerve cells entering the region of the future olfactory bulb.

At the 7th week of embryonic development, the vomeronasal and terminalis constituents continue to develop from the nasal crest localized inside the nasal pits. These nasal crest cells organize into a vomeronasal ganglion. In the final phase of the 7th week, cells and neurons of the neural crest still emerge from the nasal epithelium and form cords that migrate in the mesenchyme rich in capillaries towards the base of the prosencephalon *[Figure 13]*.

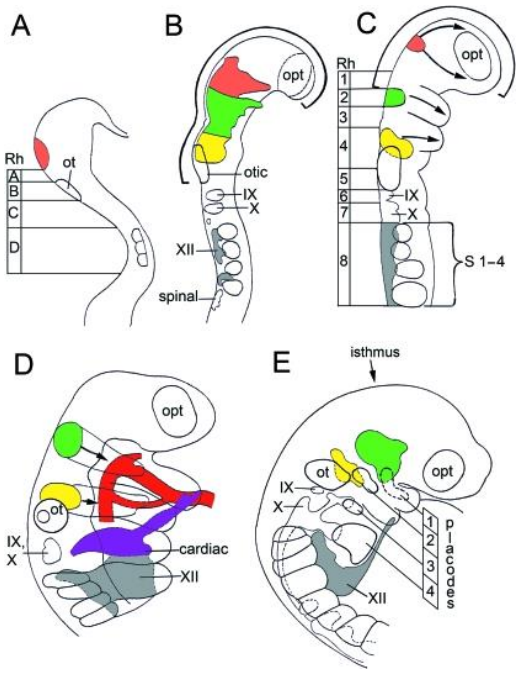

Figure 13: The neural crest in graphic reconstructions at stages 9 to 13. Right lateral views. (A) Mesencephalic crest (orange) has begun to form in stage 9. (B) Neural crest from the widely open rostral neuropore (thick curved black line) in stage 10. The preotic crest (mesencephalic, trigeminal, and facial components) is emigrating from the neural folds. The postotic and occipitospinal crest is present. (C) Trigeminal (green) and facial (yellow) ganglia have appeared in stage 11. Migration of the crest (arrows) continues. The uppermost arrow indicates a frontonasal component. Migration to pharyngeal arches 1 and 2 (arrows) is from closed neural tube. Rhombomeres 1, 3, and 5 are now seen to be crest-free. (D) The cardiac and hypoglossal crest at stage 12. The cardiac crest arises from Rh. 6 and Rh. 7 and migrates to the truncus arteriosus, which it surrounds. Hypoglossal crest at this stage occupies mainly pharyngeal arch 4. Trigeminal and facial crest migrate (arrows) into arches 1 and 2 respectively. (E) Placodal activity at stage 13. Placodes of pharyngeal arches 1–4 are indicated. The hypoglossal cord reaches pharyngeal arch 2. Adapted from "The development of the neural crest in the human" by O'Rahilly et al., 2007.

In summary, nasal placodes appear in the superficial ectoderm during the 4th week [154]. Nasal placodes emit “pioneer” cells that will give rise to the olfactory neurons as a derivative of the nasal neural crest. Remarkably, the nasal neural crest appears when the cranial neural crest has ceased to form and persists longer than other components (at least to 8th embryo week) of the cranial neural crest. Beyond olfactory neurons, the nasal neural crest provides glial cells for olfactory fibres, ganglionic cells for the vomeronasal and terminalis ganglia, and LHRH progenitors [155] that migrate to and become integrated in the anterior hypothalamus [153].

8. Characterization of stem cell /progenitor populations in the cartilage of the human, embryonic nasal septum: preliminary outcomes 2017-2018

In 2017, thanks to the collaboration with the group of Prof. Ivan Martin at the University of Basel (Switzerland) and the PhD Mobility Programme of the Molecular Medicine PhD course at University of Parma (Italy), our group headed by Prof. Roberto Toni started an experimental study to characterize the developmental phenotype of cells participating to the embryonic formation of the human nasal septum. This, with the long – term aim to clarify the possible contribution of cells from mesodermal, neuroectodermal and, possibly other embryological origins to the morphogenesis of the nasal septal cartilage. In this manner, a map of their topography in the human embryo could be obtained, making feasible an extension of this positioning to the adult human septal cartilage. As a consequence, an anatomical guide to eventual biopsies of the nasal septum *in vivo* could take advantage of different cartilage sites harbouring different types of stem cells / progenitors with potential differences in proliferation and differentiation.

As background for the research, we start from the information about these cells achieved by Basel group in the last five years. In facts, the team headed by Prof. Ivan Martin analysed the expression profile of the Hox genes and the self-renewal and plasticity of the nasal chondrocytes from *in vivo* biopsies. An Hox expression pattern consistent with that of the dental pulp was found, suggesting that nasal chondrocytes are from neural crest origin [156]. As expected for ectomesenchymal cells derived from the neural crest, these Hox-negative cells were found to adopt the Hox expression profile (Hox-positive) of the transplantation site (tibia), leading to robust bone regeneration in mice. Instead, mesoderm-derived "Hox-positive" skeletal stem/ progenitor cells failed to repair bone tissue at "Hox-negative sites like the jaw [157;158]. Finally, nasal chondrocytes were found to be easily accessible from a small biopsy of the nasal septum, with minimal donor site morbidity [156].

Remarkably, these cells showed compatibility and preclinical efficacy for articular cartilage repair much more than native articular chondrocytes. Self-renewal capacity was demonstrated after serial cloning, by the ability of cartilage formation *in vitro*, and ectopically *in vivo*. The environmental plasticity of nasal chondrocytes was monitored by the cells' ability to adapt the molecular HOX expression profile to that of the subcutaneous (human nasal chondrocytes in mice) or articular cartilage (autologous goat cells) environment. The preclinical effectiveness of nasal chondrocytes for articular cartilage repair was tested in a goat model, where tissue-engineered grafts generated by goat nasal chondrocytes or goat articular chondrocytes were implanted into articular defects of 6 mm in diameter, and tissue repair was assessed histologically 3 and 6 months after implantation. This animal trials showed that the implanted nasal cartilage cells were compatible with the knee joint environment [156;159]. These nasal chondrocytes identified for their characteristics of being able to regenerate hyaline-like cartilage tissues, were exploited for a phase I human clinical trial. In this study, patients with

symptomatic, post-traumatic full-thickness cartilage lesions on the femoral condyle or trochlea were treated at the University Hospital of Basel. Initially, chondrocytes isolated from a 6 mm nasal septum biopsy specimen were expanded and cultured onto collagen membranes to engineer cartilage grafts. Then, engineered tissues were implanted into the femoral defects via mini-arthrotomy, and assessed up to 24 months after surgery [159]. This study successfully treated about 20 patients, so that the research has now moved on to a phase II-clinical trial.

AIM OF THE STUDY

My PhD thesis has been carried under the supervision of Prof. Roberto Toni, in the Laboratory of Regenerative Morphology and Bioartificial Structures (RE.MO.BIO.S. lab.) - Unit of Biomedical, Biotechnological, and Translational Sciences - Department of Medicine and Surgery at the University of Parma, Parma, Italy.

The primary aim of my research has been to identify and characterize new sources of adult stem cells suitable for *in vitro* and *ex situ* (i.e. once used for a 3D matrix recellularization) hepatic differentiation. My interest has been focussed on the still poorly investigated differentiation potential of adult ectomesenchymal stem cells (i.e. of neural crest origin) like those expected to be found in the adult thyroid gland and the cartilage of the nasal septum, structures both developmentally contributed by the neural crest. Indeed, preliminary proteomic studies conducted in collaboration with the group of Prof. Stephen Pennington at UCD in Ireland on adult stem cells / progenitors (TSC/P) isolated by the group of Prof. Roberto Toni at UNIPR from the male rat thyroid have shown an heterogeneous protein profile composed by mesodermal, endodermal and neuroectodermal markers. Therefore, using LC-MS/MS SRM and in silico marker sequencing I have planned to confirm the embryological lineage of these TSC/P.

In a second step, I have planned to test two alternative and original protocols of hepatic differentiation to achieve hepatocyte-like features in 2D culture. As an internal control, I have applied the same differentiation procedures to adult male rat bm-MSCs, currently believed a cellular gold standard for *in vitro* hepatic differentiation

Finally, I have focussed my work on the lineage characterization of an innovative source of adult human cells, recently isolated by the group of Prof. Ivan Martin at the University of Basel, in Switzerland. These are adult nasal chondrocytes obtained by *in vivo* surgical sampling, and then *in vitro* de-differentiated. Since these are ectomesenchymal cells with mesenchymal differentiation multipotential, exhibit a number of neural crest markers, and previous collaborative studies between the groups of Prof. Toni and Martin have shown that these same markers can be found in the nasal septum of the human embryo, I have planned to study these and other protein profiles in primary cultures of human nasal chondrocytes with both immunocytochemistry and qualitative mass spectrometry (LC-LIT-Orbitrap XL). To take advantage from my PhD Mobility Program, I have also planned to interact personally with the group of Prof. Martin working in his laboratory at the University of Basel.

I expect that these human cells may represent a new source of adult stem cells suitable for differentiation to human hepatocytes, and become a very innovative tool for regenerative medicine and tissue engineering in disorders of the human liver.

MATERIALS AND METHODS

1. Animals

Sprague Dawley male rats (50-75 gr b.w.) were used as a source for isolation and characterization of both adult thyroid, stem cells and adult bone marrow – mesenchymal stromal cells. Rats were purchased from Charles River Laboratories (Calco, Lecco), and housed in temperature-controlled rooms (22 °C) with a humidity of 50% and a 12:12 hour light-dark cycle, according to the stabulary rules. All animal experimentation has been conducted in accordance with the European Communities Council Directive of 24 November 1986 (86/EEC) and approved by Ethical committees of the University of Parma, Parma, Italy.

2. Rat tail collagen extraction and HPLC-MS analysis

Sprague Dawley male rat (50- 75 gr) tails were taken following sacrifice of the animals for isolation of the thyroid gland cells, and stored at -80°C until use. Tails' collagen was extracted using an original protocol as follows:

- initially, frozen rat tails were immersed in ethanol (EtOH) 70% for 30';
- tendons were isolated using small tweezers under an inverted microscope, and rinsed in phosphate-buffered saline (PBS) 0,1 M;
- tendons were then sterilized by immersion in EtOH 100% for 2-3', then dried and weighted;
- tendons were further solubilized in acetic acid 0,5M in distilled water (dH2O) for 48-72 hours at +4°C in slow agitation;

- the ensuing solution was ultracentrifuged at 14636 x g for 1 hour, at +4°C;

- the supernatant was kept, and pellet containing undigested tendons and debris was discharged;

- the supernatant was ultracentrifuged again at 34957 x g for 45', at +4°C;

- the resulting supernatant was collected, with the presumption to contain a mixture of different collagens, and either sterilized for immediate use, or stored at +4°C for up 1 month.

High Performance Liquid Chromatography-Mass Spectrometry (HPLC-MS) was used to characterize the different types of collagen present in the extraction mixture from the rat tail tendons. The procedure was carried out at the "Centro Misure Giuseppe Casnati", in collaboration with Drs. Andrea Faccini, and Prof. Lisa Elviri, Dept. of Pharmacy, and Dr. Marco Alfieri, RE.MO.BIO.S. - lab –-Unit of Human Anatomy - S.BI.BI.T. Dept., University of Parma, Parma, Italy.

Samples were treated as follows:

- 100 µL of 5% extracted collagen solution was diluted in 100 µL of H_2O / 0.5M acetic acid mixture, to obtain a 2,5% extracted collagen solution;

- pepsin (50 mg / 0,5 mL; Sigma-Aldrich, P0525000) was added in a 1:50 pepsin : protein ratio, to digest the extracted collagen at 37°C for 72h (pH = 2,46)

- digestion was stopped with 1 µL NaOH 30%

- the sample was dried in a stream of nitrogen, then 100 µL of 50:50 H_2O / acetonitrile mixture was added.

Finally, samples were stepwise processed for MS using a LTQ Orbitrap XL (Thermo Scientific) machine, as follows:

- samples were separated by HPLC (Dionex Ultimate 3000, Thermo Scientific) by injecting 5 μL of the unknown solution in a constant flow through the chromatograph;

- then, the different chromatographed samples were ionized by a Ionization Electrospray Source (ESI), located between the HPLC and mass spectrometer;

- ions were then ready to enter the LTQ (Linear Trap Quadrupole) Orbitrap XL, able to select them through a voltage-dependent frame, and according to their m/z ratio. Protein recognition was achieved through the Proteome Discoverer™ software (Version 1.4), comparing the m/z values specific to each ion into the frequency spectrum, with the protein sequences included in Blast database. The search was restricted to the “rat ECM proteins”, with coverage ≥ 20 and score ≥ 10 as acceptable parameters for the proteins found.

3. Cell expansion and collagen coating of culture substrate

Multipotent, adult thyroid stem cells/progenitors, previously isolated and characterized by our group [108;109;110;111;160] were used in all differentiation experiments. Cells were cultured in DMEM Low Glucose (DMEM LG) with 15% serum (10% foetal bovine serum FBS + 5% foetal horse serum FHS) +1% P/S, 1% non-essential amino acids, 1% glutamine, 20μl/100ml gentamicin, and seeded on rat tail collagen-coated coverslips and dishes, at 2000 cells/cm2. Cells were grown in incubator at 37°C, in a 5% CO2 atmosphere for 4 days, up to subconfluence (80% of confluence).

Bone marrow – derived mesenchymal stem cells (bm-MSCs), isolated from adult rat (50 – 75 gr.) using a standard protocol [161], were used in all differentiation experiments. Cells at passage 4 were cultured in DMEM High Glucose (DMEM HG) with 10% serum +1% P/S, 1% non-essential amino acids, 1% glutamine, 20μl/100ml gentamicin, and seeded on rat tail

collagen-coated coverslips and dishes, at 7000 cells/cm2. Cells were grown in incubator at 37°C, in a 5% CO2 atmosphere for 4 days, up to subconfluence (80% of confluence).

About collagen coating of culture substrate, glass coverslips (1,13 cm2 surface) were used to grow and differentiate both thyroid stem cells / progenitors and bm-MSCs. Initially, coverslips were cleaned with ether 2-3 min x 2 times in agitation in a sonicator at xMhz, to eliminate all impurities deposited on the glass surface, and autoclaved at 120°C. A 1% w.v. (gr. of tendons/100ml acetic acid) solution of rat tail collagen was sterilized with chloroform vapours at +4°C overnight: specifically, pure chloroform was taken with a Pasteur pipette in a volume equal to ~10% of the collagen volume to be sterilized. Then, the chloroform was dispensed, passing through the collagen solution with the Pasteur tip, at the bottom of the collagen solution, resulting in two liquid phases, where the tail collagen remained above, and used for coating. Specifically, coverslips were immersed for 3-4 s. for 2 times in the sterile collagen solution, drained and left to dry overnight inside a 24 well plate, under UV light in a laminar flow hood. The third day, coated coverslips were put in a 2% P/S (penicillin / streptomycin) solution containing 40µl / 100ml gentamicin, and kept overnight under UV light. The same technique was applied for coating the bottom of standard, 6 well polystyrene dishes (Euroclone, ET3006) used to differentiate cells for Western Blot analysis. In particular, sterile collagen was put in each well, the excess drained off, and the remaining layer left to dry overnight under UV light in a laminar flow hood, followed by sterilization with P/S and gentamicin.

4. *In silico* analysis of adult rat thyroid stem cells / progenitors

To improve mass spectrometry analysis on adult rat thyroid stem cells / progenitors, an evaluation about endodermal, neuroectodermal and epithelial – mesenchymal transition markers was performed *[Table 3]* using LC-MS/MS SRM technique.

Protein Name	Gene Name
Paired Box 9	PAX9
C-X-C Motif Chemokine Receptor 4	CXCR4
CD117 - KIT Proto-Oncogene Receptor Tyrosine Kinase	c-KIT, KIT
Epithelial Cell Adhesion Molecule	EPCAM
T-Box 1	TBX1
GATA Binding Protein 4	GATA4
Hepatocyte Nuclear Factor 4 Alpha	HNF4A
Forkhead Box A2	FOXA2, HNF3B

Protein Name	Gene Name
Tubulin beta-3	TUBB3
Nestin	NES
DIX Domain Containing 1	DIXDC1
CD34 - CD34 Molecole	CD34
Homeobox C5	HOXC5 (debole)
Homeobox A2	HOXA2 (+)
Homeobox A3	HOXA3 (+)
Homeobox B4	HOXB4 (+)
Wnt Family Member 1	WNT1
SRY-Box 10	SOX10
Chromogranin A	CHGA
Notch 1	NOTCH1
Musashi RNA Binding Protein 1	MSI1
CD271 - Nerve Growth Factor Receptor	P75, NGFR

Protein Name	Gene Name
Atlastin GTPase 1	ATL1, FSP1
Serpin Family H Member 1	SERPINH1, HSP47 (increase)
Collagen Type I Alpha 1 Chain	COL1A1 (increase)
Collagen Type II Alpha 1 Chain	COL2A1 (increase)
Snail Family	SNAIL
Slug Family	SLUG
Twist Family	TWIST
BARX Homeobox 1	BARX1 (+)

Table 3: List of markers investigated through triple quadrupole mass spectrometry in silico analysis. In blue there are the endodermal markers, in green the neuroectodermal markers and in yellow the epithelial – mesenchymal transition markers.

In fact, the expression of these markers was very low in cell populations, also for the detection with an orbitrap investigation (considering that the weak signal is covered by the stronger ones). Triple quadrupole mass spectrometer permits to examine exactly what you are looking for, entering the exact mass/charge ratio (m/z) values of the investigated protein. In this technique, a peptide of known m/z is selected in the first quadrupole, fragmented in the second quadrupole, and monitored over time in the third quadrupole in a method called single reaction monitoring (SRM) or multiple reaction monitoring (MRM) [162]. *In silico* analysis was carried out to obtain the value of m/z ratio, as follow:

- Find the protein sequence through Uniprot protein online database (https://www.uniprot.org/)

- Put the identify code of protein sequence in a program that simulate the proteolytic cleavage of selected enzyme, as Agilent Spectrum Mill - Peptide Selector (http://128.255.119.18/millhtml/mssluice.htm)
- Insert the parameters for the simulation, like type of enzyme, database and precursor ion length
- Start the simulation.

The resulted m/z ratio was used to set up the triple quadrupole mass spectrometer in order to obtain information about the presence and the quantity of investigated protein.

LC separation has been carried out on a Agilent Poroshell 120 C18 column (75x2.1 mm, 2.7 µm), thermostated at 25°C using a gradient solvent elution system [(A) aqueous FA 0.1% solution (v/v)/(B) 0.08% (v/v) FA in AcN] delivered at 0.2 ml/min under gradient elution. The mobile phase was delivered by the Agilent HP 1260 chromatographic system (Agilent Technologies, USA) equipped with a 200-vial capacity sample tray. Injection volume was 5 µl and the concentration of each collagen standard was 1 µg/µl. A QTRAP 4000 triple quadrupole instrument (ASCIEX) equipped with a pneumatically assisted ESI interface has been used. The system was controlled by the Analyst v 1.4 software. The sheath gas (nitrogen, 99.999% purity) and the auxiliary gas (nitrogen, 99.998% purity) were delivered at flow-rates of 45 and 5 arbitrary unit, respectively. ESI conditions were set as follows: voltage 4.5 kV, capillary voltage 50 V, capillary temperature 350°C. MS/MS experiments were performed under SRM conditions with a collision gas (N_2) pressure of 2.1 × 10-3 mbar in the collision cell. The analysis was performed thanks to the collaboration with Prof. Lisa Elviri, Food and Drug Department, University of Parma (Parma).

5. Protocols for hepatic differentiation

Hepatic differentiation protocols were tested on both adult rat thyroid stem cells/progenitors and adult rat bm-MSCs at subconfluence. Cells used for immunocytochemical, histochemical, histological, and SEM analysis were seeded on rat tail collagen-coated, glass coverslips accommodated inside 24 multiwell dishes. In contrast, cells used for Western Blot analysis were seeded on rat tail collagen-coated, 6 multiwell dishes. Two different and original protocols were used, both based on different growth factors, different morphogens concentrations, and different timing of administration. Specifically, cells were cultured as follows:

Protocol 1:

- days 1 -14 : DMEM High Glucose (DMEM HG) containing 10% FBS plus 1% plus P/S, 1% non-essential AA, 1% Glutamine, 20µl / 100mL gentamicin, HGF (20ng/mL)(Recombinant Human HGF, PeproTech, 100-39), EGF (20ng/ml)(Recombinant Human EGF, PeproTech, AF-100-15) and FGF-2 (10ng/mL)(Recombinant Human FGF-basic, PeproTech, 100-18B);
- days 15 - 30: HGF (20ng/mL), OSM (20ng/mL)(Recombinant Human Oncostatin M, PeproTech, 300-10), NTA (50µg/mL)(Nicotinamide, Sigma-Aldrich, N0639) ,and Dex (10µM)(Dexamethasone, Sigma-Aldrich, D4902).

Control cells were treated with DMEM HG plus 10% FBS

Protocol 2:

- day 1: DMEM LG plus 1% P/S, 1% Glutamine, 20µl / 100ml gentamicin, without serum;
- days 2 - 3: DMEM LG with 2% FBS plus Activin A (50ng/mL)(Recombinant Human/Murine/Rat Activin A (E. Coli derived), PeproTech, 120-14E) and FGF-2 (10ng/mL);

- days 4 - 10: DMEM LG with 2% FBS, plus HGF (50ng/mL), OSM (20ng/mL), bFGF (30ng/mL), Insulin (10µg/mL)(Insulin from Bovine Pancreas, Sigma-Aldrich, 15500), Transferrin (5,5µg/mL)(Transferrin Human, Sigma-Aldrich, T8158), NTA (598µg/mL);
- days 11 - 24: DMEM LG with 2% FBS, added with HGF (40ng/mL), OSM (10ng/mL), EGF (20ng/mL), Insulin (10µg/mL), Transferrin (5,5µg/mL), and Dexametasone (1µM).

Control cells were cultured with DMEM LG plus 2% FBS.

Mediums were changed every 3-4 days, and both differentiated and control cells were stopped at different time points, chosen on the presumption of having reached each time a specific step of the rat liver organogenesis:

protocol 1: check at days 3, 7, 10, 15, 19, 30 considering

- mesodermal induction and hepatoblast phase: days 1-14
- hepatocyte phase: days 15-30

protocol 2: check at days 3, 7, 10, 15, 19, 24 considering

- mesodermal induction; days 1-3
- hepatoblast phase; day 4-10
- hapatocyte phase: days 15-24

For each time point and in each protocol, 6-8 replicas were prepared.

At the end of the differentiation period:

- cultures to be analysed by immunocytochemistry, histochemistry, histological staining, and SEM were rinsed with PBS 0,1 M (pH 7.4), then fixed in paraformaldehyde 4%, and stored into glycerol at -20°C until use;
- cultures to be analysed by Western Blot, were rinsed with PBS 0,1 M (pH 7.4), detached with trypsin 0,05% in EDTA (Euroclone, ECB3052), cells counted with the Trypan Blue exclusion

method in a Burker chamber, spun down at 272g for 10 min, and the pellets were dried, to be stored at -20°C until use.

6. Immunocytochemistry (IC)

Markers of hepatic differentiation were visualized using a well – established IC procedure as follows:

protocol 1: check HNF-3β, AFP, CK-18, CK-19, and ALB at days 3, 7, 10, 15, 19, 30

protocol 2: check HNF-3β, AFP, CK-18, CK-19, and ALB at days 3, 7, 10, 15, 19, 24.

Incubation procedure goes on for two days and consists in these steps:

Day 1

-wash with PBS 0,1M 2 times for 10’ at room temperature (RT) in agitation

-permeabilize with 0,05% Triton X100 for 5’ RT in agitation

-wash with PBS 0,1M 2 times for 5’ RT in agitation

-incubate into hydrogen peroxide (3% in PBS 0,1M) for 30’ RT

-wash with PBS 0,1M 2 times for 5’ RT in agitation

-incubate with Polypep 5% for 15’ RT in agitation

-wash with PBS 0,1M 2 times for 5’ RT in agitation

-incubate with primary antibody: rabbit anti-ALB 1:1000 (Sigma-Aldrich, SAB2100098); mouse anti-CK 1:500 (Sigma-Aldrich, C2562); rabbit anti-AFP 1:500 (Sigma-Aldrich, SAB3500533); mouse anti-HNF-3β 1:100 (Santa Cruz Biothecnology, 374375), all diluted in PBS/BSA 2%, overnight at +4°C in a humidified chamber.

Day 2

-wash with PBS 0,1M 2 times for 10’ RT in agitation

-incubate with biotinylated anti-mouse (Sigma-Aldrich, A4416) or anti-rabbit (Thermo Fisher, 31460) secondary antibody 1:200 in PBS 0,1M for 2 hours RT

-wash in PBS 0,1M 2 times for 10’ RT in agitation

-incubate with ABC complex (1A:1B:50PBS, prepared 45’ before the use, as manufacturer’s instructions) for 30’ RT in a humidified chamber (VECTASTAIN®UNIVERSAL (anti mouse IgG/rabbit IgG) Elite ABC Kit, VECTOR LABORATORIES, PK-6200)

-wash in TBS 1X (0,05M) 2 times for 15’ RT in agitation

-incubate with DAB (3,3'-Diaminobenzidine Tetrahydrochloride, 10000TBS:100DAB:10H2O2 30%) for 4’ RT in agitation in the dark (Sigma-Aldrich, D5637)

-wash with TBS 1X 2 times for 5’ RT in agitation to eliminate DAB

-wash for 1-2’ in dH2O RT

-counterstain with Mayer’s Haematoxylin 2-5’ or Eosin 6-7’ RT (protect from light). For some samples, aqueous mounting solution DAPI-DABCO were employed to counterstain the nuclei in light blue (in this case, samples were directly mounted using DAPI-DABCO and stored at -20°C protected from light).

-dehydrate in alcohol 80% for 20’’, alcohol 96% 2 times for 20’’each (change the alcohol between the first and second times), and alcohol 100% 2 times for 20’’ each (change the alcohol between the first and second times)

-clarify in xylene 2 times for 20’’-30’’ each, changing the xylene between the first and second passage

-mount with Pertex® and store at RT.

7. Histochemistry and histologic stainings

Periodic acid–Schiff (PAS) staining

Glycogen biosynthesis and storage was assessed using the periodic acid-Schiff (PAS) reaction, as follows:

-wash dishes with dH_2O RT for 5 minutes in agitation

-place dishes into periodic acid (HIO_4) 1% for 7'

-rinse in running tap water for 2'-3' RT

-wash with dH_2O for 30''-1' RT

-immerse dishes in filtered Schiff's solution for 45' RT in the dark

-rinse in running tap water for 2'-3' RT

-wash with dH_2O for 30''-1' RT

At this point, we use hematoxylin protocol to bring out the nuclei:

-stain with Hematoxylin for 1' RT in the dark

-rinse in running tap water up to the complete loss of colour of the H_2O

-wash 30''-1' with dH_2O RT

-dehydrate in alcohol 80% for 20''→ alcohol 96% 2 times for 20''each (change the alcohol between the first and second times) → alcohol 100% 2 times for 20'' each (change the alcohol between the first and second times)

-clarify in xylene 2 times for 20''-30'' each, changing the xylene between the first and second passage

-mount with Pertex® and store at RT.

Hematoxylin and Eosin (HeE)

Morphology of differentiated cells was analyzed at the light microscopic level (Zeiss Axiophot) using the contrast interference technique (Normasky optic) and the standard histological staining HeE. Images were elaborated using the imaging software AxioVision 4.8.

Method:

-wash dishes 30''-1' in dH_2O RT

-stain with filtered hematoxylin 1' RT in the dark

-rinse in running tap water up to the complete loss of colour

-wash 30''-1' in distilled dH_2O RT

-stain with filtered eosin Y 1% not acidified for 7' RT in the dark

-rinse in dH_2O up to the complete loss of colour

-dehydrate in alcohol 80% for 20''→ alcohol 96% 2 times for 20''each (change the alcohol between the first and second times) → alcohol 100% 2 times for 20'' each (change the alcohol between the first and second times)

-clarify in Xylene 2 times for 20''-30'' each, changing the xylene between the first and second passage

-mount with Pertex® and store at RT.

8. Scanning electron microscopy (SEM) analysis

Morphological changes of differentiated cells were further investigated using SEM on cell cultures at the beginning (day 3) and end (days 30 or 24) of the differentiation protocols. Cultures were fixed with paraformaldehyde 4% and dehydrated as follows:

-rinse dishes in dH_2O and start the dehydration process:

-3 times ethanol 30% for 20’

-3 times ethanol 50% for 20‘

-3 times ethanol 70% for 20’

-3 times ethanol 90% for 20’

Samples were then transferred to 100% ethanol, and subjected to critical point drying. Specimens were then mounted on aluminium stubs, and metallized for 90 s with a mixture of 60 nm, gold/palladium particles, using a sputter coating technique. Then, samples were observed with a Philips SEM501.

9. Western Blot analysis

Expression of HNF-3β, AFP, and ALB during hepatic differentiation were quantified only for protocol 1 of adult thyroid stem cells/progenitors, using Western Blot analysis at days 3, 15 and 30. The human hepatic carcinoma cell line, Hep G2 (ATCC® HB-8065™) and rat liver extracts were used as controls.

Sample preparation:

-place pelleted cells tubes on ice and add ice-cold RIPA lysis buffer (150 mM NaCl, 10 mM Tris-HCl ph7,4, 1 mM EDTA, 0,1% SDS, 0,5% Sodium deoxycholate, 1% Triton x-100): 200 µL for pellet with 2-3 million cells, 70 µL for pellet with 0,7-1 million cells.

-sonicate in ice 3 times for 20''-30'' each

-centrifugate at 4°C 16500 g for 6'

-discard cell debris pellet and transfer supernatant in a new tube

Protein Quantitation Assay: Pierce® BCA Protein Assay Kit (Thermo Scientific)

-mix 50 parts of BCA reagent A with 1 part of BCA reagent B (working solution), following the kit instructions

-prepare the diluted bovine serum albumin (BSA) standards by mixing BSA in the working solution; use dilutions 1:2 to construct a BSA calibration curve: 2000→1000→500→250→125→62,5→0 µg/ml

-put 25 µL of each BSA standard replicate into a 96 wells plate flat bottom

-put 25 µL of each sample replicate (make at least 3 replica) into the same 96 wells plate

-add 200 µL of the working solution to each wells and mix

-place in agitation for 30'' to eliminate air bubbles

-cover with Parafilm® and incubate in incubator at 37°C and 5% CO_2 for 30'

-read plate absorbance at λ=562 nm by using the program Wallac 1420 on VICTOR™ instrument (Plate Reader from PerkinElmer): the amount of protein is directly proportional to the amount of detected OD (optical density).

-determine the protein concentration of samples using the BSA calibration curve, through the straight line equation from points of BSA interpolation.

Denaturation of samples

-add sample buffer (SB) to each sample, by working in ice (sample buffer 2X composition: 2,5 mL Tris-HCl ph 6,8 (0,5 M), 2 mL glycerol, 0,4 g SDS, 0,1 mg bromophenol blue, 0,2 mL β-mercaptoethanol, add water until 10 mL and store at -20°C)

-if the protein concentration of sample is greater than 4 µg/µL use the SB 2X in 1:1 ratio; if the concentration is less than 4 µg/µL, use the SB 4X in 4:1 ratio

-boil all samples with simple buffer for 6' to complete the denaturation process.

Loading and running the gel

-load equal amounts of protein for each sample (70 µg) and controls tissue/cell into the wells of the SDS-PAGE gel (Mini-Protean® TG X™ Gels, BIO-RAD, 456-1093), along with molecular weight marker (Precision Plus Protein™ Dual Color Standard, BIO-RAD, 161-0374)

-run the gel for 1-2 h at 100-120 V, immersed in running buffer (running buffer 10X composition: trizma basic 30 g, glycine 144 g, add dH_2O until 1 L; at the use: 100 mL running buffer 10X, 10 mL Sodium Dodecyl Sulphate (SDS) 10%, add dH_2O until 1 L).

Transfer of proteins from the gel to the nitrocellulose membrane

-place the gel in contact with a nitrocellulose membrane, to assembly the sandwich, making sure that no air bubbles are trapped

-place the cassette in the transfer tank in 1X transfer buffer, then transfer overnight at +4°C, at a constant current of 34-35 V (transfer buffer 5X composition: trizma base 15 g, glycine 120 g, dH_2O until 1 L; at the use add 200 mL of methanol to 200 mL of transfer buffer 5X, and , dH_2O until 1 L)

-to verify the effective transfer, wash in dH_2O for 2-3', then colour the membrane with Ponceau S for 1-2' until the bands are seen.

Immunoblotting

-wash the membrane 3-4 times for 3-5' each in dH_2O, next in PBS-tween-20 0,1% RT in agitation, until the Ponceau S disappear

-saturate in BSA 5% in PBS-tween-20 0,1% for 60' RT in agitation

-incubate in slow agitation with primary antibody, diluted in PBS-tween-20 0,1% at +4°C overnight (rabbit anti-ALB 1:10000 (Sigma-Aldrich, SAB2100098); rabbit anti-AFP 1:5000 (Sigma-Aldrich, SAB3500533); mouse anti-Hnf-3β 1:1000 (374375)); we have used β-Actin (Mouse monoclonal anti-β-Actin 1:5000, Sigma-Aldrich, A5441) diluted in BSA 5% in PBS-tween-20 0,1%, as control protein, and incubation was performed in slow agitation RT for 30'

-wash membrane 3 times for 10' in PBS-tween-20 0,1% RT in agitation

-incubate with secondary antibody in slow agitation RT for 60' (anti-mouse-HRP 1:2000 (Sigma-Aldrich, A4416) and anti-rabbit-HRP 1:2000 (Thermo Fisher, 31460), both diluted in PBS-tween-20 0,1%)

-wash 3 times for 10' in PBS-tween-20 0,1% RT in agitation

-apply the chemiluminescent substrate to the membrane: incubate with ECL standard (mix 1:1 reagent A and reagent B) for 4' RT in the dark (Thermo Scientific, 34080), or with ECL ultra (mix 1:1 reagent A and reagent B, then dilute the mixture 1:1 in dH_2O) for 1' RT in the dark (Perkin Elmer, NEL112001EA)

-impress and develop the film by using darkroom development techniques for chemiluminescence.

Densitometric analysis and quantitation of immunoreactions product

-scan the film impressed into the dark room, at 300 dpi resolution and in a grey scale

-use image analysis softwares (e.g. Photoshop or Gimp 2) to improve the image quality

-import the image in Image J software, then select the band corresponding to each specific marker: the software is able to calculate the Optical Density (OD) of each bands, expressed as an area of each specific peak generated.

-normalize the target protein OD value by using the loading control protein (β-Actin) OD, for both differentiated and control group of each time analysed

-calculate the OD difference between differentiated and control group for each time

-use the difference calculated to obtain a percentage of increase or decrease in differentiated cells with respect to controls, for each expressed marker in each time considered.

10. Nasal chondrocytes culture method and expansion

Primary cells used in this project were made available by Prof. Ivan Martin, Department of Surgery and Biomedicine, Laboratory of Tissue Engineering, University Hospital, Basel, Switzerland as collaborative project. We used three different cellular type from different donor and for different study line: NC (101,176, 183, P0), BM (253, 270) *[Table 4]*.

Code	Gender	Age	Donor	Institute/Hospital	Date of tissue biopsy collection
NC101	Male	75y	cadaver	IPB*	10.02.2009
NC176	Male	67y	patient	UHB°	06.11.2015
NC183	Female	49y	patient	UHB°	23.03.2016
BM253	Female	49y	patient	UHB°	25.11.2016
BM270	Female	52y	patient	UHB°	27.06.2018

Table 4: Donor specifications of the cell strains used in this analysis.

**IPB: Instititute of Pathology, Basel. Samples were collected with 24-hour post-mortem*

°UHB: University-Hospital Basel. Fresh samples collected during the surgery.

NC cells were human nasal chondrocytes harvested from biopsy of the nasal septum of three different donor, in accordance with the local ethics committee. NC P0 instead were cell culture derived from NC 101 that were expanded for 2 weeks in chondrogenic direction with appropriate medium *[Table 5]*, trying to mimic the condition of primary nasal cartilage biopsy cultures *[Figure 14]*.

Basic Serum Free Medium		
PSG (Penicillin-Streptomycin Glutammine)	1%	Gibco 10378-16 (Thermo Fisher Scientific, Waltham, MA, USA)
Sodium Pyruvate	1%	Gibco 11360-039 (Thermo Fisher Scientific, Waltham, MA, USA)
Hepes buffer (1M)	1%	Gibco 15630-056 (Thermo Fisher Scientific, Waltham, MA, USA)
HSA 100x (Human Serum Albumin)	1%	43075 (CSL Behring, Pennsylvania, PA, USA)
ITS-A (Insulin-Transferrin-Selenium-Sodium Pyruvate)	1%	Gibco 51300-044 (Thermo Fisher Scientific, Waltham, MA, USA)
Linoleic Acid	0,56%	62240 (Sigma-Aldrich, St. Louis, MO, USA)
DMEM High glucose 4.5%, NEAA, no glutammine	94,44%	Gibco 10938-25 (Thermo Fisher Scientific, Waltham, MA, USA)
Additional supplements for chondrogenic medium		
Ascorbic acid 2-Phosphate (AA) 0.1 mM	0.1 mM	A-8960 (Sigma-Aldrich, St. Louis, MO, USA)
Dexamethasone 10-5 M (Dex)	10-4 mM	D-2915 (Sigma-Aldrich, St. Louis, MO, USA)
TGFβ3	10 ng / mL	TGFB3- (Novartis International AG, Basel, Switzerland)

Table 5: Specification for chondrogenic medium (CHM) starting from basic serum free medium.

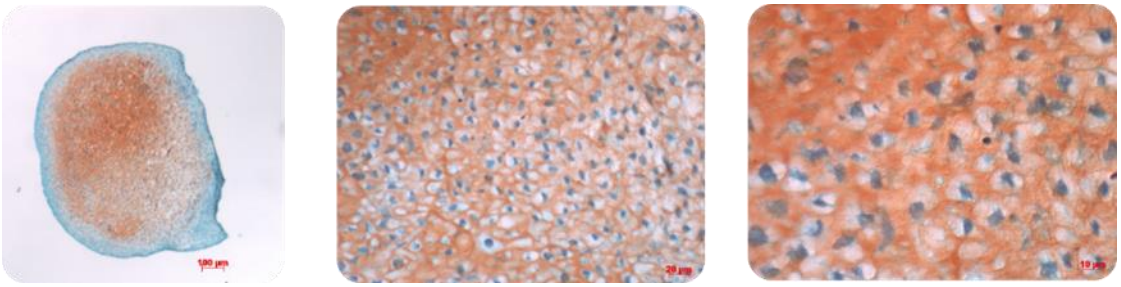

Figure 14: Safranin-O staining for nasal chondrocytes differentiated in pellets. In red the collagen II and the glycosaminoglycans were stained, while in blue the collagen I and the cytoplasm.

BM were human bone marrow stromal cells obtained during routine orthopaedic surgical procedures involving exposure of the iliac crest, after informed consent. BM cells were used as a control to test difference with NC cells in considered markers expression profile.

NC cells were isolated by 22 hours of incubation at 37°C in 0.15% type II collagenase, following the protocol described by Candrian et al., 2008 [163], while BM cells were isolated using a density gradient solution, as described by Frank et al., 2002 [164]. After isolation, the cells were counted, and several pellets were made frozen in liquid nitrogen and subsequently thawed for analysis.

All culture work was carried out using standard aseptic techniques, unless otherwise specified. Different types of basic growth media have been used for cell manipulations. Dulbecco's Modified Eagle Medium (DMEM) for chondrocytes *[Table 6]*, while Minimum Essential Medium Eagle Alpha (α-MEM) for bone marrow stromal cells *[Table 7]*.

Dulbecco's Modified Eagle's Medium (DMEM) Complete Medium		
Basic for culture defrost and manipulation		
DMEM High glucose 4.5%, NEAA, no glutammine	87%	Gibco 10938-25 (Thermo Fisher Scientific, Waltham, MA, USA)
FBS (Fetal Bovine Serum)	10%	Gibco 102701-06 (Thermo Fisher Scientific, Waltham, MA, USA)
Hepes buffer (1M)	1%	Gibco 15630-056 (Thermo Fisher Scientific, Waltham, MA, USA)
PSG (Penicillin-Streptomycin Glutammine)	1%	Gibco 10378-16 (Thermo Fisher Scientific, Waltham, MA, USA)
Sodium Pyruvate	1%	Gibco 11360-039 (Thermo Fisher Scientific, Waltham, MA, USA)
Additional supplements for expansion		
TGFβ-1	1 ng / mL	240B0-10 (R&D Systems, Minneapolis, USA)
FGF-2	5 ng / mL	233-FB-025 (R&D Systems, Minneapolis, USA)

Table 6: Specification for Dulbecco's Modified Eagle's Medium (DMEM) culture complete.

Minimum Essential Medium Eagle - alpha modification (α-MEM) Complete Medium		
Basic for culture defrost and manipulation		
α-MEM with ribonucleotides and deoxyribonucleosides	87%	Gibco 22571-020 (Thermo Fisher Scientific, Waltham, MA, USA)
FBS (Fetal Bovine Serum)	10%	Gibco 102701-06 (Thermo Fisher Scientific, Waltham, MA, USA)
Hepes buffer (1M)	1%	Gibco 15630-056 (Thermo Fisher Scientific, Waltham, MA, USA)
PSG (Penicillin-Streptomycin Glutammine)	1%	Gibco 10378-16 (Thermo Fisher Scientific, Waltham, MA, USA)
Sodium Pyruvate	1%	Gibco 11360-039 (Thermo Fisher Scientific, Waltham, MA, USA)
Additional supplements for expansion		
FGF-2	5 ng / mL	233-FB-025 (R&D Systems, Minneapolis, USA)

Table 7: Specification for Minimum Essential Medium Eagle - alpha modification (α-MEM).

Before characterizing these cells through cytofluorimetric analysis, cell expansion and passage were performed to increase number of proliferating cells in their living space. Subsequently, once they arrived at sub-confluence, the cells were collected and utilized for analysis. The procedure of expansion was carried out as follows:

Calculate the volume of cell suspension;

- Resuspend the cells in medium containing the appropriate growth factors;
- Seed uniformly the cell suspension in the appropriate T150 flasks (90150 VENT, TPP Techno Plastic Products, Trasadingen, Switzerland);
- Incubate the cells in an air-incubator (Heracell 150, Thermo Fisher Scientific, Waltham, MA, USA) under 5% CO2 at 37°C;
- Change media twice a week and detach them until they are sub-confluent.

Instead, the cell collection procedure was as follows:

- Remove old medium from culture flask and wash the cells briefly with 10 mL of phosphate buffered saline (PBS, 20012-068, Gibco, Thermo Fisher Scientific, Waltham, MA, USA);
- Add 5 mL of trypsin, then incubate the cells with trypsin, for 5 minutes in an air-incubator at 37°C and 5 % CO2;
- After incubation, check the cells to ensure full release from the culture flask;
- Quench trypsin with 20 mL of complete medium and spin-down the total volume at 1500 rpm for 3 minutes;
- Discard the supernatant and resuspend the pellet in an adequate volume of complete medium.

11. Immunocytochemistry for human nasal chondrocytes

To check the presence of both neuroectodermal and primitive mesoderm markers in expanded human nasal chondrocytes, an immunocytochemistry analysis was performed *[Table 8]*.

	Definitive markers list	Description
1	SOX10	neural crest markers
2	MSX1	
3	NESTIN	
4	NOTCH1	
5	SOX2	
6	WNT1	
8	Neuron Specific Enolase (NSE)	
9	Musashi1 (MSI1)	
10	p75	
11	DIX Domain Containing 1 (DIXDC1)	positive regulator of the Wnt/β-catenin pathway highly expressed in neural crest-derived tissues
12	Brachyury (T)	Primitive endoderm marker

Table 8: Neural crest and primitive mesoderm markers for IC of human nasal chondrocytes.

In particular:

- Rinse with buffer PBS 1x 2 times for 10’ in agitation
- Permeabilize with Triton X100 (0,05% in PBS) for 5’ RT in slow agitation
- Rinse with buffer PBS 1x 2 times for 5’
- Blocking solution with serum (3% with 0,3% Tween 20 in PBS) from the animal origin corresponding to the secondary antibody for 30’ RT
- Rinse with buffer PBS 1x 2 times for 5’
- Primary antibody overnight at 4°C or 2h at RT (humid chamber):
    - BRACHYURY (rabbit) 1:100 in blocking solution
    - Sox2 (rabbit) 1:100 in blocking solution
    - MSX1 (goat) 1:400 in blocking solution
    - NSE (mouse) 1:1000 in blocking solution

- DIXDC1 (goat) 1:13 in blocking solution
- WNT1 (rabbit) 1:50 in blocking solution
- NESTIN (rabbit) 1:50 in blocking solution
- Sox10 (goat) 1:50 in blocking solution
- P75 (rabbit) 1:200 in blocking solution
- NOTCH (rabbit) 1:200 in blocking solution
- MSI1 (rabbit) 1:250 in blocking solution

- Rinse with buffer PBS 1x 2 times for 10'
- Secondary antibody 60-70' at RT in a humid chamber:
    - Goat Anti-Rabbit 1:300 in blocking solution
    - Rabbit Anti-Goat 1:200 in blocking solution
    - Goat Anti-Mouse 1:200 in blocking solution
- Rinse with buffer PBS 1x 2 times for 10'
- Vectastain ABC / AP complex Kit (Linaris AK-5000) for 45' at RT in a humid chamber (1ml PBS + 10µl A solution + 10µl B solution; prepare the complex 30 min before use and store at 4°C).
- Rinse with buffer TBS° 1x 2 times for 10'
- Vector Red Alcaline phosphatase substrate kit + Levamisole (Linaris SK-5100) for 1-30' (5ml Tris pH 8.25 + 2 drop of Reagent 1 + 2 drop of Reagent 2 + 2 drop of Reagent 3 + 1 drops of Levamisole). The staining is developing better in the dark.
- Rinse with buffer TBS° 1x for 1'
- Rinse with tap water for 1'
- Counterstain the nuclei with haematoxylin for 30 – 40''

- Rinse with tap water until it is clean
- Dehydrate with ethanol 70%, ethanol 95%, ethanol 100%, xylol I and xylol II
- Apply the Pertex mounting medium.

As controls, we used positive controls (to check the efficiency of each antibody dilution), adult human septal cartilage (“native cartilage”, to compare the expression of expanded nasal chondrocytes with adult cartilage), and human embryos (7th week of gestational age) from the collection of the University Museum of Biomedicine - BIOMED (Scientific Director, Prof. Dott. Roberto Toni) in Parma (to confront the expression pattern of the neural crest and primitive mesoderm markers between embryo and expanded nasal chondrocytes).

12. Flow cytometry for characterize nasal chondrocytes

Flow cytometry is a technology that simultaneously measures and then analyzes multiple physical characteristics of single particles, usually cells, as they flow in a fluid stream through a beam of light. The properties measured include a particle’s relative size, relative granularity or internal complexity, and relative fluorescence intensity. These characteristics are determined using an optical-to-electronic coupling system that records how the cell or particle scatters incident laser light and emits fluorescence.

In this study different protocols were used, alternating direct cytometry, in which the primary antibody is directly conjugated to a fluorescent tracer *[Table 9]*, to the indirect antibody (which uses the secondary antibody bound to a fluorescent dye) *[Table 10]* and using surface and intracellular antibodies (which need different buffers) in combined-mode (surface and intracellular) analysis. The protocols used, collected in a single, are presented below.

PRIMARY ANTIBODY	CLONE	FLUOROCHROME	DILUTION	TARGET	SOURCES
Brachyury	Rabbit	Unconjugated	1:200	Nucleus	ab209665 (Abcam, Cambridge, UK)
Lgr-5	Mouse	DyLight 488	1:10	Membrane	TA400002 (OriGene Technologies, Inc, Rockville, USA)
SSEA-4	Mouse	FITC	1:80	Membrane	FAB1435F (R&D Systems, Minneapolis, USA)
SSEA-4	Mouse	APC	1:80	Membrane	FAB1435A (R&D Systems, Minneapolis, USA)
FoxF1	Rabbit	Unconjugated	1:1000	Nucleus	ab168383 (Abcam, Cambridge, UK)
P75	Mouse	APC	1:50	Membrane	345107 (BioLegend, San Diego, USA)
Dixdc1	Goat	Unconjugated	1:20	Cytoplasm	PA5-48086 (Thermo Fisher Scientific, Waltham, MA, USA)
Nestin	Mouse	PE	1:50	Cytoplasm	561230 (BD Biosciences, Franklin Lakes, USA)
FoxD3	Rabbit	Unconjugated	1:100	Nucleus	ab64807 (Abcam, Cambridge, UK)

Table 9: Sources, fluorochromes, dilution and condition of the primary antibodies used in this study.

Specification for fluorochromes: FITC= Fluorescein isothiocyanate; APC=Allophycocyanin; PE= Phycoerythrin; Unconjugated= Antibody requires a conjugated secondary antibody.

SECONDARY ANTIBODY	CLONE	FLUOCORHROME	DILUTION	SOURCERS
Donkey-Anti-Rabbit	Donkey	FITC	1:1000	ab6798 (Abcam, Cambridge, UK)
Donkey-Anti-Rabbit	Donkey	Alexa 568	1:1000	a10040
Rabbit-Anti-Goat	Rabbit	Alexa 488	1:1000	A21222
Donkey-Anti-Mouse	Donkey	Alexa 488	1:100	A4416 (Sigma-Aldrich, St. Louis, MO, USA)

Table 10: Sources, fluorochromes, dilution and condition of the secondary antibodies used in flow cytometry for the primary unconjugated antibody.

Specification for fluorochromes: FITC= Fluorescein isothiocyanate.

Flow Cytometry Protocol

1. Collect cells;
2. Centrifuge cells (at 1500 rpm for 3 minutes) and resuspend in an appropriate volume of Flow Cytometry Staining Buffer (PBS + 0.1% HSA + 2 mM EDTA) so that the final cell concentration is 5 x 106 cells/mL;
3. Aliquot 50 µL of cell suspension (250.000) to each well.
    - Note: Proceed to Step 15 if all membrane primary antibodies were directly conjugated to fluorochromes. For Nestin-PE proceed until step 10. Resuspend in 50 µL 1X Permeabilization Buffer (1:10 stock solution 10X in sterile dH2O, 00-8333-56 eBioscience, Thermo Fisher Scientific, Waltham, MA, USA). Proceed to Step 15;
4. Stain cell surface markers;
5. Centrifuge cells at room temperature. Discard the supernatant;
6. Add 200 µL of Foxp3 Fixation/Permeabilization (3 diluent buffer + 1 Permeabilization, 00-5521-00 Invitrogen, Thermo Fisher Scientific, Waltham, MA, USA) working solution to each well. Pipetting;
7. Incubate for 45 minutes on ice. Protect from light;
8. Centrifuge at room temperature. Discard the supernatant;
9. Add 200 µL 1X Permeabilization Buffer to each well. Pipetting. Centrifuge at room temperature. Discard the supernatant;
10. Repeat Step 9;
    - Note: For Nestin-PE. Resuspend in 50 µL 1X Permeabilization Buffer. Proceed to Step 15;
11. Combine the recommended quantity of each primary antibody in an appropriate volume of 1X Permeabilization Buffer so that the final staining volume is 100 µL. Pipetting;

12. Incubate for 60 minutes on ice. Protect from light;
13. Add 200 µL of 1X Permeabilization Buffer to each well and centrifuge samples at room temperature. Discard the supernatant;
14. Repeat Step 13;
15. 15.
    - Dilute the appropriate fluorochrome-labeled secondary reagent in 100 µL of 1X Permeabilization Buffer and add to the cells. Pipetting to mix. Incubate for at least 30 minutes on ice. Protect from light.
    - Primary antibodies directly conjugated to fluorochromes: Combine the recommended quantity of each primary antibody in an appropriate volume of Flow Cytometry Staining Buffer (or Permeabilization Buffer for Nestin-PE) so that the final staining volume is 100 µL (i.e. 50 µL of cell sample + 50 µL of antibody mix => concentrate antibodies aliquots two times) and add to cells. Pipetting to mix. Incubate for 60 minutes on ice. Protect from light;
16. Add 200 µL of 1X Permeabilization Buffer / Flow Cytometry Staining Buffer to each well;
17. Centrifuge at room temperature. Discard the supernatant;
18. Add 200 µL of 1X Permeabilization Buffer / Flow Cytometry Staining Buffer to each well and centrifuge at room temperature. Discard the supernatant;
19. Resuspend stained cells in 150 µL of Flow Cytometry Staining Buffer;
20. Analyze by flow cytometer.

Stainings for flow cytometry were performed as described, using unstained controls (only cells without antibody, to check their autofluorescence), isotype controls (an antibody provides with the staining kit, to verify antibody aspecific bonds) and fluorescence minus one controls (a specific control for each fluorochrome utilized, which permits the best gates placement during

the following software analysis, during a combined-mode experiment). Cells were acquired with CytoFLEX (Beckman Coulter, Pasadena, CA, USA), previewed with CytExpert Software (Beckman Coulter, Pasadena, CA, USA) and analyzed using FlowJo 9.3.2 Software (FlowJo LLC, Ashland, OR, USA).

13. Mass spectrometry analysis

Mass spectrometry (MS) is an analytical technique that measures the mass-to-charge ratio of ions derived from the digestion of proteins. The results are typically presented as a mass spectrum, a plot of intensity as a function of the mass-to-charge ratio.

To perform mass spectrometry analysis, samples were lysate and protein denaturate using 2 different methods: for hepatic differentiation, because some samples had been used for WB analysis, cell pellets has been treated with RIPA buffer and boiled for 6'. Subsequently, in order to further purify the samples from WB solution residues (SDS, bromophenol blue and β-mercaptoethanol), a buffer exchange through FASP method was performed. Instead, for human nasal chondrocyte pellets, the lysis and denaturation were achieved through sonication of samples at 42kHz in an ultrasonic bath (Bransonic ultrasonic cleaner 2510E) at 60°C for 3 hours. Then, resulting samples were centrifuge and processed via mass spectrometry protocol.

FASP Method – buffer exchange

FASP (Filter Aided Sample Preparation) method was performed with Amicon Ultra - 0,5 mL centrifugal filters (ultracel - 3 kDa) (Sigma Aldrich UFC500324) according with protocol:

- filters hydration with 500 µl of H2O milliQ;
- centrifugation at 4°C for 3 min at 15.000 rpm;

- loading samples;
- centrifugation at 4 °C for 3 min at 15.000 rpm;
- addition of 200 µl of buffer (RIPA buffer for hepatic differentiation and ammonium bicarbonate for nasal chondrocytes);
- centrifugation at 4°C for 3 min at 15.000 rpm;
- addition of 300 µl of buffer (for three times);
- centrifugation at 4°C for 3 min at 15.000 rpm;

Reached the volume of 100 µl in the filters, the latter have been flipped in a new eppendorf and centrifugated at 4 °C for 3 min at 15.000 rpm.

Sample preparation protocol for Mass Spectrometry

Cell lysate samples for mass spectrometry analysis have been processed as follow:

- resuspension with 100 µl of Urea 6M;
- centrifugation at 4°C at 10.000 rpm for 5 min;
- supernatant collection and protein quantification (Bradford kit/BCA kit);
- addition of ammonium bicarbonate to dilute urea until 2M (alternatively, the buffer exchange FASP method can be used to remove urea);
- reduction of the bi-sulfur bound with dithiotreitol (DTT) (Sigma Aldrich D0632) 5mM at 37°C for 55 min;
- alkylation with iodoacetamide (IAA)(Sigma Aldrich 1149) 10mM for 30 min in the dark at RT;
- reduction with DTT 5mM at 37°C for 15 min;
- digestion of proteins with trypsin 5µg/µl (Sigma Aldrich T4799) for a final 1:25 enzyme/substrate ratio at 37 °C for 24 hrs;

- stop trypsin digestion with 3µl of acetic acid 98 %.

To reduce salt content, the desalting procedure was performed on digested samples:

- membrane C18 Supelco hydration with 1 mL of methanol;
- wash with 1 mL of solution 1 (H2O + 1% TFA);
- loading samples;
- wash with 500 µl of solution 2 (H2O + 0,1 % TFA);
- peptides elution with 1 mL of H_2O/acetonitrile (40:60) mixture + 0,1 % TFA;

Subsequently, all samples were dried in a stream of nitrogen and resuspended in 100µl of H_2O/acetonitrile (50:50) mixture + 0,1 % TFA.

The samples were then loaded and analyzed using a High Performance Liquid Chromatography-Mass Spectrometry (HPLC-MS) linear trap quadrupole (LTQ) Orbitrap XL at the “Centro Misure Giuseppe Casnati”, in collaboration with Drs. Andrea Faccini, and Prof. Lisa Elviri, Dept. of Food and Drug.

14. Data processing analysis

The raw data from the Orbitrap Fusion were visually analysed with Xcalibur™ software, then MaxQuant computational proteomics platform (version 1.6.2.10) was used for processing the data. Proteins identification was made by Andromeda search engine against the Rattus Norvegicus database (Uniprot proteome ID: UP000002494), containing 29,941 proteins, and Homo Sapiens database (Uniprot proteome ID: UP000005640), consisting of 74,034 proteins. Trypsin was chosen as a specific digestion mode with up to two missed cleavages. Proteins N-

terminal acetylation and oxidation of methionine was set as variable modifications and carbamidomethylation of cysteine as a fixed modification. Minimum peptide length was fixed at 7, mass tolerances and false discovery rate (FDR) for both peptides and proteins were set at 1%.

Analysis of the biological relevance of data from MaxQuant was made with Perseus (version 1.6.1.1). In order to facilitate the calculation of the protein's expression fold change, samples were grouped and values were transformed to a log2 scale. Overlap and variability between biological replicates was reported as Venn diagrams, scatter plot and multiple scatter plots. Hierarchical clustering with Euclidean distances and HeatMap graphic representation were performed after z-score normalization, and up- and down-regulated proteins analyzed. GO analysis for biological processes and molecular function annotations was performed with Perseus and STRING (Search Tool for the Retrieval of Interacting Genes/Proteins) version 10.5.

RESULTS

1. Rat tail collagen HPLC-MS analysis

High Performance Liquid Chromatography-Mass Spectrometry (HPLC-MS) was performed to analyze the collagen composition of extraction mixture from the rat tail tendons.

- *Figure 15* shows the different types of collagen revealed by HPLC-MS analysis. The resulting collagens are sorted from higher to lower score, each score used as an indirect index to estimate the amount of each collagen subtype. Collagen I resulted the more expressed subtype. The typical liver collagens are highlighted in red. Note that the analysis revealed also the presence of elastin.

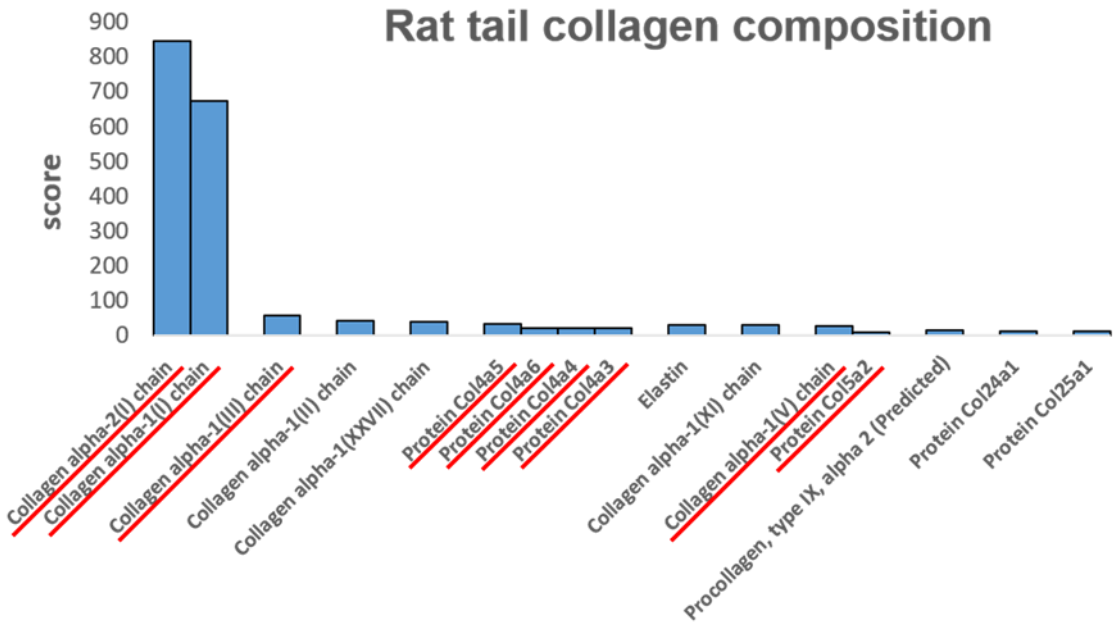

Figure 15: Different types of collagen (and elastin) resulting from HPLC-MS analysis of rat tail extraction mixture. The typical rat liver collagens are underlined in red.

2. Triple quadrupole *in silico* characterization of TSC/P

To improve Orbitrap mass spectrometry analysis on adult rat thyroid stem cells / progenitors, an evaluation about endodermal, neuroectodermal and epithelial-mesenchymal transition markers was performed, employing triple quadrupole mass spectrometer.

- *Figure 16* shows results from *in silico* mass spectrometry analysis for the stem cells TSC/P and primary culture cells THY. For neuroectodermal markers, HoxA2, HoxC5 and Tubulin b3 were found in both THY and TSCS/P. Similar, endodermal markers Pax9 and HNF-4a were expressed by both cell types. Epithelial – mesenchymal transition marker Snail-Slug was appeared in THY and TSC/P, while the other epithelial – mesenchymal transition marker Twist was detected only in TSC/P cells.

Interestingly, in the TSC/P population there is an increase of some neuroectodermal markers, while endodermal markers decrease, as expected from a stem cells / progenitors population.

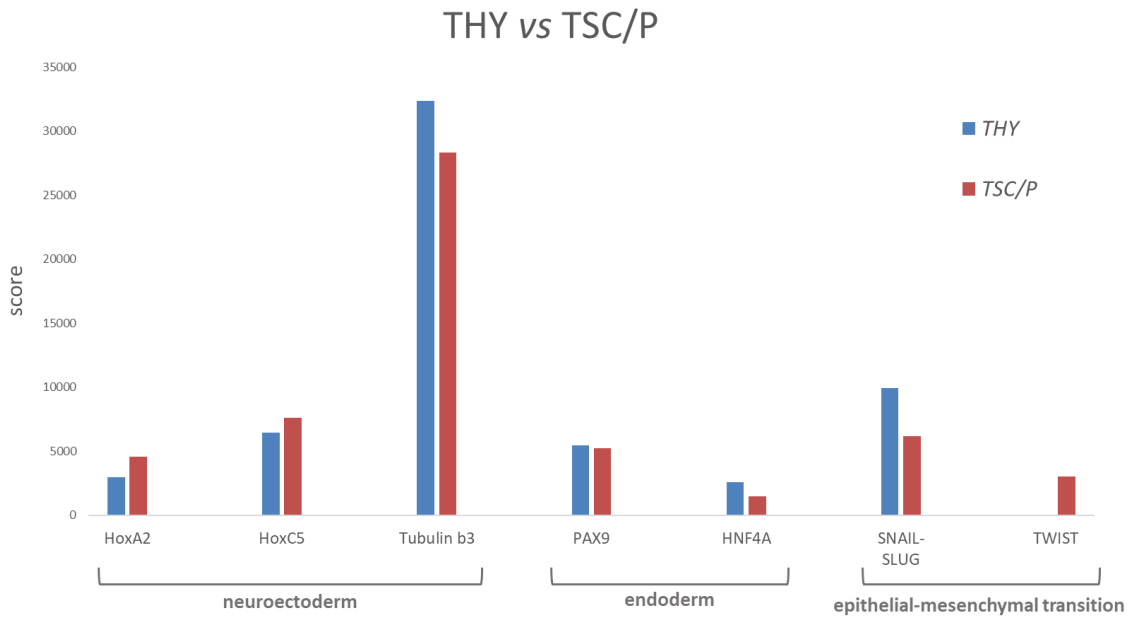

Figure 16: histogram of neuroectodermal, endodermal and epithelial – mesenchymal transition markers resulted by in silico triple quadrupole mass spectrometry analysis. Primary thyroid culture cells (THY) are represented in blue, thyroid stem cells / progenitors (TSC/P) are represented in red.

3. Immunocytochemistry (IC) for hepatic markers

Cells on coverslips were analysed by IC for expression of typical hepatic marker including α-fetoprotein (AFP), Hepatocyte Nuclear Factor-3β (HNF-3β), Cytokeratin-18 and 19 (CK-18 and CK-19), and Albumin (ALB). Specifically:

- *Figures 17a* and *17b* show the distribution of AFP in control (ctrl) and differentiated (diff) thyroid stem cells / progenitors (TSC/P) cultures, using either protocol 1 or protocol 2. With protocol 1, AFP immunoproduct resulted highly expressed in the cytoplasm at days 7 and 10, progressively reduced at days 15 -19, and almost disappeared at days 30. In contrast, with protocol 2, a low AFP expression was observed between days 7 - 10, with only occasional polygonal cells at day 19 days.

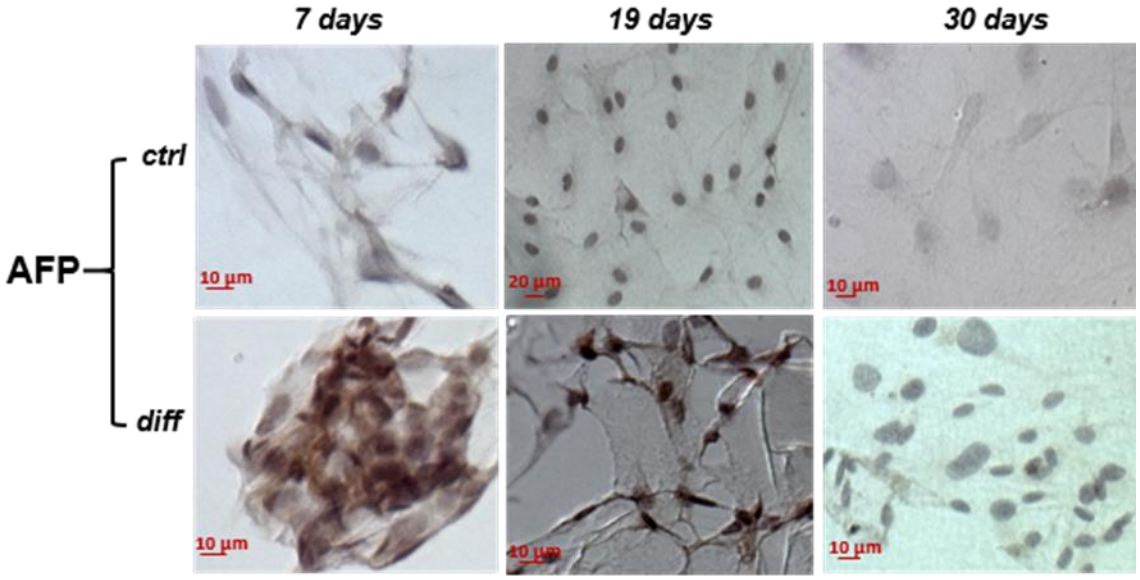

Figure 17a: IC for α-fetoprotein in control (above) and differentiated (below) TSC/P at 7,19 and 30 days using protocol 1; nuclei are stained in violet, positive signal is in brown (DAB staining).

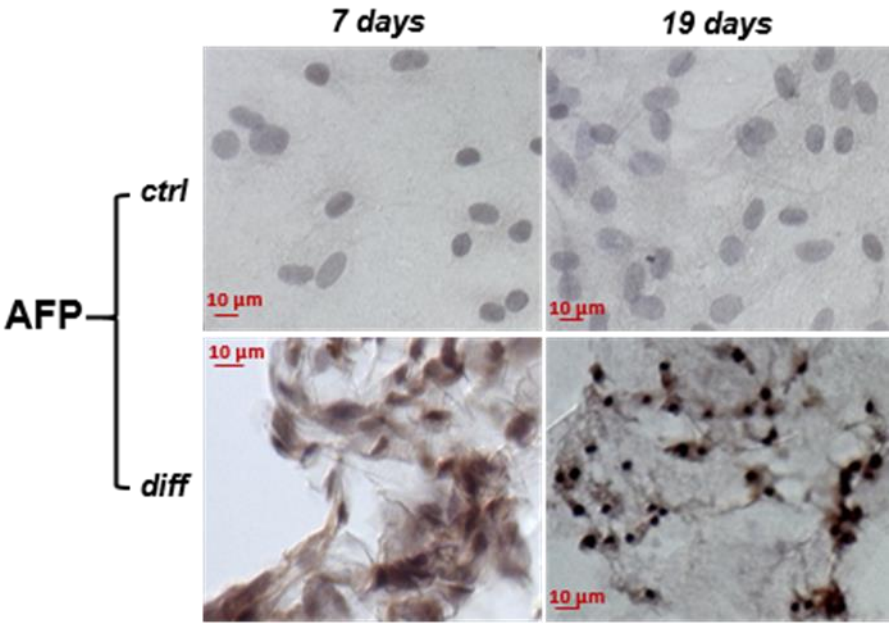

Figure 17b: IC for α-fetoprotein in control (above) and differentiated (below) TSC/P at 7 and 19 days using protocol 2; nuclei are stained in violet, positive signal is in brown (DAB staining).

- *Figures 17c* and *17d* show the distribution of AFP in control (ctrl) and differentiated (diff) bone marrow – derived mesenchymal stem cells (bm-MSC) cultures, using either protocol 1 or protocol 2. With protocol 1, AFP immunoproduct resulted highly expressed in the cytoplasm at day 3, progressively reduced at days 7 – 10, and almost disappeared at the end of the differentiation period. In protocol 2, a low AFP expression in single cells was observed at day 3, increasing at day 7 and disappearing with differentiation progress.

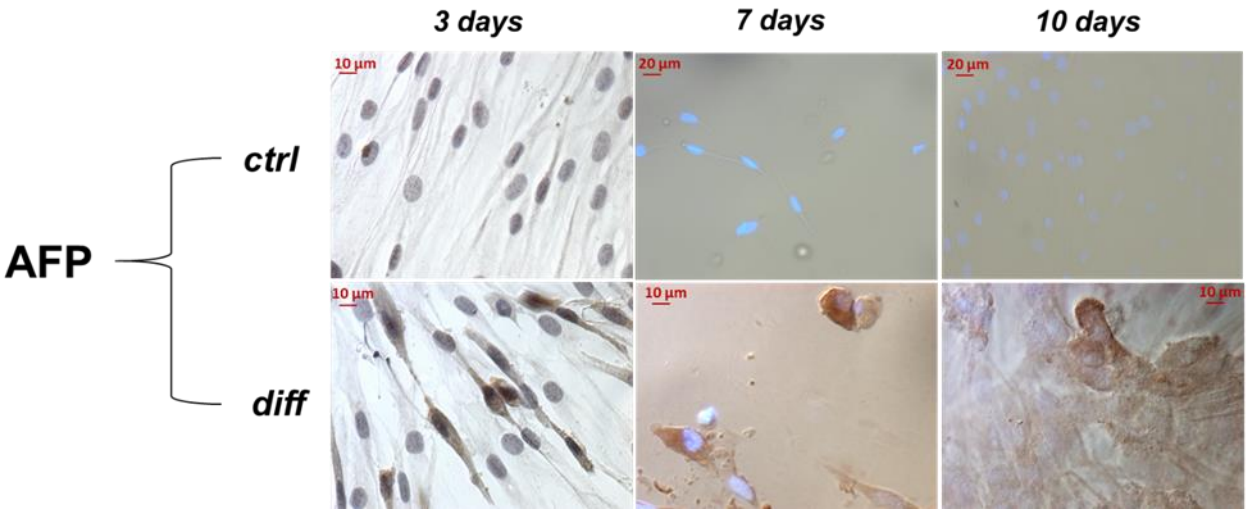

Figure 17c: IC for α-fetoprotein in control (above) and differentiated (below) bm-MSCs at 3, 7 and 10 days using protocol 1; nuclei are stained in violet or fluorescent in light blue, positive signal is in brown (DAB staining).

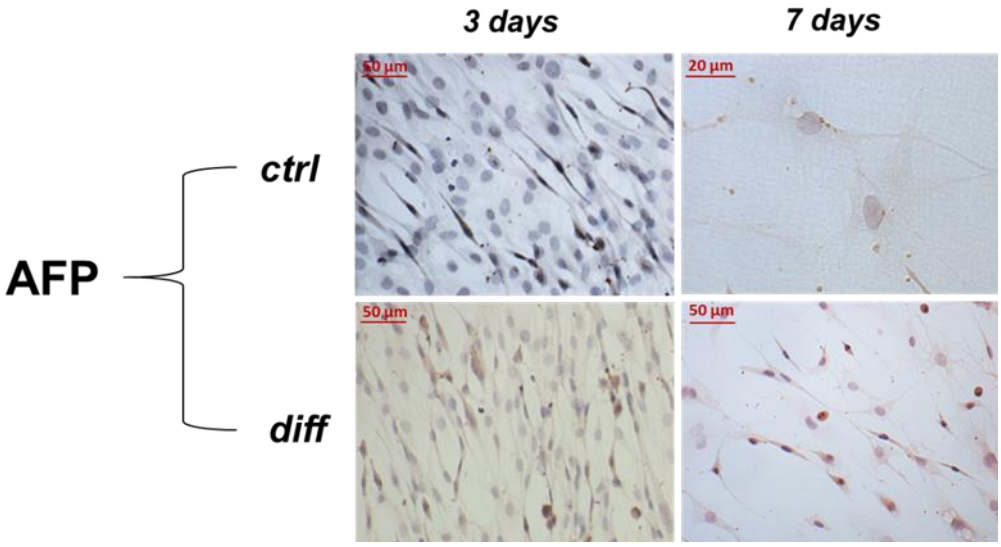

Figure 17d: IC for α-fetoprotein in control (above) and differentiated (below) bm-MSCs at 3 and 7 days using protocol 2; nuclei are stained in violet, positive signal is in brown (DAB staining).

- *Figures 18a* and *18b* show the distribution of HNF-3β in control and differentiated TSC/P cultures, using either protocol 1 or protocol 2. With protocol 1, a weak HNF-3β nuclear immunoreactivity was present at day 3, reaching a peak between days 7 -10, and returning to low levels at day 19. In contrast, with protocol 2 HNF-3β immunopositive nuclei were seen only ad day 10.

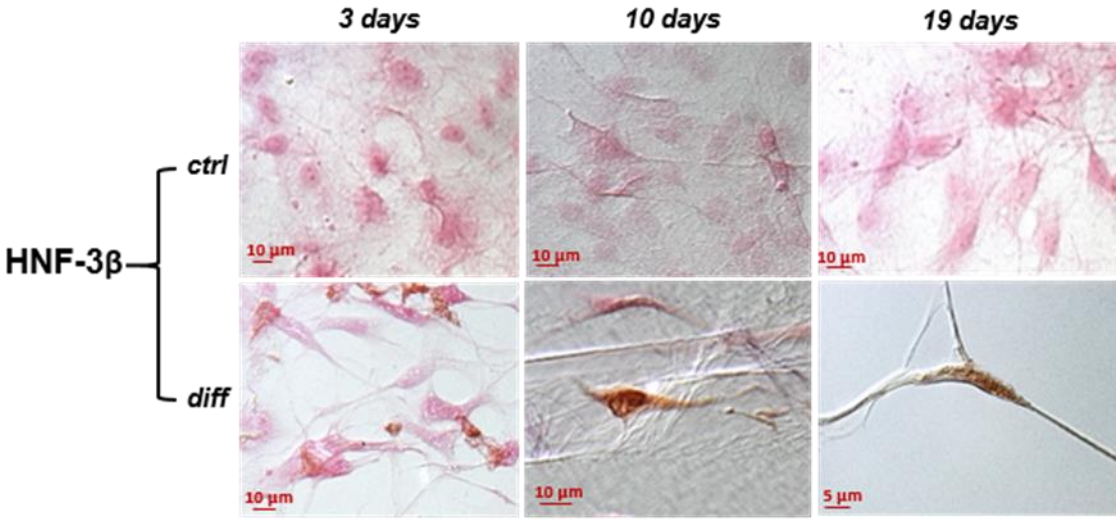

Figure 18a: IC for Hepatocyte Nuclear Factor-3β in control (above) and differentiated (below) TSC/P at 3, 10 and 19 days using protocol 1; nuclei and cytoplasm are stained in pink, positive signal is in brown (DAB staining).

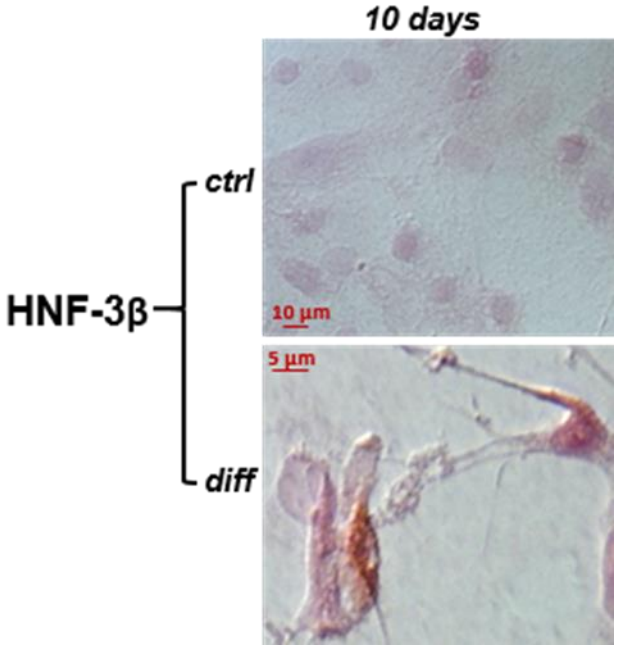

Figure 18b: IC for Hepatocyte Nuclear Factor-3β in control (above) and differentiated (below) TSC/P at 10 days using protocol 2; nuclei and cytoplasm are stained in pink, positive signal is in brown (DAB staining).

- *Figures 18c* and *18d* show the distribution of HNF-3β in control and differentiated bm-MSC cultures, using either protocol 1 or protocol 2. With protocol 1, only a weak HNF-3β nuclear immunoreactivity was present at day 7. In contrast, with protocol 2 weak immunopositive nuclei

were seen in single cells during all differentiation period, with an increase of positivity at the end of differentiation.

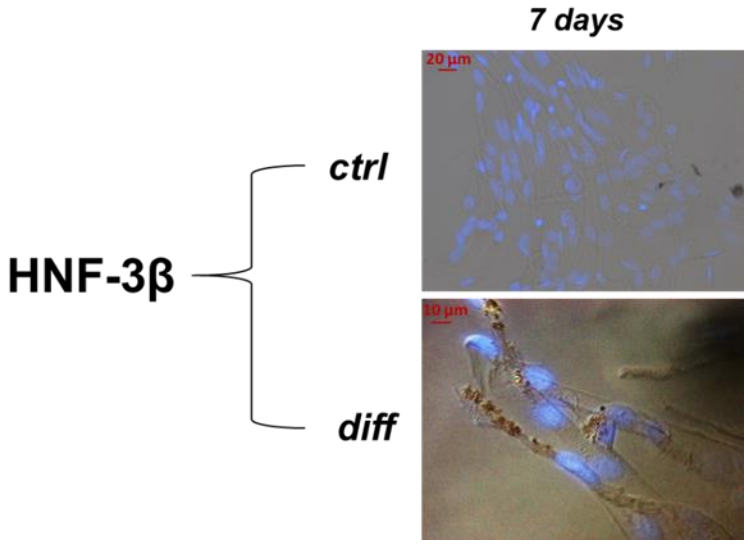

Figure 18c: IC for Hepatocyte Nuclear Factor-3β in control (above) and differentiated (below) bm-MSCs at 7 days using protocol 1; nuclei are fluorescent in light blue, positive signal is in brown (DAB staining).

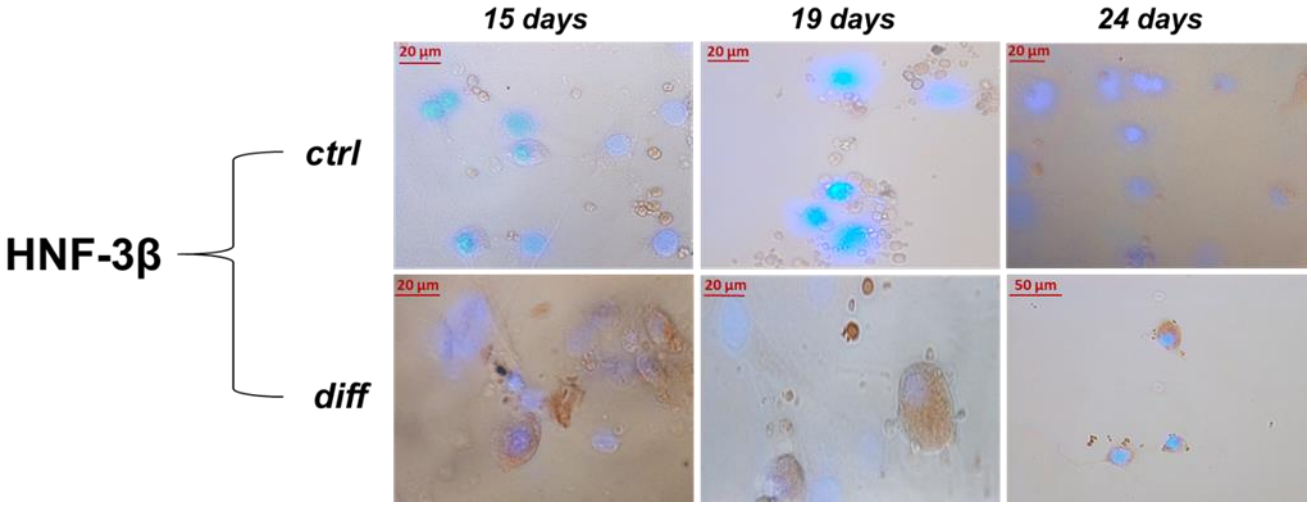

Figure 18d: IC for Hepatocyte Nuclear Factor-3β in control (above) and differentiated (below) bm-MSCs at 15, 19 and 24 days using protocol 2; nuclei are fluorescent in light blue, positive signal is in brown (DAB staining).

- *Figures 19a* and *19b* show the distribution of isoforms 18 and 19 of CK in controls and differentiated TSC/P cultures, using either protocol 1 or protocol 2. With protocol 1, a weak cytoplasmic CK immunopositivity was present at day 3, increasing at day 7 primarily in cluster

cells, and reaching a peak between days 10 - 19. Similar, with protocol 2 a low cytoplasmic CK immunostaining was observed at day 7, reaching a peak between days 10-19 when cells exhibited a clear change in morphology.

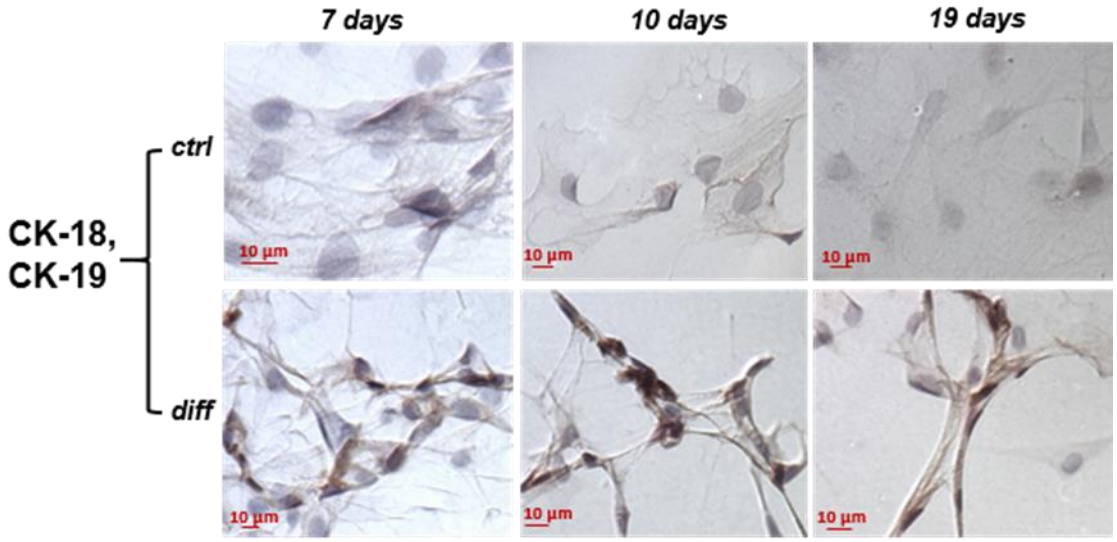

Figure 19a: IC for cytokeratins in control (above) and differentiated (below) TSC/P at 7, 10 and 19 days using protocol 1; nuclei are stained in violet, positive signal is in brown (DAB staining).

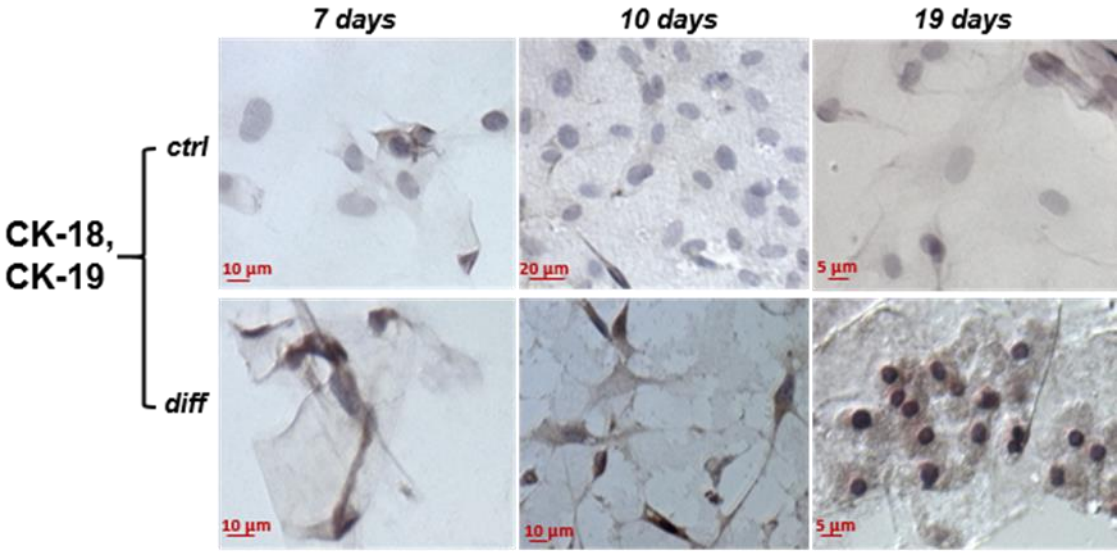

Figure 19b: IC for cytokeratins in control (above) and differentiated (below) TSC/P at 7, 10 and 19 days using protocol 2; nuclei are stained in violet, positive signal is in brown (DAB staining).

- *Figures 19c* and *19d* show the distribution of isoforms 18 and 19 of CK in controls and differentiated bm-MSC cultures, using either protocol 1 or protocol 2. With protocol 1, a weak cytoplasmic CK immunopositivity was present only at day 3, with several cells that exhibit immunoreaction. For protocol 2, a well evident cytoplasmic CK immunostaining was observed at day 15 in different cell groups, with some of these positive cell groups that was seen also at 10 and 19 days.

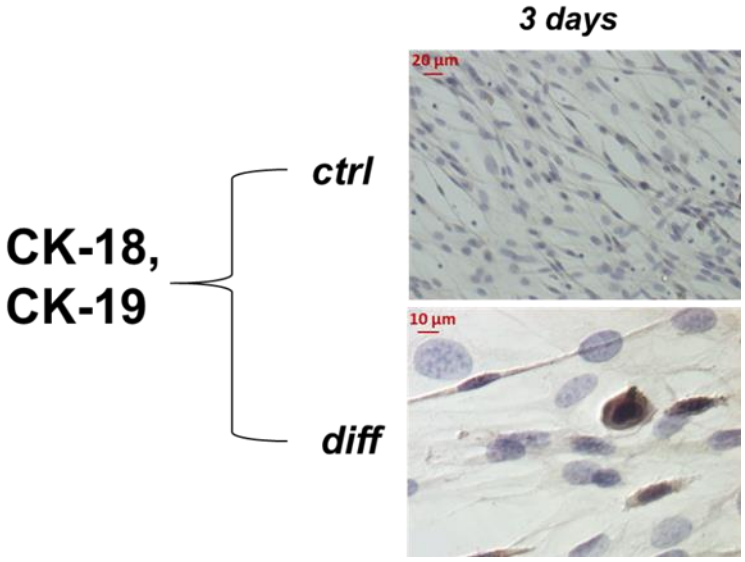

Figure 19c: IC for cytokeratins in control (above) and differentiated (below) bm-MSCs at 3 days using protocol 1; nuclei are stained in violet, positive signal is in brown (DAB staining).

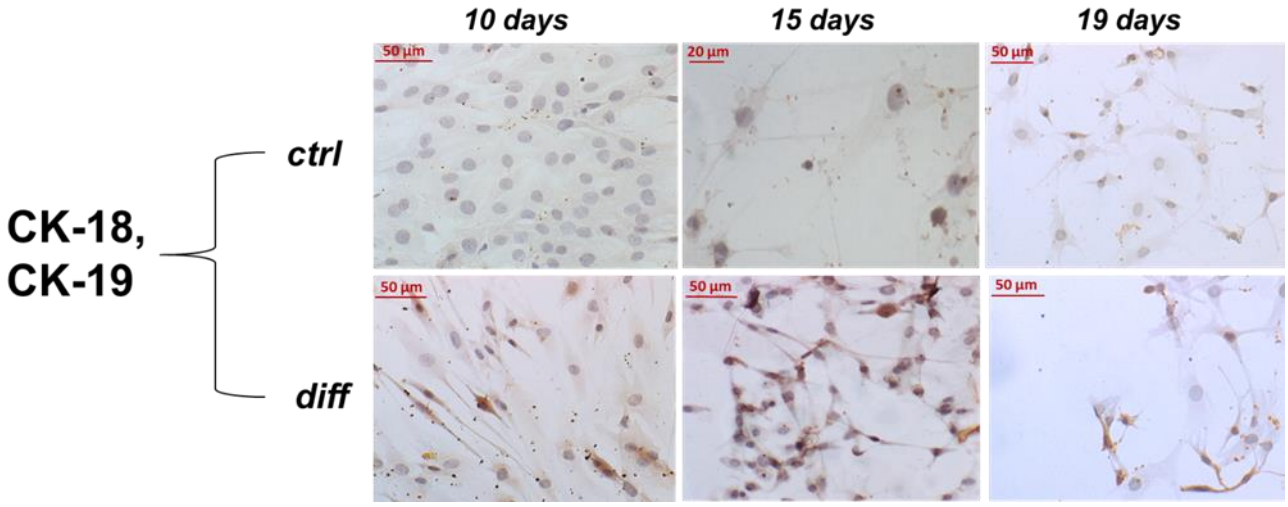

Figure 19d: IC for cytokeratins in control (above) and differentiated (below) bm-MSCs at 10, 15 and 19 days using protocol 2; nuclei are stained in violet, positive signal is in brown (DAB staining).

- *Figures 20a* and *20b* show the distribution of ALB in controls and differentiated TSC/P cultures, using either protocol 1 or protocol 2. With protocol 1, clear ALB immunoreactivity was present between days 7-15, reaching a peak at days 30. In contrast, with protocol 2 some ALB immunopositive cells were detected at day 7, but immunostaining was very faint at days 24.

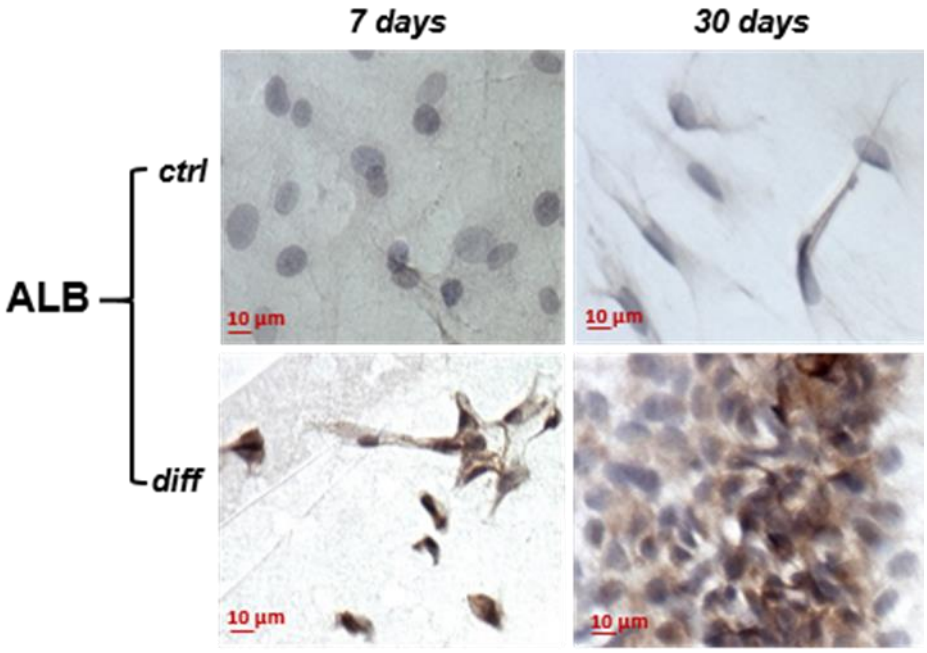

Figure 20a: IC for albumin in control (above) and differentiated (below) TSC/P at 7 and 30 days using protocol 1; nuclei are stained in violet, positive signal is in brown (DAB staining).

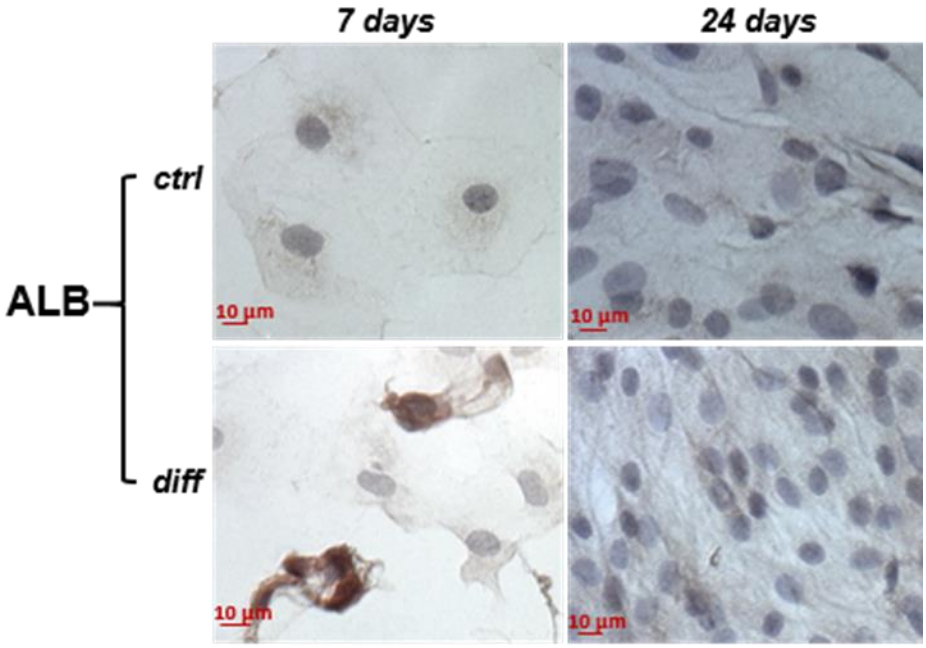

Figure 20b: IC for albumin in control (above) and differentiated (below) TSC/P at 7 and 24 days using protocol 2; nuclei are stained in violet, positive signal is in brown (DAB staining).

- *Figures 20c* and *20d* show the distribution of ALB in controls and differentiated bm-MSC cultures, using either protocol 1 or protocol 2. With protocol 1, clear ALB immunoreactivity was present at 10 days, despite it disappear at 30 days except for few isolated cells. In contrast, with protocol 2 ALB immunoreactivity was observed at 15 days in cell groups that exhibit a polygonal morphology with round and central nuclei. A positive signal was still present in few groups of cells also at the last time points of differentiation.

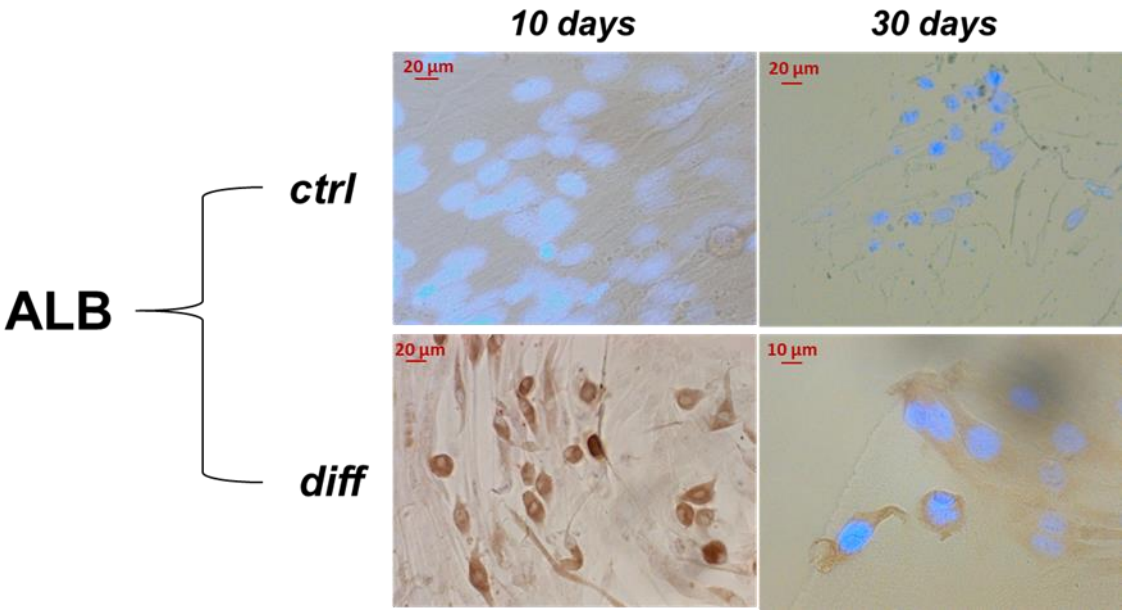

Figure 20c: IC for albumin in control (above) and differentiated (below) bm-MSCs at 10 and 30 days using protocol 1; nuclei are fluorescent in light blue, positive signal is in brown (DAB staining).

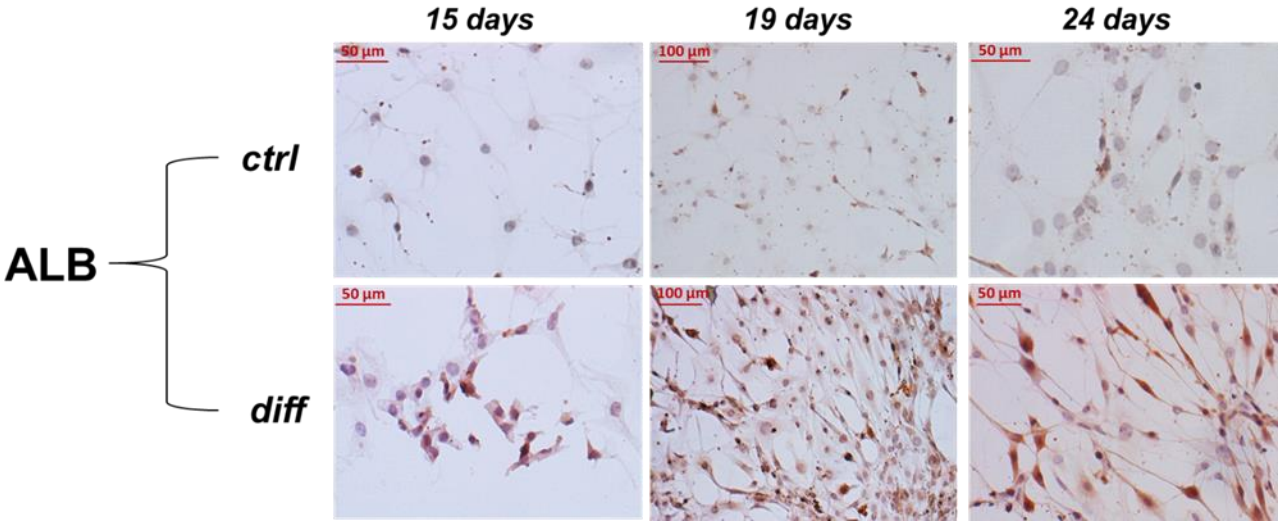

Figure 20d: IC for albumin in control (above) and differentiated (below) bm-MSCs at 15, 19 and 24 days using protocol 2; nuclei are stained in violet, positive signal is in brown (DAB staining).

4. Histochemistry for glycogen, and histological staining for cell morphology

The capacity of differentiated cells to synthesize and store glycogen was investigated using the histochemical Periodic acid–Schiff (PAS) reaction, performed at days 3 (initial differentiation period), 15 (intermediate differentiation period) and 24 or 30 (final differentiation period). In particular:

- *Figures 21a* and *21b* show the PAS reaction staining in controls and differentiated TSC/P cultures, using either protocol 1 or protocol 2. With protocol 1, PAS-positive cells resulted mostly segregated into clusters at day 3, with the number of clusters increasing at day 15. During this time lag, cells started to change from fibroblast-like morphology to a more polygonal geometry with respect to controls. Finally, PAS staining reached a peak of intensity at day 30, with PAS-positive cells moving at the periphery of the clusters.

In contrast, with protocol 2 only very few PAS-positive cells were observed at day 3, remaining almost undetectable at day 15, whereas only scattered PAS-positive cells were visible at day 24.

Single PAS-positive cells were also detected in the control group, primarily at early time frames, as expected by the fact that adult thyroid stem cells / progenitors are endodermal in origin and, as such may share with the hepatic lineage the capacity to synthesize small amounts of glycogen.

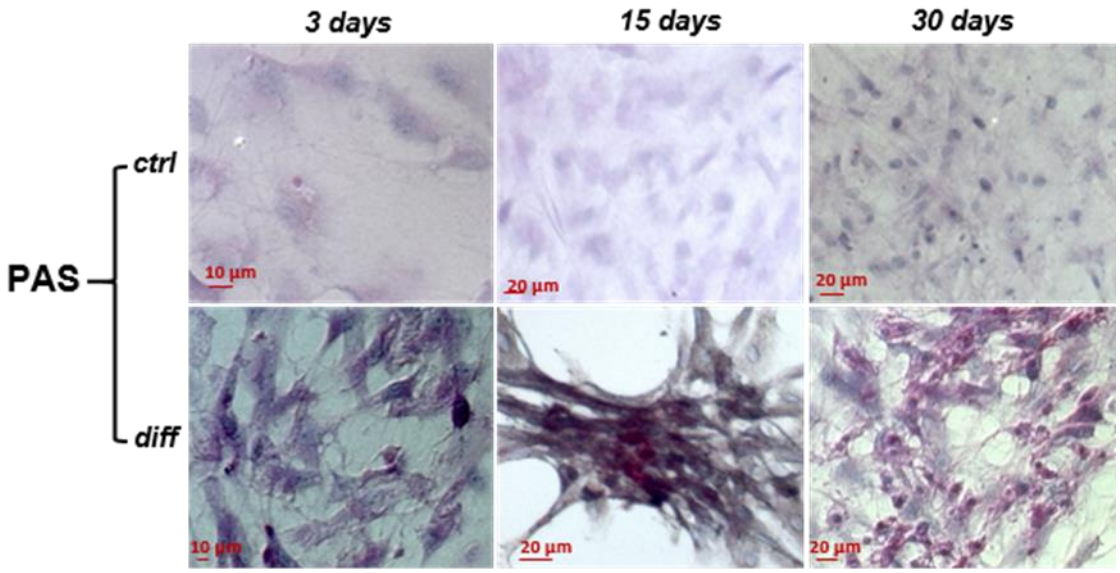

Figure 21a: Periodic acid–Schiff (PAS) staining in control (above) and differentiated (below) TSC/P at 3, 15 and 30 days using protocol 1; nuclei are stained in violet, positive signal in pink.

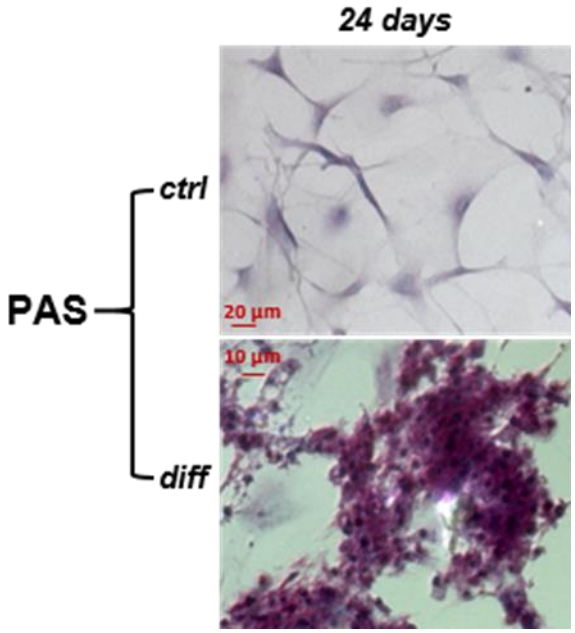

Figure 21b: Periodic acid–Schiff (PAS) staining in control (above) and differentiated (below) TSC/P at 24 days using protocol 2; nuclei are stained in violet, positive signal in pink.

- *Figure 21c* shows the PAS reaction staining in controls and differentiated bm-MSC cultures, for protocol 1. Using this protocol, cells started to store glycogen at 3 days, with an increase of number of cell cluster and PAS-positive cells at 15 days of differentiation. The presence of

positive cells within the clusters was observed also at 30 days, confirming the acquired capacity of these cells to store glycogen.

Few Single PAS-positive cells were also detected in the control group.

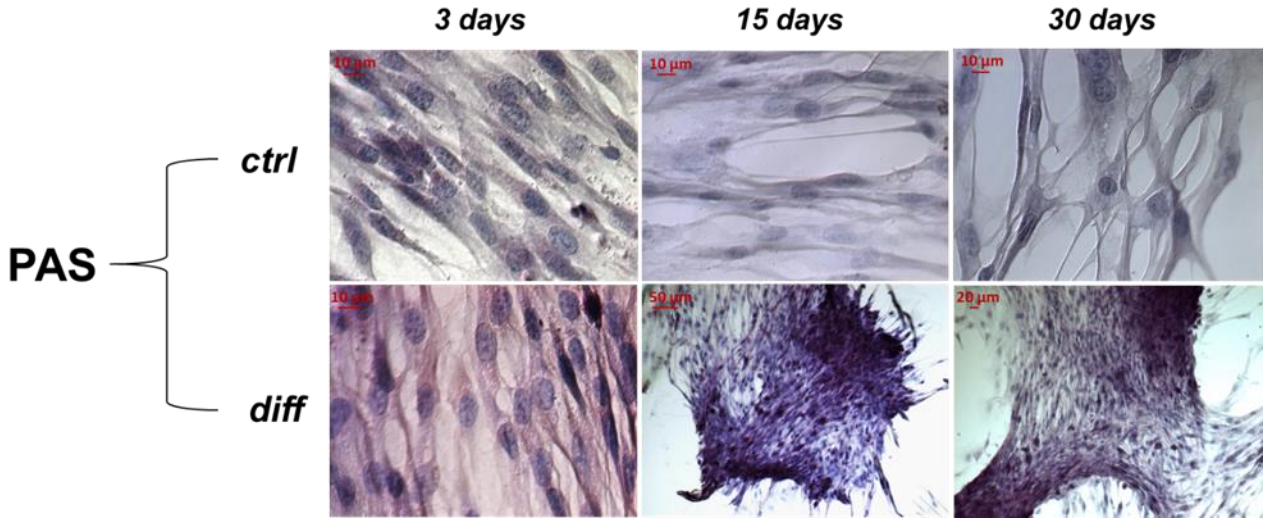

Figure 21c: Periodic acid–Schiff (PAS) staining in control (above) and differentiated (below) bm-MSCs at 3, 15 and 30 days using protocol 1; nuclei are stained in violet, positive signal in pink.

Changes in the morphology of differentiating cells were followed using the classical Hematoxylin and Eosin (HeE) histological staining. In particular:

- *Figures 22a* and *22b* show the cell morphology at the light microscopic level in controls and differentiated TSC/P cultures, using either protocol 1 or protocol 2. With protocol 1, differentiated cells depicted large and monomorphic, round and central nuclei already at day 19. These nuclei were strikingly different from those of the control group, that appeared heterogeneously oval in cells with a fibroblast-like shape. At end of differentiation process, i.e. at days 30, hepatic – like groups of cells were observed, in which cells exhibited a hepatocyte-

like geometry with large, round and central nuclei and a flat, polygonal shape. In contrast, with protocol 2 many stellate cells were visible at day 19, although a progression to more polygonal elements was observable at day 24.

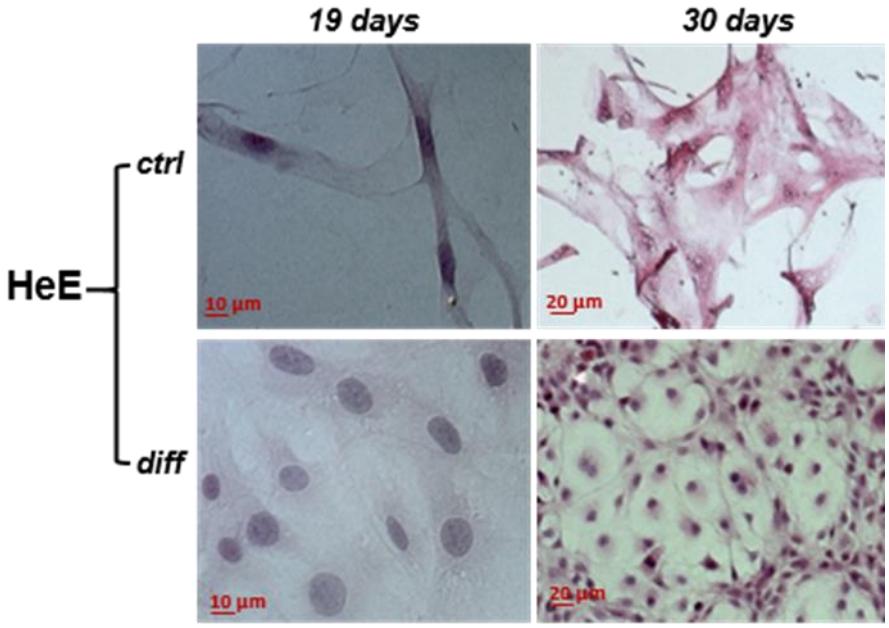

Figure 22a: Hematoxylin and Eosin (HeE) staining in control (above) and differentiated (below) TSC/P at 19 and 30 days using protocol 1; nuclei are stained in violet, while cytoplasm are stained in pink.

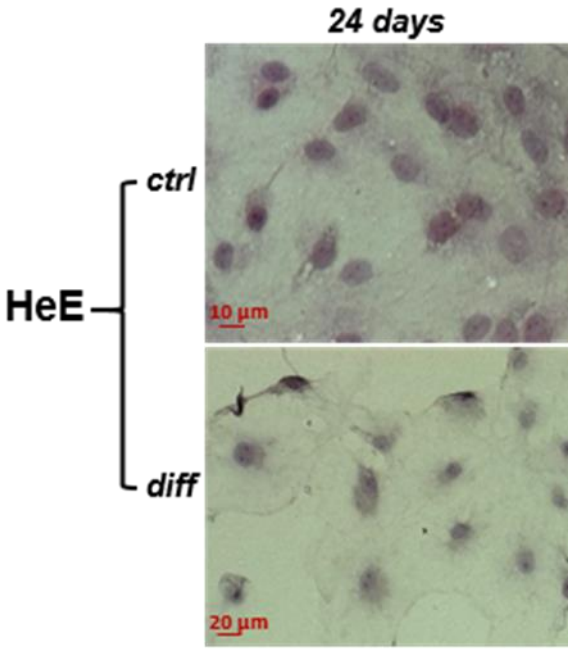

Figure 22b: Hematoxylin and Eosin (HeE) staining in control (above) and differentiated (below) TSC/P at 24 days using protocol 2; nuclei are stained in violet, while cytoplasms are stained in pink.

- *Figure 22c* shows the cell morphology at the light microscopic level in controls and differentiated bm-MSC cultures, using protocol 1. With protocol 1, first changes in cell morphology occurred starting from day 19, in which differentiated cells appeared large and monomorphic, with round and central nuclei, in contrast to control cells that still exhibited a fibroblast – like morphology, typical of mesenchymal stromal cells. At the end of the differentiation period, i.e. day 30, some hepatic – like well – organized groups of cells were noticed, characterized by cells with hepatocyte – like geometry, as a polygonal shape and large, round and central nuclei.

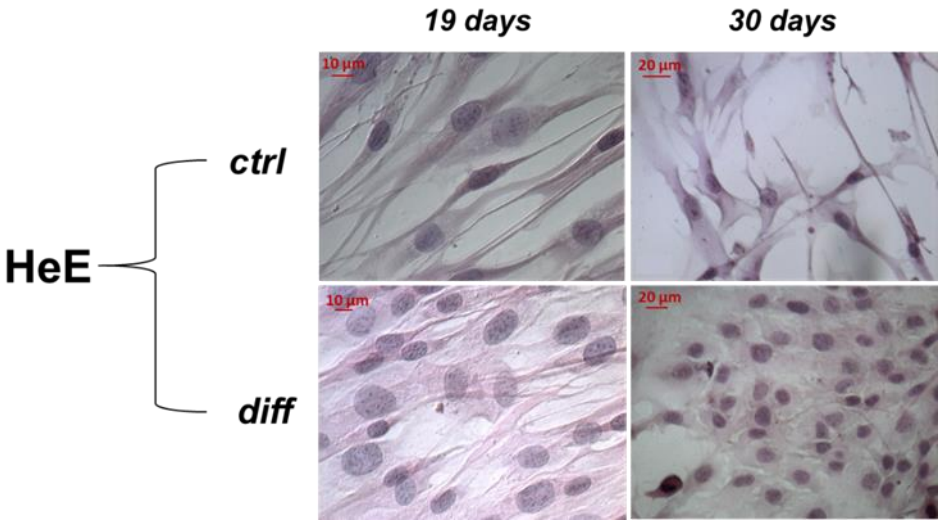

Figure 22c: Hematoxylin and Eosin (HeE) staining in control (above) and differentiated (below) bm-MSCs at 19 and 30 days using protocol 1; nuclei are stained in violet, while cytoplasm are stained in pink.

5. Scanning Electron Microscopy (SEM)

Ultrastructural features of the cell morphology in differentiating cells were investigated using SEM at days 3 (initial differentiation period) and either 30 or 24 (final differentiation period). In particular:

- *Figures 23a* and *23b* show ultrastructural details of the cell morphology at SEM in controls and differentiated TSC/P cultures, using either protocol 1 or protocol 2. With both protocols 1 and 2, a multipolar morphology resulted evident at day 3, likely compatible with the thyrogenic origin of the stem cells / progenitors used. However, with protocol 1 cells at day 30 consistently displayed a hepatocyte-like shape with round and central nuclei, a degree of binucleation, retracted borders, and a propensity to clustering. In some areas, clusters of large polygonal

cells were also seen surrounded by smaller oval-like cells. In contrast, with protocol 2 only few cells were noted at day 24 to have a classical flat and polygonal morphology like that expected for mature hepatocytes.

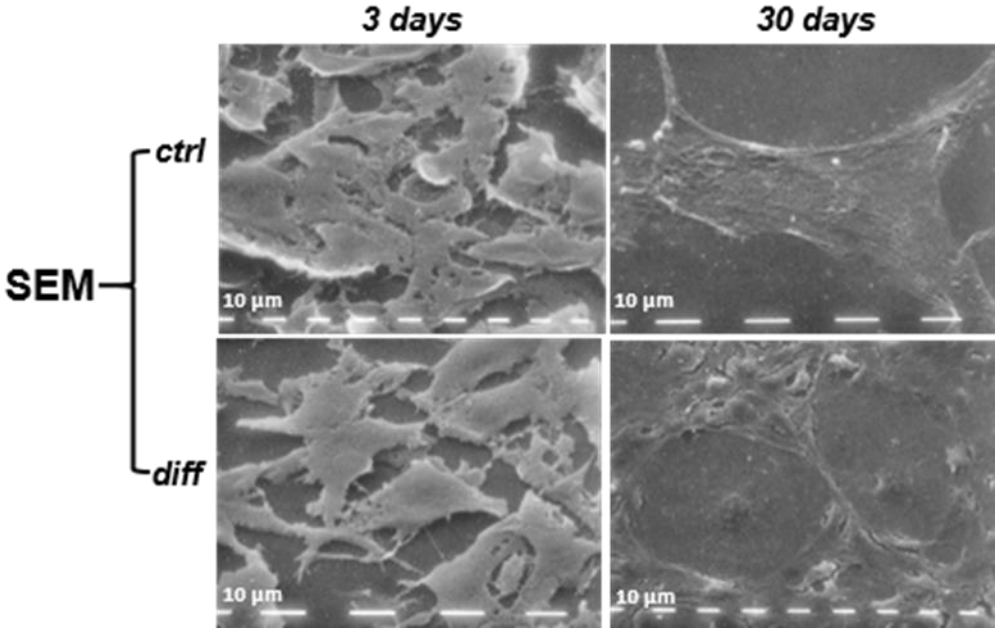

Figure 23a: Scanning Electron Microscopy (SEM) images in control (above) and differentiated (below) TSC/P at 3 and 30 days using protocol 1.

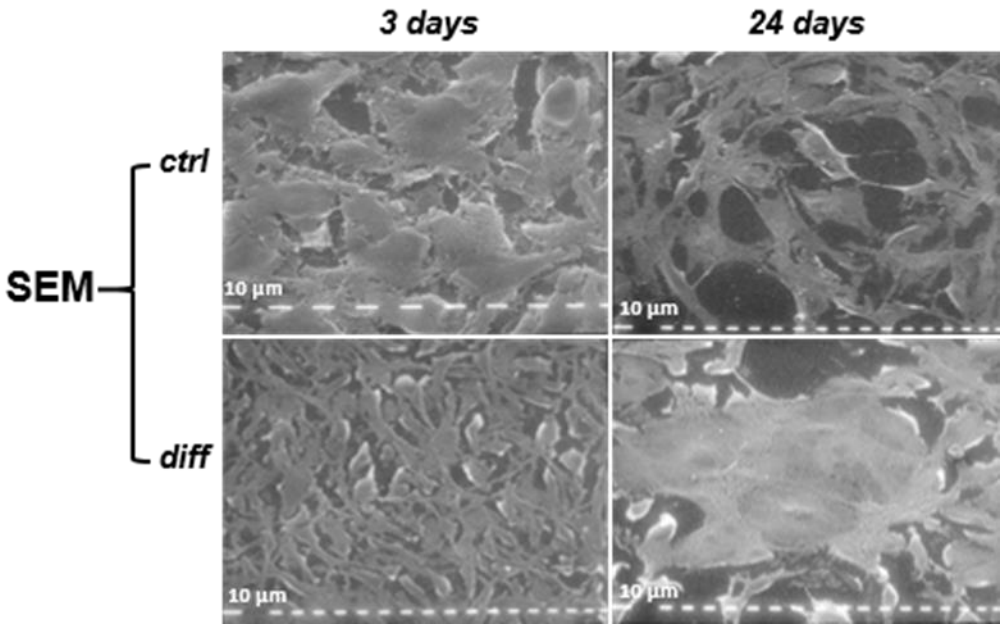

Figure 23b: Scanning Electron Microscopy (SEM) images in control (above) and differentiated (below) TSC/P at 3 and 24 days using protocol 2.

- *Figure 23c* shows ultrastructural details of the cell morphology at SEM in controls and differentiated bm-MSC cultures, for protocol 1. Hepatocyte-like morphology was evident at 30 days of differentiation, with cells characterized by round and central nuclei, the typical polygonal shape, and a clear propensity to clustering. Contrariwise, a well different situation was observed in the control group, in which cells exhibit a multipolar / fibroblast – like morphology, compatible with the mesenchymal origin of these cells.

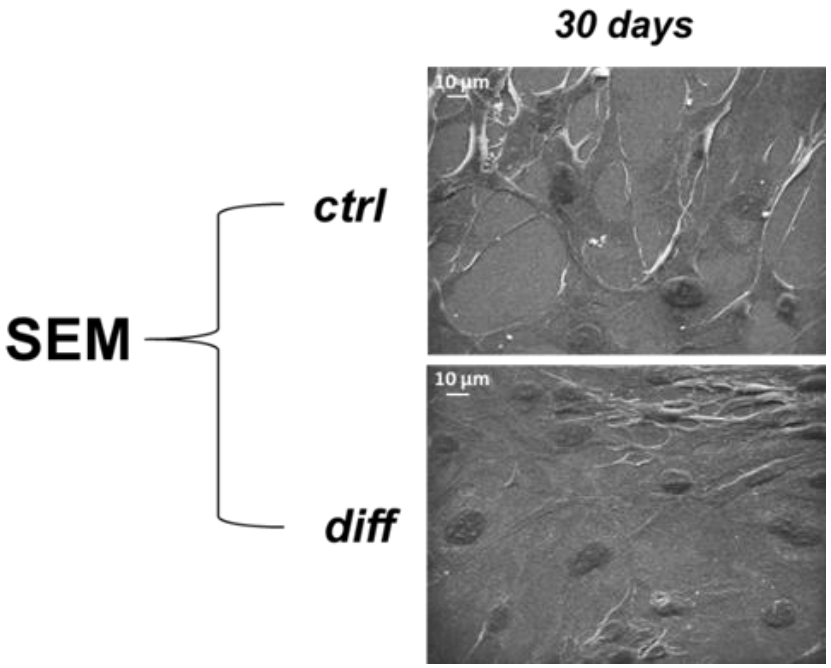

Figure 23c: Scanning Electron Microscopy (SEM) images in control (above) and differentiated (below) bm-MSCs at 30 days using protocol 1.

6. Western Blot and densitometric analysis

Quantitation of AFP, HNF-3β, and ALB biosynthesis in controls and differentiated cultures was performed by WB and densitometric analysis of the ensuing bands. The study was carried out only for TSC/P with protocol 1 at days 3, 15, and 30, and values expressed as percentage of increase respect to control. In particular:

- *Figure 24* shows that AFP increased at day 3 in differentiated cells of 56% when compared to the control.

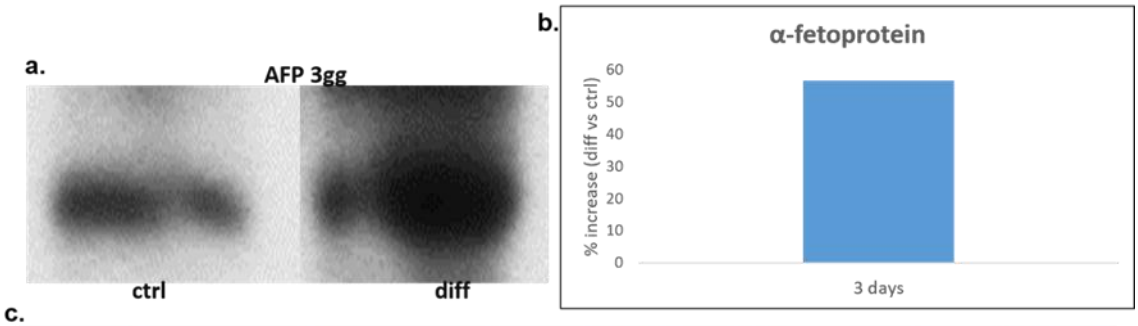

c.

OD		Afp	Act	Afp/Act	Difference	Increase %
3 days	ctrl	10.416.983	19.160.296	0,543675473	0,3084	56,73159543
	diff	18.461.054	21.665.075	0,852111244		

Figure 24: ***a.*** *Photo of the bands of α-fetoprotein obtained by Western Blot (WB) procedure.* ***b.*** *Histogram of percentage increase of target protein in differentiated cells.* ***c.*** *table with values of control (above) and differentiated (below) group, obtained by densitometric analysis.*

- *Figure 25* shows that HNF-3β increased progressively in differentiated cells between days 3 and 15 of 8% and 130% as compared to the control, respectively.

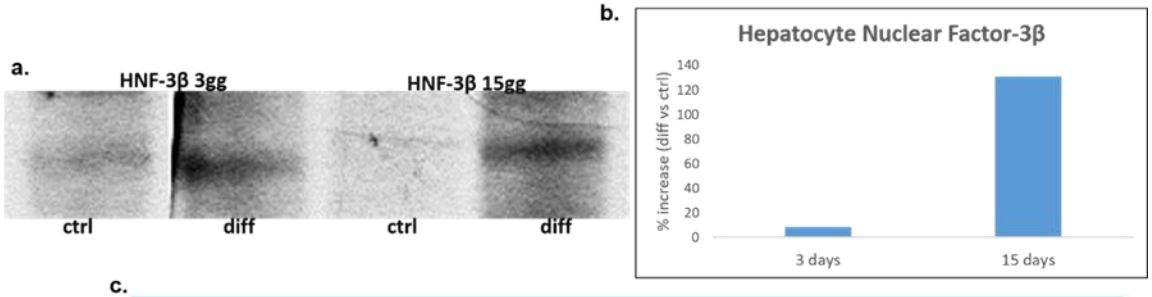

c.

OD		Hnf-3β	Act	Hnf-3β/Act	Difference	Increase %
3 days	ctrl	14.143.811	30.480.530	0,464027725	0,0383	8,256379742
	diff	19.701.276	39.219.037	0,502339616		
15 days	ctrl	3.298.749	19.381.125	0,170204206	0,2225	130,7196765
	diff	17.247.447	43.920.765	0,392694594		

Figure 25: ***a.*** *Photo of the bands of Hepatocyte Nuclear Factor-3β obtained by Western Blot (WB) procedure.* ***b.*** *Histogram of percentage increase of target protein in differentiated cells.* ***c.*** *table with values of control (above) and differentiated (below) group, obtained by densitometric analysis.*

- *Figure 26* shows that ALB increased in differentiated cells at day 30 of 330% when compared to control.

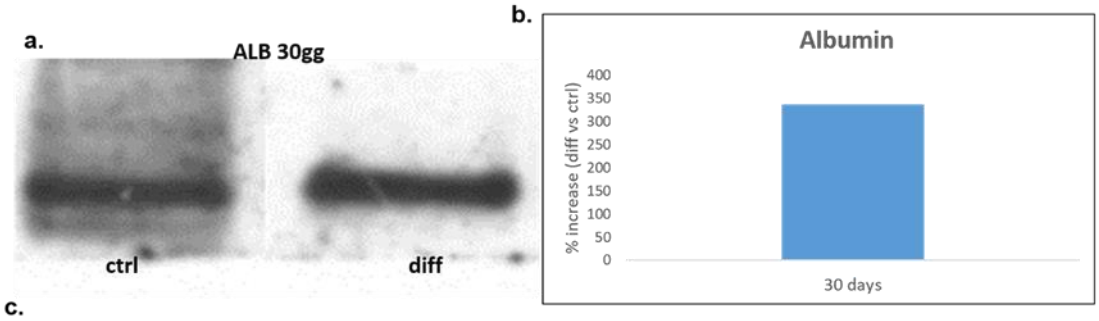

c.

OD		Alb	Act	Alb/Act	Difference	Increase %
30 days	ctrl	9.437.205	33.710.915	0,279945086	0,9430	336,8358326
	diff	12.333.933	10.085.803	1,222900447		

Figure 26: ***a.*** *Photo of the bands of albumin obtained by Western Blot (WB) procedure.* ***b.*** *Histogram of percentage increase of target protein in differentiated cells.* ***c.*** *table with values of control (above) and differentiated (below) group, obtained by densitometric analysis.*

7. Mass spectrometry analysis of hepatic differentiation process

Treated and control cells subjected to differentiation process were analyzed using a mass spectrometer. Cell pellets for both bm-MSCs and TSC/P at different time point (3, 15 and 30 days for protocol 1 and 3, 10 and 24 days for protocol 2) during differentiation were collected and digested for obtain their proteomic profile via mass spectrometry.

- *Figure 27* displays Venn's diagram overlaps of proteomic expression of TSC/P during the differentiation period (3, 15 and 30 days) using protocol 1. The protein expression results different in number between the 3 samples, and it progressively changes proceeding with

differentiation. In fact, although 5,9% of proteins remain expressed during all differentiation time, the common proteins between 3 and 15 days represent the 33,3% (67% and 40% of the total proteins expressed by 3 and 15 days respectively), and between 15 and 30 days are the 7,3% (8% and 52% of the total proteins expressed by 15 and 30 days respectively).

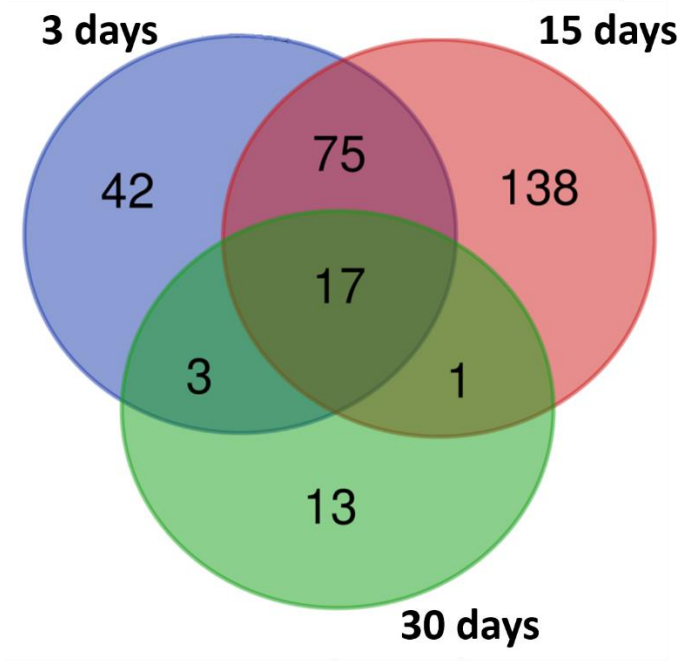

Figure 27: Venn's diagram of protein expression overlap in treated TSC/P during the protocol 1 differentiation process.

- *Figure 28* shows Venn's diagram overlaps of proteomic expression of TSC/P during the differentiation period (3, 10 and 24 days) using protocol 2. As for protocol 1, the protein expression results different in number between the 3 samples, although it exhibits a lower change during the differentiation process. In fact, the common proteins for the 3 time point are 14,9%, while the shared proteins between 3 and 10 days represent the 34,3% (54% and 48% of the total proteins expressed by 3 and 10 days respectively), and between 10 and 24 days are the 22,2% (24% and 73% of the total proteins expressed by 10 and 24 days respectively).

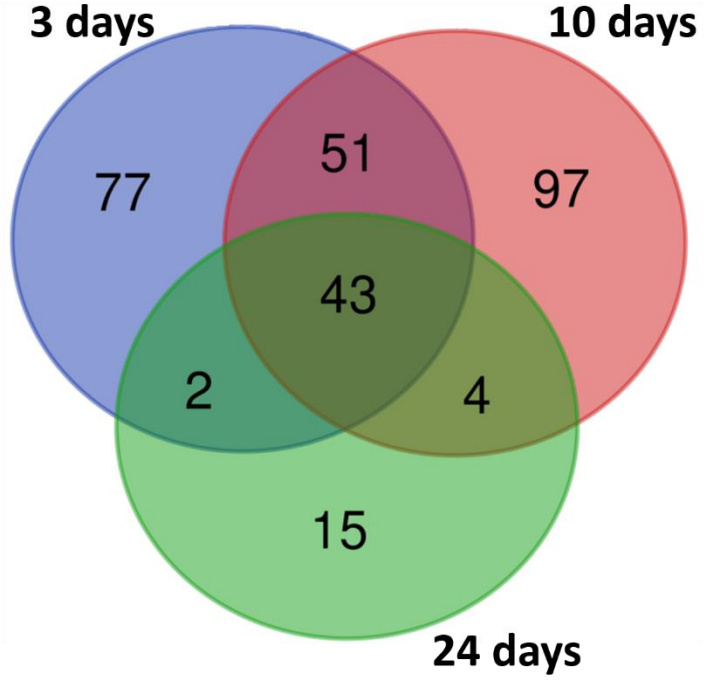

Figure 28: Venn's diagram of protein expression overlap in treated TSC/P during the protocol 2 differentiation process.

- *Figure 29* exhibits the differences in protein expression of TSC/P between protocol 1 and protocol 2 in treated cell group at 3 and 24/30 days. The thyroid cells responded immediately and similarly at the different growth factors of 2 protocols. In fact, at 3 days we observe only the 29,2% of common protein, a sign that the changes due to the differentiation factors begin to influence the cells in culture. At 24/30 days, the shared proteins still represent the 21,0%, confirming a stable and different protein expression between the 2 protocols also at the end of differentiation.

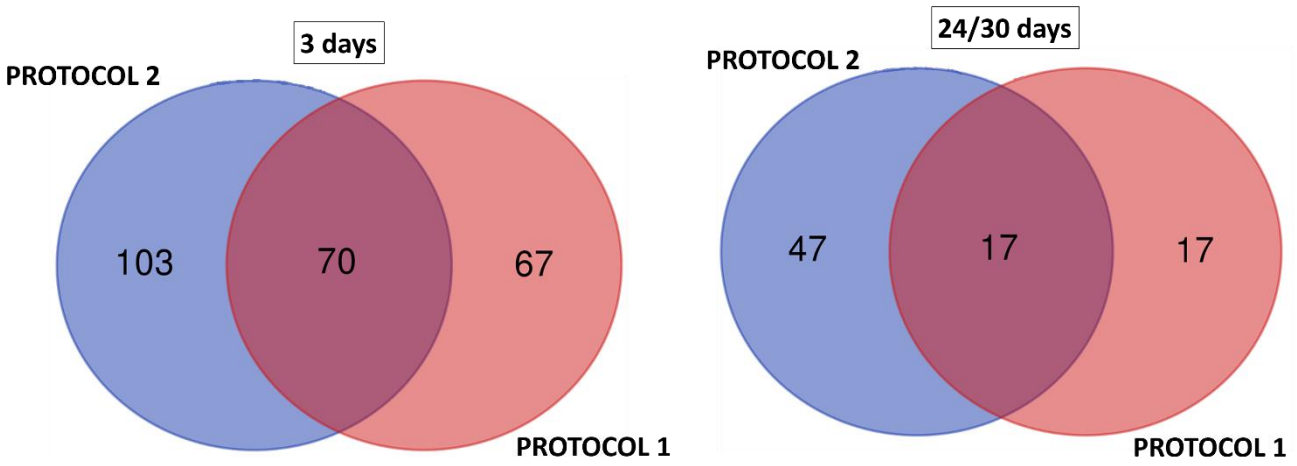

Figure 29: Venn's diagrams of differences in protein expression of TSC/P between protocol 1 and protocol 2 in treated cell group at 3 and 24/30 days.

- *Figure 30* represent a Venn's diagram of protein expression overlap between protocol 1 and protocol 2 in treated bm-MSCs at 3 and 24/30 days. Different from TSC/P, bone marrow stromal cells resent less of growth factor in the initial phase, as proved by the 46,9% of proteins in common. In the late phase, bm-MSCs treated with the 2 protocols shared only 15,9% of proteins, although these proteins represent the 100% of sample treated with protocol 2.

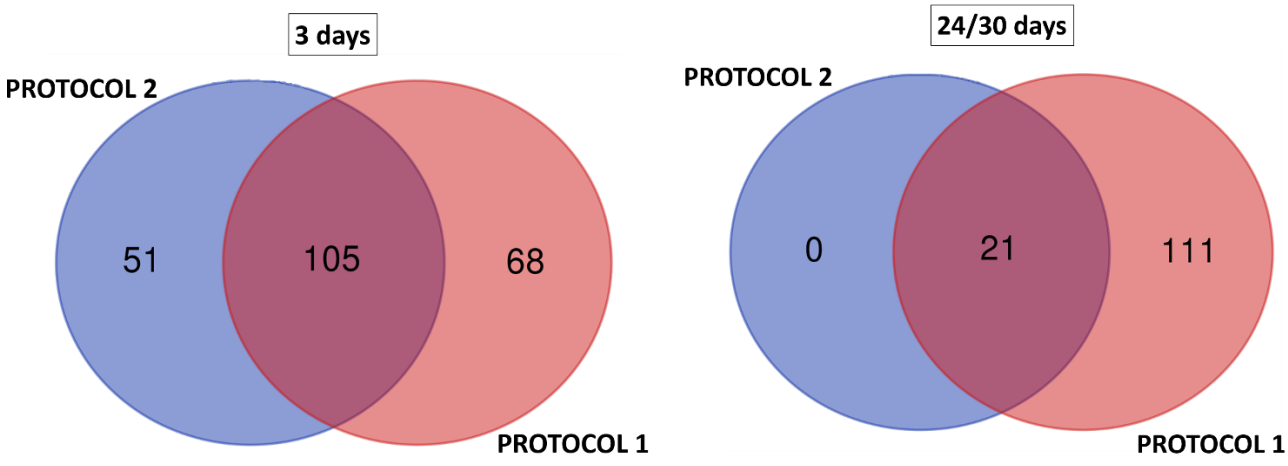

Figure 30: Venn's diagrams of differences in protein expression of bm-MSCs between protocol 1 and protocol 2 in treated cell group at 3 and 24/30 days.

- *Figure 31* shows the differences in protein expression at 3 and 30 days of protocol 1, in differentiated and control TSC/P. As observed before, the overlapping of the protein expression progressively decreases during differentiation (46,6% at 3 days against 30,0% at 30 days), confirming the hypothesis that TSC/P reacts to the differentiation stimuli and progressively changes their proteomic signature.

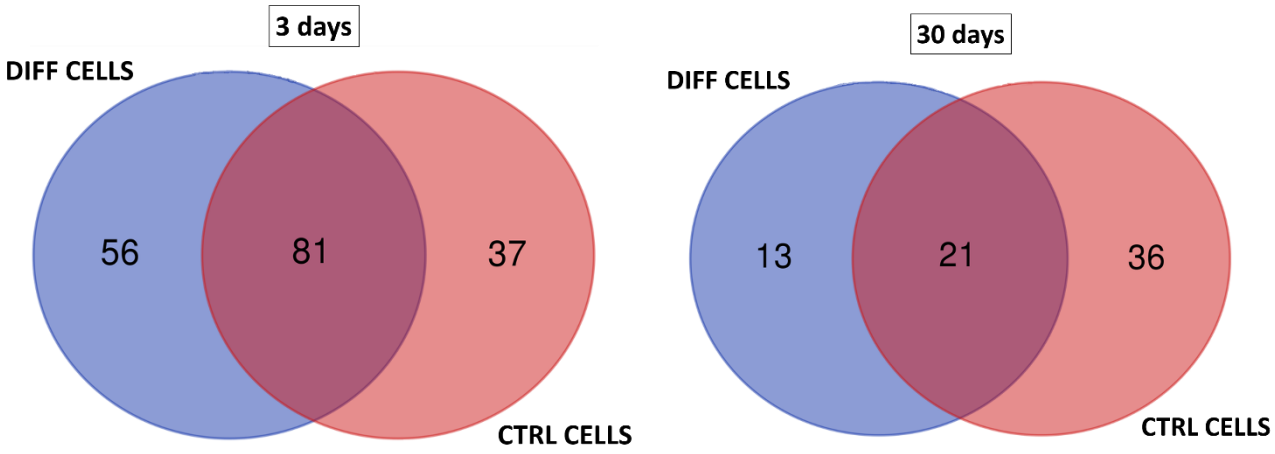

Figure 31: Venn's diagrams of proteins expression overlap between treated and control group of TSC/P using protocol 1 at 3 and 30 days.

- *Figure 32* represents the HeatMap of TSC/P protein expression at 3 and 30 days in differentiated and control cells using protocol 1. The Hierarchical clustering associated with the HeatMap highlights the similarity between differentiated and control cells at the beginning of differentiation process (3 days), while at 30 days the control sample resulted more similar at the 3 days samples respect to the 30 days treated sample, demonstrating the efficiency of the differentiation protocol.

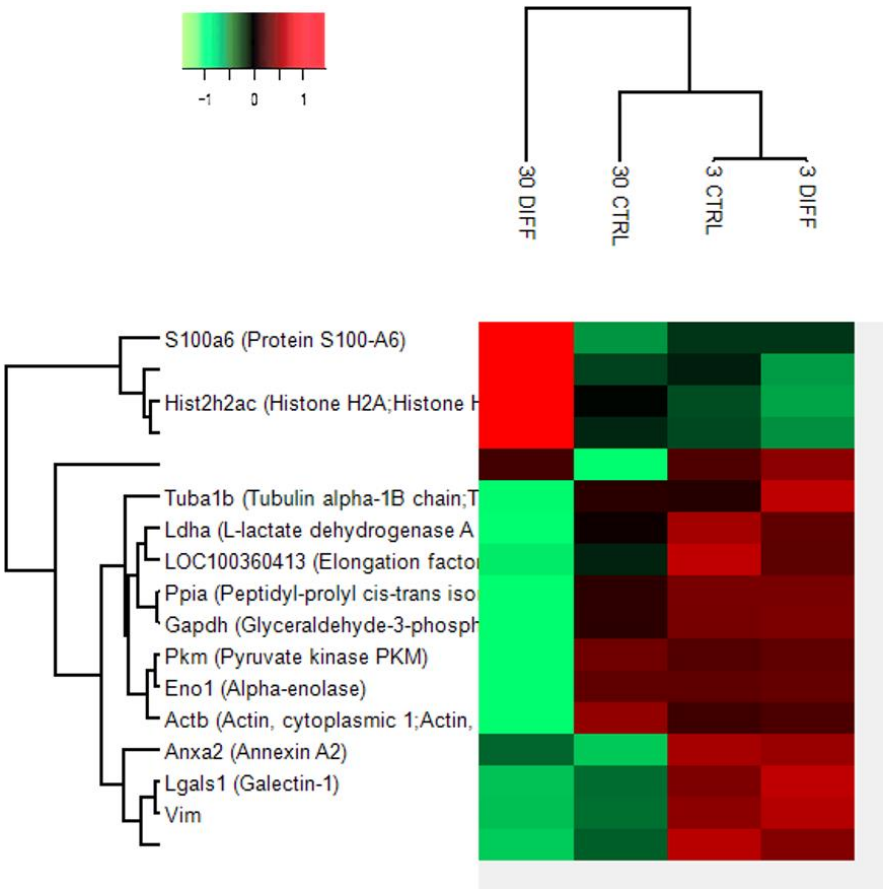

Figure 32: HeatMap and Hierarchical clustering of TSC/P protein expression at 3 and 30 days in differentiated and control cells using protocol 1. The expression pattern is represented by colours, from light green (-1) to light red (1).

- *Table 11* shows the down- and up-regulated proteins of differentiated TSC/P respect to control cells at 30 days using protocol 1. Interestingly, some down-regulated proteins in differentiated cells are implicated in catabolic / metabolic processes, while in up-regulated scheme, except for protein S100-A6, are present only proteins involved in cell assembly, regulation, organization, development and morphogenesis. Remarkably, in up-regulated table there is also Albumin, an essential marker for hepatic differentiation, found also with immunocytochemistry analysis.

DOWN-REGULATED		
PROTEIN NAME	GENE NAME	GO BIOLOGICAL PROCESS
Tubulin alpha-1B chain;Tubulin alpha-4A chain	Tuba1b;Tuba4a	cellular component assembly
L-lactate dehydrogenase A chain	Ldha	alcohol catabolic process;alcohol metabolic process
Elongation factor 1-alpha;Elongation factor 1-alpha 1	Eef1a1	biological regulation;catabolic process
Peptidyl-prolyl cis-trans isomerase A;Peptidyl-prolyl cis-trans isomerase A, N-terminally processed	Ppia	biological regulation;cellular macromolecule metabolic process
Glyceraldehyde-3-phosphate dehydrogenase	Gapdh	alcohol biosynthetic process;alcohol catabolic process
Pyruvate kinase PKM	Pkm	alcohol catabolic process;alcohol metabolic process
Alpha-enolase	Eno1	alcohol catabolic process;alcohol metabolic process
Actin, cytoplasmic 1;Actin, cytoplasmic 1, N-terminally processed	Actb	anatomical structure morphogenesis
Galectin-1	Lgals1	B cell activation; biological regulation;carbohydrate homeostasis
Vimentin	Vim	actin cytoskeleton organization; anatomical structure development
AHNAK nucleoprotein	Ahnak	structural molecule activity conferring elasticity; protein complex oligomerization

UP-REGULATED		
PROTEIN NAME	GENE NAME	GO BIOLOGICAL PROCESS
Protein S100-A6	S100a6	calcium-dependent protein binding; ion transmembrane transporter activity
Histone H2A;Histone H2A type 2-A	Hist2h2ac;Hist2h2aa3; Hist2h2ab	cellular component assembly;cellular component organization
Keratin, type II cytoskeletal 1	Krt1	biological regulation;complement activation
Serum albumin	Alb	anatomical structure development;anatomical structure morphogenesis;behavior;biological regulation
Annexin A2	Anxa2	anatomical structure formation involved in morphogenesis; angiogenesis;biological regulation

Table 11: Schemes of down- and up-regulated protein of differentiated TSC/P respect to control cells at 30 days using protocol 1. Catabolic and metabolic process are underlined in down-regulated proteins, while cell assembly, organization, regulation, development and morphogenesis process are underlined in up-regulated proteins.

8. Immunocytochemistry for human nasal chondrocytes

In order to evaluate the presence of a subpopulation of cells with high differentiation capacity into the nasal chondrocytes population, we analyzed in immunocytochemistry the neuroectodermal / neural crest markers Nestin, Notch1, NSE, P75, Sox2, Sox10, Wnt1, Dixdc1, MSX1 and Musashi 1, and the primitive mesoderm marker Brachyury (T).

- *Figure 33* shows results of immunocytochemistry analysis of human nasal chondrocytes, after their *in vitro* expansion (using expansion culture medium). The positivity was seen for the neural crest markers Dixdc1, Nestin and p75, as well as for the primitive mesoderm marker Brachyury.

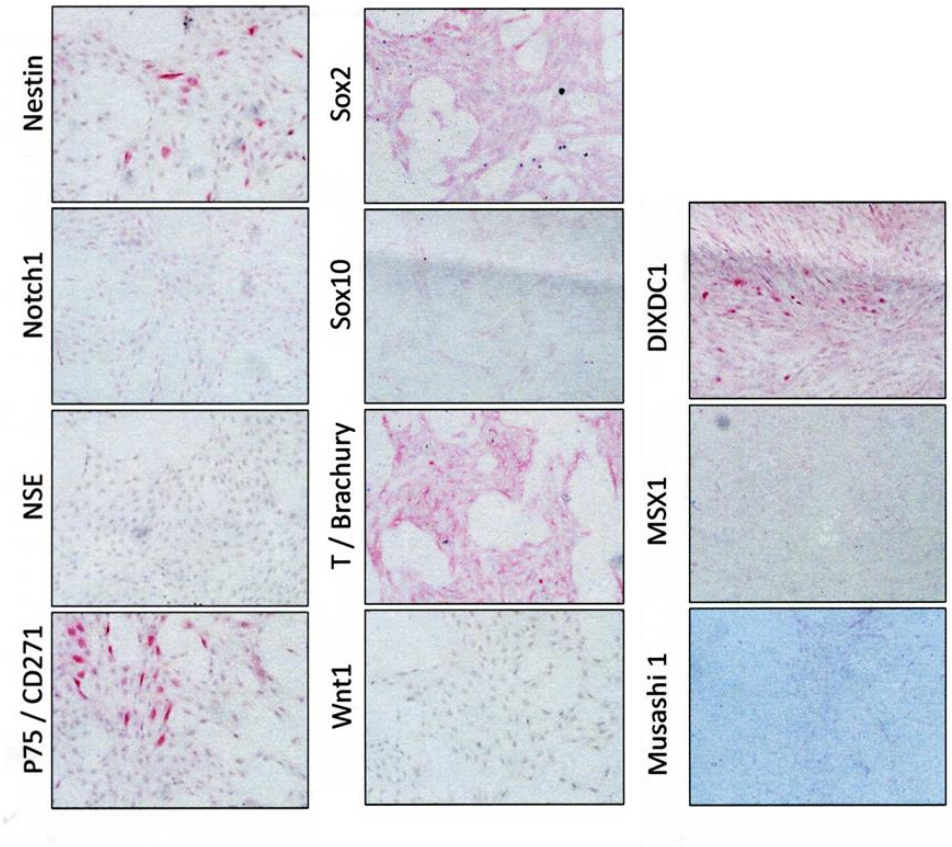

	NC in culture
DIXDC1	+
MSX1	-
Musashi 1	-
Nestin	+
Notch1	-
NSE	-
p75	+
Sox2	-
Sox10	-
T	+
Wnt1	-

Figure 33: IC analysis of human nasal chondrocytes for neural crest (Nestin, Notch1, NSE, P75, Sox2, Sox10, Wnt1, Dixdc1, MSX1 and Musashi 1) and the primitive mesoderm (Brachyury) markers. Positive cells are in pink-red for the use of alkaline phosphatase as substrate. The table summarizes results for each marker.

Moreover, to compare the obtained results from human nasal chondrocytes with human adult septal cartilage and human embryos, an immunohistochemical analysis was performed (data not shown).

- *Figure 34* displays all the results obtained, summarized in a Venn's diagram. The investigations on the primary cultures of nasal chondrocytes (NC in culture) showed immunoreactivity for p75, Dixdc1, Nestin and Brachyury, as observed also in adult human

septal cartilage (Native NC), with the addiction of Musashi 1 (Msi1). Instead, the septal cartilage of human embryos displayed positivity for Wnt1, Sox10, Chromogranin A, Msi and Brachyury.

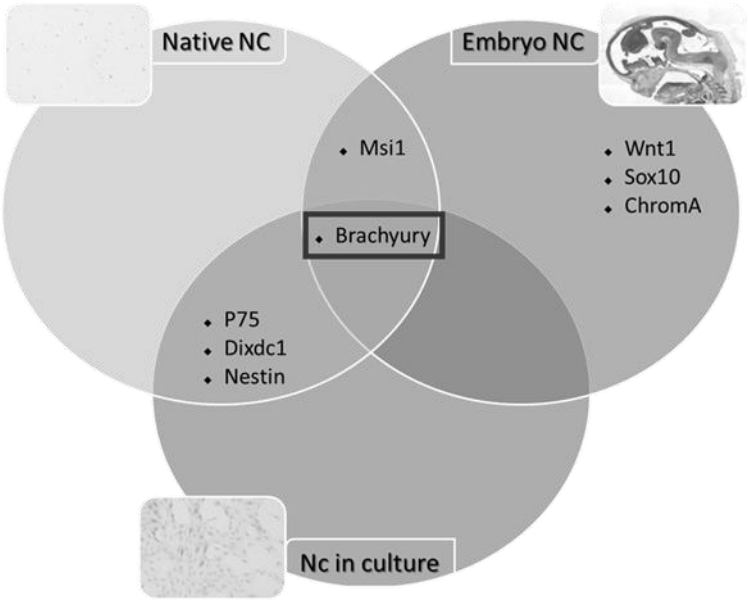

Figure 34: immunocytochemical investigations in the septal cartilage of human embryos (7th week), in comparison to the adult human septal cartilage (Native NC), and primary cultures of these latter cells (NC in culture).

9. Flow cytometry – titration

At the beginning of the cytometry experiment, titrations were made for each individual antibody, using increasing dilutions, in order to identify the minimum fluorescence intensity and to obtain optimal results.

- *Figure 35* shows an example of antibody titration, in particular for the mesodermal marker FoxF1 using its isotype control, cellular control and increasing dilutions (shown from bottom to top), starting from the dilution recommended by the manufacturer (1:100).

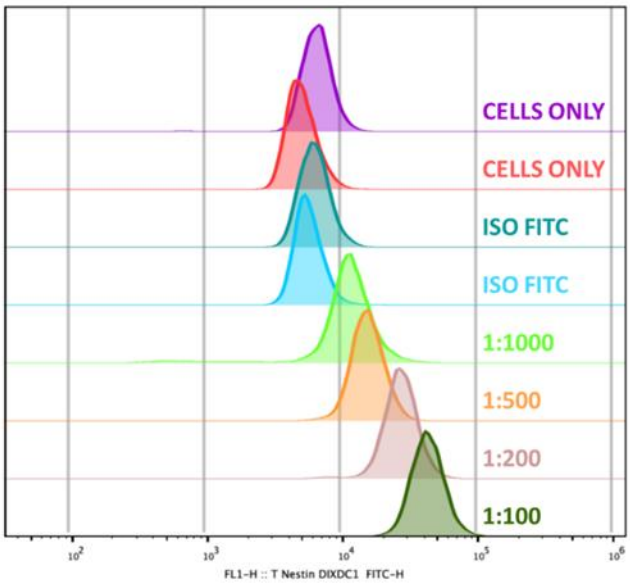

Figure 35: Example of titration experiment for flow cytometry marker. In this case is show the mesodermal marker FoxF1 using its isotype control (ISO FITC), cellular control (CELLS ONLY) and increasing dilutions starting from the dilution recommended by the manufacturer (recommended 1:100).

10. Flow cytometry characterization of nasal chondrocytes

Once all the antibodies were titrated, we proceeded to characterize human nasal chondrocytes (NC), expanded with a culture medium that stimulates stemness, using two different controls as a comparison: human bone marrow cells (BM) and human chondrocytes NC differentiated (P0) to simulate a primary culture derived directly from cartilage biopsy.

- *Figure 36* shows part of the graphical outputs of the combined analysis of SSEA-4 (plasma membrane mesodermal marker) with the intracellular markers of the mesodermal lineage (Brachyury and FoxF1) for the treaties (NC cells) and controls (BM cells). Table 10 shows the quantitative values derived from all combinations performed in the combined expression of the

mesodermal markers. Based on these results, up to 90% of these cells exhibit positivity to mesodermal lineage markers.

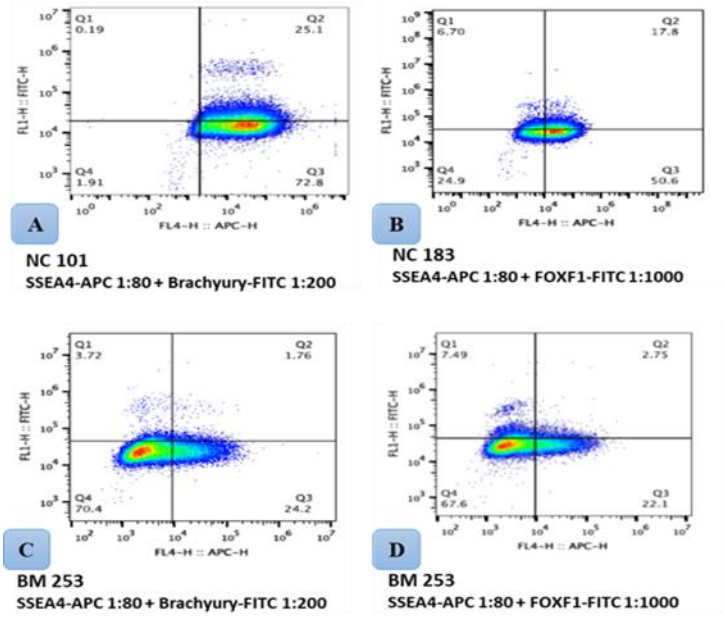

	Brachyury			FoxF1		
Brach +	1,31%		3,72%	/		
FoxF1 +	/			5,46%	4,12%	7,49%
SSEA4 +	69,60%		24,20%	36,63%	69,80%	22,10%
Double +	18,00%		1,76%	47,27%	17,80%	2,75%
Double -	11,09%		70,32%	10,64%	8,30%	67,66%
	Nasal	P0	CTRL	Nasal	P0	CTRL

Figure 36: flow cytometry outputs of the combined analysis between: ***a.*** *SSEA-4 and Brachyury in NC 101;* ***b.*** *SSEA-4 and FoxF1 in NC 183;* ***c.*** *SSEA-4 and Brachyury in BM 253;* ***d.*** *SSEA-4 and FoxF1 in BM 253. Brachyury or FoxF1 positive cells are represented in the quadrant 1 (Q1). SSEA-4 positive cells are represented in the quadrant 3 (Q3). Double positive cells are represented in the quadrant 2 (Q2), while double negative cells are represented in quadrant 4 (Q4).*

- *Figure 37* shows part of the graphical outputs of the combined analysis of P75 (plasma membrane neuroectodermal marker) with the intracellular markers of the neuroectodermal lineage (Dixdc1, Nestin and FoxD3) for the treaties (NC cells) and controls (BM cells). Table 11 shows the quantitative values derived from all combinations performed in the combined expression of the neuroectodermal/neural crest markers. Based on these results, up to 80% of these cells exhibit positivity to neuroectodermal lineage markers.

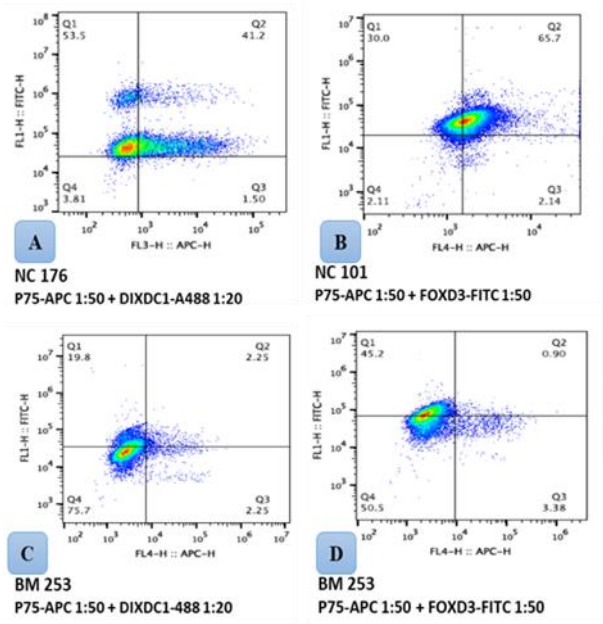

	Dixdc1			Nestin			FoxD3		
Dixdc1 +	37,03%	13,20%	19,80%	/			/		
Nestin +	/			2,86%		0,97%	/		
FoxD3 +	/			/			39,93%	76,90%	45,20%
P75 +	5,57%	4,66%	2,25%	12,55%		5,10%	4,01%	1,31%	3,38%
Double +	**16,13%**	**4,69%**	**2,25%**	**0,60%**		**0,10%**	**45,53%**	**14,90%**	**0,90%**
Double -	**41,27%**	**77,45%**	**75,70%**	**84,00%**		**93,83%**	**12,52%**	**6,89%**	**50,52%**
	Nasal	P0	CTRL	Nasal	P0	CTRL	Nasal	P0	CTRL

Figure 37: flow cytometry outputs of the combined analysis between: ***a.*** *P75 and Dixdc1 in NC 176;* ***b.*** *P75 and FoxD3 in NC 101;* ***c.*** *P75 and Dixdc1 in BM 253;* ***d.*** *P75 and FoxD3 in BM 253. Dixdc1 or FoxD3 positive cells are represented in the quadrant 1 (Q1). P75 positive cells are represented in the quadrant 3 (Q3). Double positive cells are represented in the quadrant 2 (Q2), while double negative cells are represented in quadrant 4 (Q4).*

- *Figure 38* shows part of the graphical outputs of the combined analysis of P75 (plasma membrane neuroectodermal marker) with SSEA-4 (plasma membrane mesodermal marker) for the treaties (NC cells) and controls (BM cells). Table 12 shows the quantitative values derived from all combinations performed in the combined expression between the neuroectodermal and mesodermal marker. Based on these results, up to 16% of these cells exhibit positivity to both neuroectodermal and mesodermal lineage markers.

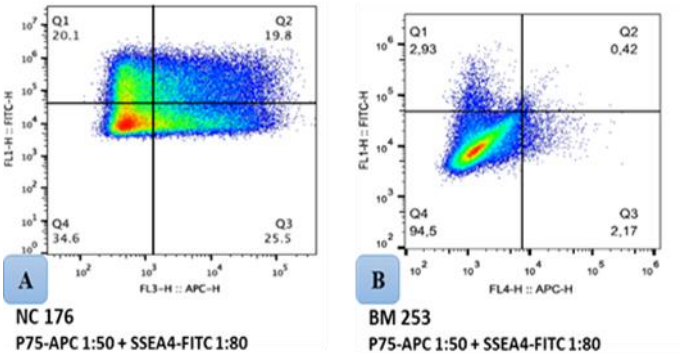

	SSEA4		
P75 +	14,87%	0,69%	2,17%
SSEA4 +	30,83%	7,94%	2,93%
Double +	**13,26%**	**16,00%**	**0,42%**
Double -	**41,00%**	**90,99%**	**94,50%**
	Nasal	P0	CTRL

Figure 38: flow cytometry outputs of the combined analysis between: ***a.*** *P75 and SSEA-4 in NC 176;* ***b.*** *P75 and SSEA-4 in BM 253. SSEA-4 positive cells are represented in the quadrant 1 (Q1). P75 positive cells are represented in the quadrant 3 (Q3). Double positive cells are represented in the quadrant 2 (Q2), while double negative cells are represented in quadrant 4 (Q4).*

- *Figure 39* shows part of the graphical outputs of the combined analysis of P75 (plasma membrane neuroectodermal marker) with the intracellular markers of the mesodermal lineage (Brachyury and FoxF1) for the treaties (NC cells) and controls (BM cells). Table 13 shows the quantitative values derived from all combinations performed in the combined expression between neuroectodermal and mesodermal lineage markers. Based on these results, up to 30% of these cells exhibit positivity to both neuroectodermal and mesodermal lineage markers.

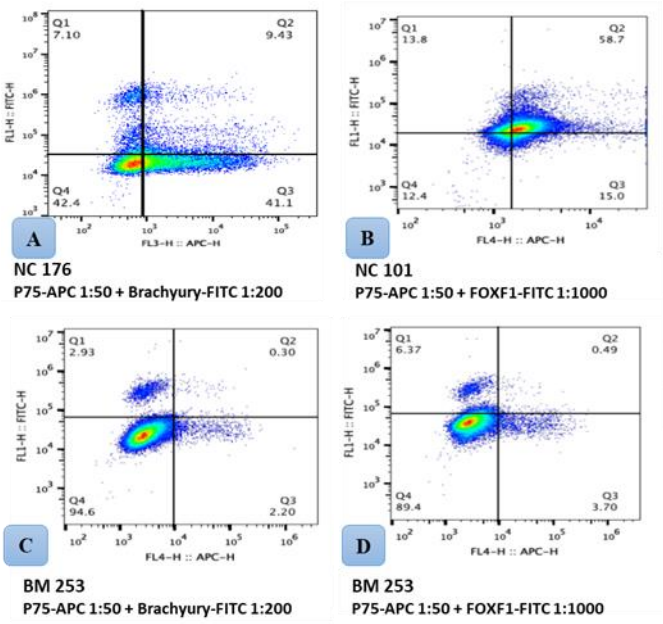

	Brachyury			FoxF1		
Brach +	23,93%	13,50%	2,93%	/		
FoxF1 +	/			20,96%	13,40%	6,37%
P75 +	11,42%	15,30%	2,17%	14,66%	6,14%	3,70%
Double +	**6,84%**	**7,82%**	**0,42%**	**32,16%**	**6,23%**	**0,49%**
Double -	**57,81%**	**63,40%**	**94,50%**	**33,20%**	**74,23%**	**89,44%**
	Nasal	P0	CTRL	Nasal	P0	CTRL

Figure 39: flow cytometry outputs of the combined analysis between: ***a.*** *P75 and Brachyury in NC 176;* ***b.*** *P75 and FoxF1 in NC 101;* ***c.*** *P75 and Brachyury in BM 253;* ***d.*** *P75 and FoxF1 in BM 253. Brachyury or FoxF1 positive cells are represented in the quadrant 1 (Q1). P75 positive cells are represented in the quadrant 3 (Q3). Double positive cells are represented in the quadrant 2 (Q2), while double negative cells are represented in quadrant 4 (Q4).*

- *Figure 40* shows part of the graphical outputs of the combined analysis of SSEA-4 (plasma membrane mesodermal marker) with the intracellular markers of the neuroectodermal lineage (Dixdc1, Nestin and FoxD3) for the treaties (NC cells) and controls (BM cells). Table 14 shows the quantitative values derived from all combinations performed in the combined expression between neuroectodermal and mesodermal lineage markers. Based on these results, up to 80% of these cells exhibit positivity to both neuroectodermal and mesodermal lineage markers.

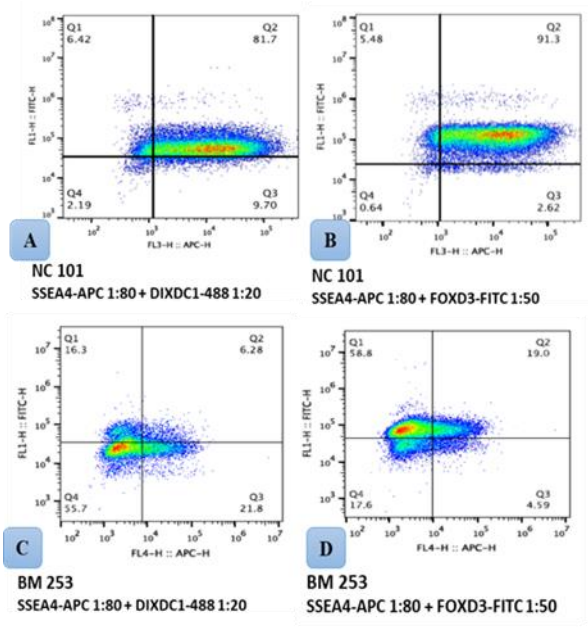

	Dixdc1			Nestin			FoxD3		
Dixdc1 +	6,64%	6,59%	16,30%	/			/		
Nestin +	/			1,96%		0,42%	/		
FoxD3 +	/			/			12,06%	8,80%	58,80%
SSEA4 +	20,69%	56,00%	21,80%	66,30%		26,20%	4,14%	16,20%	4,59%
Double +	65,33%	26,30%	6,28%	2,13%		0,13%	81,87%	66,70%	19,00%
Double -	7,34%	11,11%	55,62%	29,62%		73,25%	1,93%	8,22%	17,60%
	Nasal	P0	CTRL	Nasal	P0	CTRL	Nasal	P0	CTRL

*Figure 40: flow cytometry outputs of the combined analysis between: **a.** SSEA-4 and Dixdc1 in NC 101; **b.** SSEA-4 and FoxD3 in NC 101; **c.** SSEA-4 and Dixdc1 in BM 253; **d.** SSEA-4 and FoxD3 in BM 253. Dixdc1 or FoxD3 positive cells are represented in the quadrant 1 (Q1). SSEA-4 positive cells are represented in the quadrant 3 (Q3). Double positive cells are represented in the quadrant 2 (Q2), while double negative cells are represented in quadrant 4 (Q4).*

11. Proteomic signature of human nasal chondrocytes

Human nasal chondrocytes (NC) were analyzed using a high-performance liquid chromatographer coupled with a mass spectrometer, in order to obtain information about the protein expression of these cells. In particular, we analyzed the nasal septal cells from 2 different patients (NC101 and NC176), and we added to the analysis another type of cell, the differentiated nasal chondrocytes (P0), deriving from NC101 submitted to differentiation medium (see materials and methods, chapter 10).

- *Figure 41* displays Scatter Plot and Multiple Scatter Plot graphs for NC176, NC101 and P0 samples. The replicates of each group show a high similarity in protein expression, confirming the success of the mass spectrometry analysis and the consistence of the obtained results.

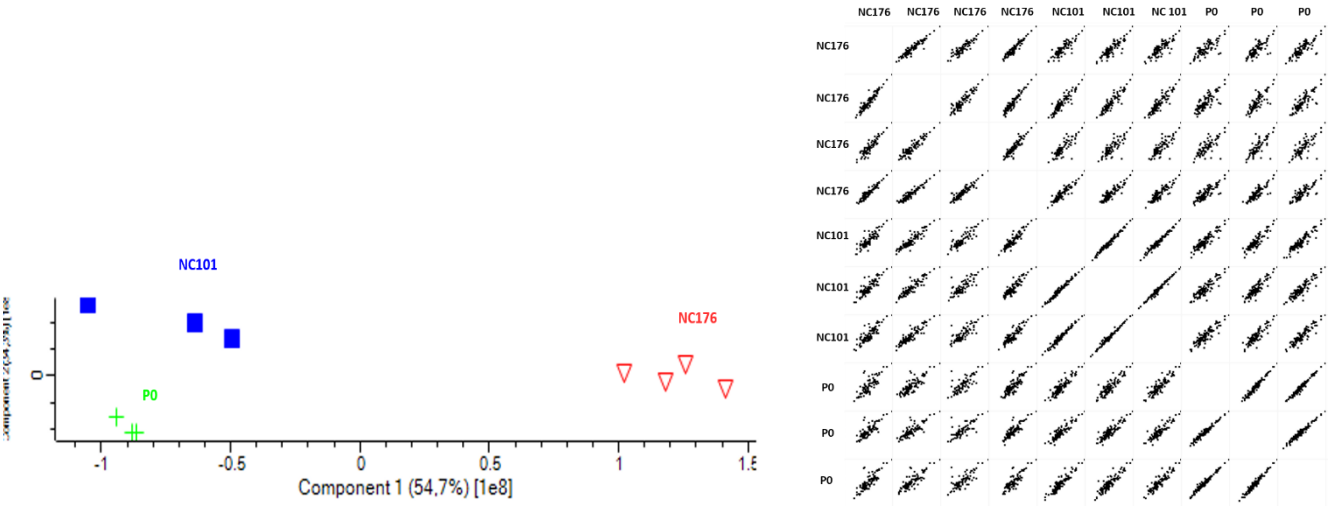

Figure 41: Similarities in protein expression between replicates of each sample group (NC176, NC101 AND P0). Scatter Plot (left) and Multiple Scatter Plot (right) graphs.

- *Figure 42* shows Venn's diagram of protein expression overlapping between the nasal chondrocytes and differentiated nasal cells. As expected, the common protein expression is very low, demonstrating the adequacy of chondrocyte differentiation protocol, and also the effective functionality of the expansion/dedifferentiation medium used for NC cells. The overlap of the protein results 27,0% between NC176 and P0, and 25,2% between NC101 and P0. The NC176 *vs* NC101 protein expression exhibits a more shared expression (35,2%), although the variability between patients remain elevated (data not shown).

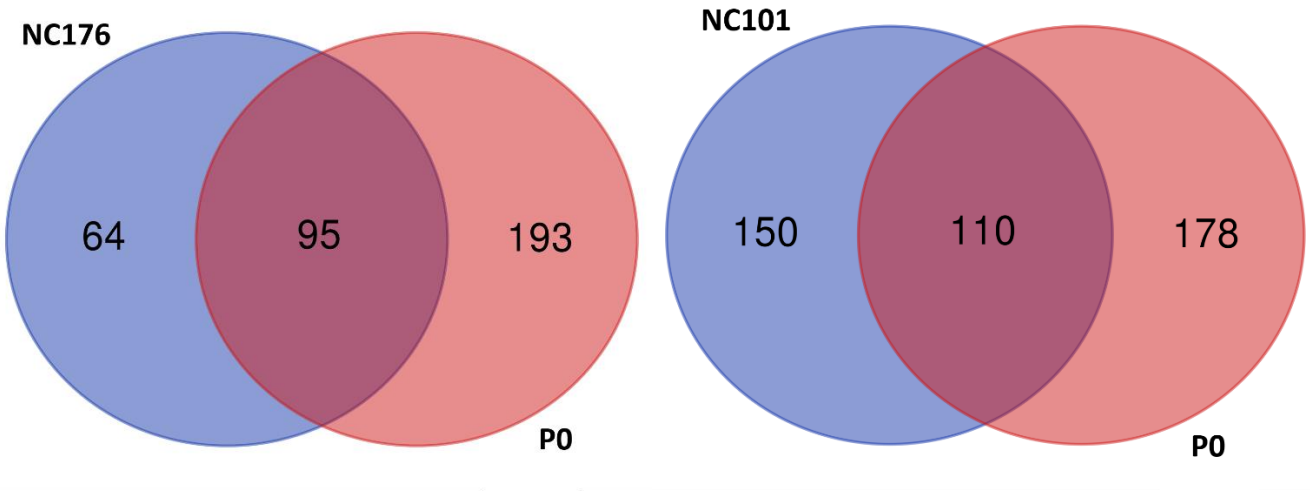

Figure 42: Venn's diagrams of protein expression overlap between NC176 and P0 (left) and NC101 and P0 (right).

- *Figure 43* displays the HeatMap of protein expression comparison between NC176, NC101 and P0. The Hierarchical clustering associated with HeatMap highlights the similarity of the replicates of each sample group, and exhibits a greater analogy between NC176 and NC101 cells, respect to P0.

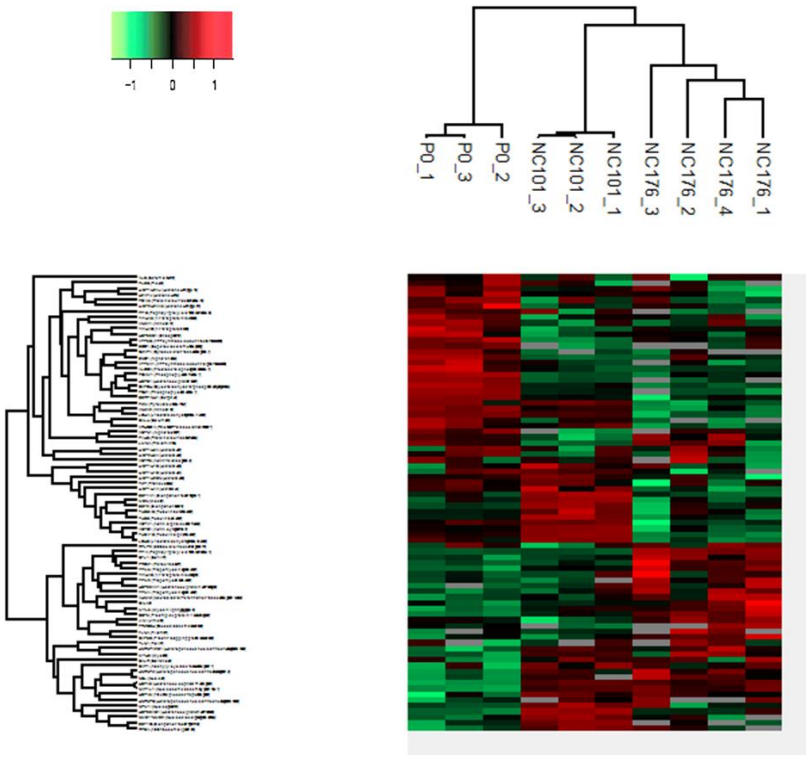

Figure 43: HeatMap and Hierarchical clustering of protein expression comparison between NC176, NC101 and P0. The expression pattern is represented by colours, from light green (-1) to light red (1). Grey bands depict a protein not identified in the sample.

- *Table 12* represents the 20 most down- and up-regulated proteins in human nasal chondrocytes NC176 respect to differentiated P0 cells. Down- and up-regulated proteins between the 2 samples are very similar considering the biological functions. In fact, both schemes contain about the same number of catabolic / metabolic process and cell morphogenesis, development, regulation and organization mechanisms.

DOWN-REGULATED		
PROTEIN NAME	GENE NAME	GO BIOLOGICAL PROCESS
L-lactate dehydrogenase A chain	LDHA	alcohol catabolic process;alcohol metabolic process;carbohydrate catabolic process
Phosphoglycerate kinase 1	PGK1	alcohol biosynthetic process;alcohol catabolic process;alcohol metabolic process
Heat shock protein beta-1	HSPB1	biological regulation;cell death
Serpin H1	SERPINH1	biological regulation;biosynthetic process;cellular component organization
Annexin A2	ANXA2;ANXA2P2	anatomical structure development;anatomical structure formation involved in morphogenesis;angiogenesis;biological regulation
Phosphoglycerate mutase 1	PGAM1	alcohol biosynthetic process;alcohol catabolic process;alcohol metabolic process
Histone H2A.V	H2AFV;H2AFZ	cellular component assembly;cellular component organization
Cytoskeleton-associated protein 4	CKAP4	cytoskeleton-linking membrane protein
Histone H2A type 2-A	HIST2H2AA3;HIST2H2AC	cellular component assembly;cellular component organization
Glyceraldehyde-3-phosphate dehydrogenase	GAPDH	alcohol biosynthetic process;alcohol catabolic process;alcohol metabolic process
Calumenin	CALU	cell activation;cellular process;establishment of localization
Histone H4	HIST1H4A	anatomical structure homeostasis;ATP-dependent chromatin remodeling;biological regulation;cellular component assembly
Histone H2B	HIST1H2BN;HIST1H2BM;HIST1H2BH;HIST2H2BF;HIST1H2BC;HIST1H2BD;HIST1H2BL	cellular component assembly;cellular component organization
Actin, alpha skeletal muscle	ACTA1;ACTC1	actin cytoskeleton organization;actin filament organization
Peptidyl-prolyl cis-trans isomerase B	PPIB	cellular component organization
Tubulin alpha-1B chain	TUBA1B;TUBA4A	cell activation;cell cycle process;cell division;cellular component assembly
Histone H2A type 1-J	HIST1H2AJ;HIST1H2AH;HIST1H2AG;H2AFJ;HIST1H2AD;HIST2H2AB;H2AFX	biological regulation;cell cycle checkpoint;cell cycle phase;cell cycle process
Fructose-bisphosphate aldolase A	ALDOA	actin cytoskeleton organization;actin filament organization
Plectin	PLEC	cell junction assembly;cell junction organization;
14-3-3 protein zeta/delta	YWHAZ	amine transport;biological regulation;cell activation;cellular component organization

UP-REGULATED		
PROTEIN NAME	GENE NAME	GO BIOLOGICAL PROCESS
Cofilin-1	CFL1	actin cytoskeleton organization;actin filament depolymerization
Nucleolin	NCL	anatomical structure formation involved in morphogenesis;angiogenesis;developmental process
Peptidyl-prolyl cis-trans isomerase A	PPIA	biological regulation;biosynthetic process;cell activation;cell migration;cell motility
Filamin-A	FLNA	actin crosslink formation;actin cytoskeleton organization; anatomical structure formation involved in morphogenesis
Tropomyosin alpha-3 chain	TPM3	actin filament-based movement;actin filament-based process;actin-mediated cell contraction
Nucleosome assembly protein 1-like 1	NAP1L1	biological regulation;biosynthetic process;cellular biosynthetic process;cellular component assembly
Neuroblast differentiation-associated protein AHNAK	AHNAK	anatomical structure development;developmental process;nervous system development
Myosin-9	MYH9	actin cytoskeleton organization;actin cytoskeleton reorganization;actin filament-based movement
T-complex protein 1 subunit epsilon	CCT5	cellular macromolecule metabolic process;cellular metabolic process
Heat shock cognate 71 kDa protein	HSPA8	biological regulation;biosynthetic process;cellular biosynthetic process;cellular component organization
78 kDa glucose-regulated protein	HSPA5	activation of signaling protein activity involved in unfolded protein response;anatomical structure arrangement;anatomical structure development
Myosin light polypeptide 6	MYL6	actin filament-based movement;actin filament-based process;actin-mediated cell contraction
Heat shock protein HSP 90-alpha	HSP90AA1	apoptosis;axon guidance;biological regulation;cardiac muscle cell apoptosis;cell cycle process;cell death;cell migration;cell motility
Calmodulin-3	CALM3	response to amine stimulus;response to amphetamine;response to chemical stimulus
Adenylyl cyclase-associated protein 1	CAP1	actin cytoskeleton organization;actin filament-based process;activation of adenylate cyclase activity
Tropomyosin beta chain	TPM2	actin filament-based movement;actin filament-based process;actin-mediated cell contraction
Peroxiredoxin-1	PRDX1	anatomical structure development;biological regulation;catabolic process;cell killing;cell proliferation
Heterogeneous nuclear ribonucleoprotein K	HNRNPK	biological regulation;cellular macromolecule metabolic process;cellular metabolic process
Heterogeneous nuclear ribonucleoproteins C1/C2	HNRNPC	cellular macromolecule metabolic process;cellular metabolic process
F-actin-capping protein subunit beta	CAPZB	actin cytoskeleton organization;actin filament capping;actin filament-based process;biological regulation

Table 12: Schemes of the 20 most down- and up-regulated proteins in human nasal chondrocytes NC176 respect to differentiated P0 cells. Catabolic and metabolic process are underlined in black, while cell organization, regulation, development and morphogenesis mechanisms are underlined in red.

- *Table 13* shows the 20 most down- and up-regulated proteins in human nasal chondrocytes NC101 respect to differentiated P0 cells. Several proteins of both down- and up-regulated schemes are involved in the cell regulation, organization, development and morphogenesis. However, among the up-regulated proteins was observed a decrease of the catabolic / metabolic ones, with an increase in regulation, organization, developmental and morphogenetic mechanisms.

DOWN-REGULATED		
PROTEIN NAME	GENE NAME	GO BIOLOGICAL PROCESS
Phosphoglycerate kinase 1	PGK1	alcohol biosynthetic process;alcohol catabolic process;alcohol metabolic process
Heat shock protein beta-1	HSPB1	biological regulation;cell death
Phosphoglycerate mutase 1	PGAM1	alcohol biosynthetic process;alcohol catabolic process;alcohol metabolic process
Serpin H1	SERPINH1	biological regulation;biosynthetic process;cellular component organization
Cytoskeleton-associated protein 4	CKAP4	cytoskeleton-linking membrane protein
Alpha-actinin-1	ACTN1	actin crosslink formation;actin cytoskeleton organization
L-lactate dehydrogenase A chain	LDHA	alcohol catabolic process;alcohol metabolic process
Histone H2A type 2-A	HIST2H2AA3;HIST2H2AC	cellular component assembly;cellular component organization
Superoxide dismutase [Cu-Zn]	SOD1	activation of MAPK activity;aging;amine metabolic process
Histone H2A.V	H2AFV;H2AFZ	cellular component assembly;cellular component organization
14-3-3 protein theta	YWHAQ	biological regulation;cellular component organization
Prelamin-A/C	LMNA	activation of signaling protein activity involved in unfolded protein response;anatomical structure development;biological regulation
Protein disulfide-isomerase	P4HB	4-hydroxyproline metabolic process;amine metabolic process
14-3-3 protein zeta/delta	YWHAZ	amine transport;biological regulation;cell activation;cellular component organization
Annexin A2	ANXA2;ANXA2P2	anatomical structure development;anatomical structure formation involved in morphogenesis; angiogenesis;biological regulation
Glyceraldehyde-3-phosphate dehydrogenase	GAPDH	alcohol biosynthetic process;alcohol catabolic process;alcohol metabolic process
Fructose-bisphosphate aldolase A	ALDOA	actin cytoskeleton organization;actin filament organization
ATP synthase subunit beta, mitochondrial	ATP5B	anatomical structure formation involved in morphogenesis;angiogenesis; ATP biosynthetic process
Alpha-enolase	ENO1	alcohol biosynthetic process;alcohol catabolic process;alcohol metabolic process
Plectin	PLEC	cell junction assembly;cell junction organization;cellular component assembly

UP-REGULATED		
PROTEIN NAME	GENE NAME	GO BIOLOGICAL PROCESS
Moesin	MSN	biological adhesion;biological regulation; cell migration;cell motility
Nucleolin	NCL	anatomical structure formation involved in morphogenesis;angiogenesis; developmental process
Heat shock protein HSP 90-beta	HSP90AB1	anatomical structure development;axon guidance;biological regulation;cellular component organization
Nucleosome assembly protein 1-like 1	NAP1L1	biological regulation;biosynthetic process; cellular component assembly
Myosin-9	MYH9	actin cytoskeleton organization
Nucleophosmin	NPM1	aging;ATP-dependent chromatin remodeling;biological regulation;cell aging;cell cycle process
Elongation factor 2	EEF2	biosynthetic process;cellular macromolecule biosynthetic process
78 kDa glucose-regulated protein	HSPA5	activation of signaling protein activity involved in unfolded protein response;anatomical structure development;biological regulation
Heat shock cognate 71 kDa protein	HSPA8	biological regulation;biosynthetic process; cellular component organization
Adenylyl cyclase-associated protein 1	CAP1	actin cytoskeleton organization;actin filament-based process
Tubulin beta chain	TUBB	biological regulation;cell cycle process;cell division;cell killing;cellular component assembly
Histone H1.5	HIST1H1B	cellular component assembly;cellular component organization
Elongation factor 1-alpha 1	EEF1A1;EEF1A1P5	biological regulation;biosynthetic process;catabolic process
Cofilin-1	CFL1	actin cytoskeleton organization;actin filament depolymerization
Tubulin beta-4B chain	TUBB4B;TUBB4A	biological regulation;cell cycle process;cell killing;cellular component assembly
Tropomyosin alpha-3 chain	TPM3	actin filament-based movement
Elongation factor 1-gamma	EEF1G	multi-organism process;response to biotic stimulus
40S ribosomal protein SA	RPSA	biological adhesion;biosynthetic process;catabolic process
Nucleoside diphosphate kinase	NME1-NME2; NME2;NME2P1	biological adhesion;biological regulation;biosynthetic process
Myosin light polypeptide 6	MYL6	actin filament-based movement;actin-mediated cell contraction

Table 13: Schemes of the 20 most down- and up-regulated proteins in human nasal chondrocytes NC101 respect to differentiated P0 cells. Catabolic and metabolic process are underlined in black, while cell organization, regulation, development and morphogenesis mechanisms are underlined in red.

DISCUSSION

1. *In silico* mass spectrometry analysis of adult rat thyroid stem cells / progenitors

As show previously, adult male rat TSC/P tend to express both endoderm/epithelial and mesenchyme markers, with a slightly predominance of the latter. Moreover, a small percentage is represented by neuroectodermal markers, in agreement with very recent evidence that the neural crest contribute to the development of the thyroid gland giving rise to its stromal matrix and, possibly to other still unknown progenitor cells [165]. This evidence implies a heterogeneity of this cell population (58% Mesoderm – 36% Endoderm – 6% Neuroectoderm), probably due to both the tissue source used for the primary culture and the starvation process to isolate the staminal counterpart. To further study the proteomic signature of these cells, a triple quadrupole analysis was carried out, thanks to the collaboration with Prof. Lisa Elviri, Food and Drug Department, University of Parma. The resulted semiquantitative evaluation based on score values depicted an increase in the number of markers of neuroectodermal lineage, with few markers of endoderm and an evidence of some proteins of epithelial-mesenchymal transition.

In particular, endodermal marker hepatocyte nuclear factor HNF-4a, a transcription factor expressed early in endoderm formation [166;167], was detected in both THY and TSC/P cells, with a slightly predominance in primary culture thyrocytes. This factor is also not expressed in differentiated thyroid cells [168]. In addition, expression of HNF-4a is not detectable in cells of neuroectodermal origin [166;169], confirming another time the heterogeneity of the population.

Similar, also endodermal marker PAX9 has been found in THY and TSC/P, which represents a marker of pharyngeal endoderm and then specific for cells in a non-differentiated state [170;171].

These evidences indicate the presence of a percentage of undifferentiated endodermal stem cells also in the population of differentiated thyrocytes.

Neuroectodermal markers HoxA2 and HoxC5 were detected in both THY and TSC/P, with a slightly predominance in the thyroid stem/progenitor population. It was demonstrated that Hox-positive neural crest–derived cells from posterior rhombomeres could not substitute for Hox-negative cells after transplantation into anterior domains, but by contrast, Hox-negative neural crest–derived cells could replace Hox-positive cells, leading to normal tissue formation [172]. HoxA2, a Hox-positive neural crest markers, is important for the developmental potentials of the Neural crest cells (NCCs), because targeted mutation of Hox-A2 in mice leads to partial duplication of the lower jaw at the expense of the normal BA2 skeleton (the hyoid cartilage) [173;174;175;176]. HoxC5, instead, can be inserted in the group of Hox-negative neural crest marker, although it could be weakly expressed sometimes. This Hox-negative status was proposed to reflect a higher level of self-renewal capacity in totipotent human embryonic stem cells [177] and functionally distinct human stem cell populations derived from cord blood [178]. Therefore, the Hox genes in THY and TSC/P suggests the presence of a neuroectoderm / neural crest group of cells into the population, confirming the Orbitrap analysis results.

Similar, Tubulin-b3 (TUBB3) is a well – known neuroectodermal marker found in both THY and TSC/P populations, confirming what affirmed before. In fact, TUBB3 is an element of microtubules, which are dynamic components of the intracellular cytoskeleton that have been linked to NC cell migration [179;180]. TUBB3 is an established marker of proliferative and terminally differentiated neurons [181;182;183], and it resides in cells that are either

differentiating into, or have already become neurons, because its expression overlaps with cells that will become both the central nervous and peripheral nervous systems [184].

Epithelial -mesenchymal transition marker (EMT) Snail/Slug transcription factor is one prominent example of a common downstream target of various signalling pathways that regulates EMT. Of the three vertebrate Snail family members of zinc finger proteins (Snail1, Snail2, and Snail3), the functionally equivalent Snail1 and Snail2 (which was formerly known as Slug) mediate EMT. In fact, all known EMT events during development, cancer, and fibrosis appear to be associated with Snail activation [185]. In fact, the Snail/Slug signal regulates various aspects of the EMT phenotype, such as increased expression of mesenchymal cell / fibroblast markers (fibronectin and vitronectin), decreased expression of various epithelial markers (claudins, occludins, and cytokeratins), inhibition of proliferation through suppression of cyclin D proteins and cyclin-dependent kinase 4 (CDK4), increased MMP expression, and protection from cell death (through suppression of expression of caspases, DNA fragmentation factor, and Bcl – interacting death agonist) [186].

Twist, another EMT marker, is a basic helix-loop-helix protein that is transcriptionally active during lineage determination and cell differentiation. It is upregulated during early embryonic morphogenesis [187;188], tissue fibrosis [189;190], and cancer metastasis [191]. In the development of metastatic cancer cells by type 3 EMT, Twist can act independently of Snail to repress E-cadherin [192] and to upregulate fibronectin and N-cadherin [193]. Together with Snail/Slug marker, it is a key factor for both *in vitro* and *in vivo* EMT transition [186].

In silico LC-MS/MS SRM analysis results support the evidence derived from the previous analysis, in which the population exhibited not only mesodermal markers, but also endodermal and specially neuroectodermal markers, as well as epithelial – mesenchymal transition markers. These clues seem to confirm the original assumption of our group that a large fraction

of our rat TSC/P are ectomesenchymal cells of neural crest origin, although a minor effect on the induction of a mesenchymal phenotype was triggered by the monolayer culture *per se*, as suggested by the presence of few markers of epithelial-mesenchymal transition.

2. Hepatic differentiation of adult rat thyroid stem cells / progenitors

Adult multipotent stem cells and, possibly also uncommitted progenitors of the male rat thyroid gland have been used to set up an original and alternative method of hepatic differentiation, allowing for *in vitro* long – term establishment and maintenance of a hepatocyte-like cell source. The common endodermic origin shared by thyroid and hepatic stem cells/progenitors has been exploited for this aim; in particular, the knowledge that both differentiated thyrocytes and hepatocytes express the hepatocyte growth factor (HGF) receptor Met [194] has suggested to us that the mitogenic action of its ligand HGF [195;196] might exert a key role to induce hepatic differentiation of multipotent adult, thyroid stem cells.

Based on these premises, two original protocols of hepatic differentiation have been developed, with the intent to *in vitro* mimic the three classical phases of differentiation *in vivo* including mesodermic induction, hepatoblast, and hepatocyte steps thus preventing cells to shift towards the cholangiocyte lineage [80;197]. To this aim, each protocol had its own cocktail of growth factors added in sequence and at difference dosages, to provide a temporal gradient as expected for morphogens during liver organogenesis [3;49].

Protocol 1

Protocol 1 was characterized by the very early presence and long-term administration of moderate concentrations of HFG (also known as Scatter Factor), whose pleiotropic activity comprises stimulation of growth, migration, and morphological changes of a variety of mesodermal and endodermal cell types, including those of the hepatic lineage [194]. HGF was coupled to equal dosages of the potent, tyrosine kinase-dependent epithelial growth activator, EGF. EGF is one of the primary mitogens for mammalian hepatocytes [198] *in vitro* and has been shown to trigger liver regeneration after partial hepatectomy in the rat *in vivo* (similar to HGF). As such, it is believed to be essential to program a hepatic commitment during the first differentiation phase, in particular from day 3 to 15 (mesodermic induction and hepatoblast step). However, in our system it is unlikely that EGF regulates the development of epithelial intermediate filaments like cytokeratins, as suggested by their equal variations in differentiating cells irrespective of its presence or absence in the culture medium (see below protocol 2).

Protocol 1 was also constantly supplemented with the mesenchymal regulator bFGF, a pleiotropic growth factors that control cell proliferation, migration and differentiation, that has been shown to be released *in vivo* in high dose by the cardiogenic mesoderm during the very early induction phase [3;49], and known also for its markedly increase after liver injury [79]. Using this growth factor combination, adequate biosynthesis of early hepatic markers was achieved, including AFP and HNF-3β production. This prompt differentiation response to protocol 1 was supported by the consistent cytoplasmic accumulation of glycogen, as shown by the PAS reaction and the progressive changes in cell morphology from a multipolar and/or spindle-like shape to a classical, hepatoblast-like polygonal geometry, within the first 15 days of culture as observed by light microscopic and SEM analysis.

Finally, since HGF concentration did not change during the last 15 days of differentiation but:

a) the process of morphological adequacy progressed to give rise to a pavement-like organization of polygonal elements with classical features of hepatocytes, including large and round nuclei, frequent binucleation, retracted borders, clustering and juxtaposition of cells as in the mature liver tissue, and oval-shaped satellite-like cells around the clusters and,

b) the biosynthesis of ALB became prominent,

we conclude that factors other than HGF in the differentiation medium should have played a determinant role for the hepatic phenotype progression. To this purpose, the presence of NTA as a source of NAD and NADP coenzymes is expected to have boosted a number of intracellular redox chains critical for maturation of the hepatocyte-like cells. In particular, it is well known that NTA promotes the maintenance of cytochrome P450 in rat hepatocyte cultures [199], preserves rat hepatocyte function in primary cultures [200], and increases rat hepatocyte proliferation using standard media [201]. In contrast, the high dose of the long-acting steroid hormone dexamethasone, a well know factor for differentiation of mammalian mesenchymal stromal cells [202;203], might have favoured the commitment of hepatoblast-like cells to a definitive hepatocyte-like phenotype [96]. Similar, the use of the Jak-Stat activator, oncostatin at the early mesodermal phase might have concurred to the committment to the hepatic phenotype, through its well – known capacity to stimulate the epithelial-mesenchymal transition of hepatic cells [204;205] that is also one of the key mechanisms that allows for the endodermal hepatic bud to become sensitive to the influence of the surrounding mesoderm (later to become the septum transversum), and to its specification clues [43; 44].

Adult rat thyroid stem cells / progenitors subjected to hepatic differentiation were analyzed in mass spectrometry at 3 different time point, early (3 days), intermediate (15 days) and late (30 days). The analysis shows that only 5,9% of protein remain expressed during all differentiation time, confirming the change in marker expression seen in immunocytochemistry for these cells.

In addition, it was observed a trend of shared proteins to decrease during differentiation time, as expected using a differentiation protocol. Remarkably, comparing treated TSC/P cells in protocol 1 with those of protocol 2, we observed a similar response to stimuli but a different protein expression. In fact, although both protocols cause an early change in proteome of thyroid stem cells, the diverse growth factors and administration timing bring to a different protein expression between the 2 protocols during all differentiation time (29,2% of shared proteins at 3 days of differentiation and 21,0% at 24/30 days). Another consideration is about the different expression observed between treated TSC/P and control cells at the beginning (3 days) and at the end (30 days) of the differentiation process using protocol 1. Indeed, the common proteins between differentiated and control cells seems to decrease with the progress of differentiation, as confirm by the 46,6% of shared proteins at 3 days against 30,0% of shared proteins at 30 days. Taking together, these evidences bring at the conclusion that protocol 1 causes not only the expression of typical hepatic markers and morphology, but also a progressively change in proteomic signature of this cells during differentiation time.

The HeatMap and Hierarchical clustering of differentiated and control TSC/P at 3 and 30 days of protocol 1 confirm the change in proteome occurred during differentiation period. In fact, differentiated 3 days, control 3 days and control 30 days samples resulted more similar then differentiated 30 days sample, highlighting the efficacy of the protocol 1. Moreover, another important information derives from the down- and up-regulated proteins observed in differentiated TSC/P at the end of differentiation period. Several down-regulated proteins in our differentiated cells are involved in catabolic / metabolic processes. In particular, L-lactate dehydrogenase, Glyceraldehyde-3-phosphate dehydrogenase, Pyruvate kinase and Alpha-enolase are proteins implicate in glycolysis, a very important pathway for the maintenance of a stemness state. In this sense, it is widely thought that the high rate of glucose uptake and

glycolysis is required to meet the needs of rapid proliferation of mouse PSCs [206], similar to the situation of cancer cells in the Warburg effect [207]. The Warburg effect operates predominantly in highly proliferative cells, such as cancer cells, to accumulate glycolytic intermediates for rapid proliferation while minimizing reactive oxygen species (ROS)-induced damage. Then, down-regulation of proteins involved in glycolytic pathway in TSC/P at the end of differentiation can be due to the fact that these cells leave their stemness state, characterized by high proliferation rate, and begin to differentiate (differentiation state is featured by strong decrease of cell proliferation).

On the other side, up-regulated protein in treated cells at the end of differentiation process are implicated in cell assembly, regulation, organization, development and morphogenesis. All these mechanisms are essential to permit proteomic and morphological cellular changes important for shift the initial peculiarity to the new ones, achieving the mature differentiated phenotype. Furthermore, the presence of Albumin in the up-regulated protein list is another attestation of the hepatic differentiation success using protocol 1, as observed also in immunocytochemistry. Also, Annexin II (Anx2), a Ca(2)-dependent phospholipid- and membrane-binding protein which has been reported to be up-regulated in fetal hepatoblasts during rat fetal development [208], resulted up-regulated in our differentiated TSC/P at 30 days, confirming the evidences derived by immunocytochemistry about the presence of hepatoblast-like cells. Interestingly, the most up-regulated protein in differentiated sample is Protein S100-A6 (also known as Calcyclin), a calcium-binding protein that belongs to the family of S100 proteins. Functions of Calcyclin pertaining to cell proliferation, cytoskeletal dynamics, and tumorigenesis are known for some cells and tissues [209], and it is well recognized also the important role of this protein to promote the proliferation of activated hepatic stellate cells (HSC). In fact, S100-A6 is secreted from HSCs and induces the proliferation of activated HSC

[210] probably via mitogen-activated protein kinase (MARK) activation, as reported in literature both *in vitro* using a recombinant S100-A6 for HCT116 cells and *in vivo* in tumor growth [211]. Moreover, Xia et al. [212] exhibit though cell cycle analysis as human recombinant S100-A6 could significantly induce the transition from S to G2 stage, leading to replication and cell proliferation. Kristensen et al. [210] demonstrate that the 3 growth- and proliferation-associated proteins, calcyclin, calgizzarin, and galectin-1, become heavily up-regulated in activated stellate cells. They show also as hepatocytes do not express calcyclin and galectin-1, which are markers for only hepatic stellate cells. In this sense, we could speculate that the up-regulation of S100-A6 protein and the down-regulation of galectin-1 and vimentin, another marker used for hepatic stellate cells [213], could be represent an intermediate state characterized by the presence of hepatic stellate-like cells (in a not still mature state) surrounded by hepatoblasts / hepatocytes, indicating as TSC/P, submitted to protocol 1, are able not only to differentiate *in vitro* in hepatoblasts and hepatocytes, but also to achieve hepatic stellate cells features. In addition, since the latter are a normal component of the liver *in vivo*, and are of mesodermal origin, the present *in vitro* evidence supports the original assumption that the large majority of our TSC/P are cell from an ectomesenchymal, neural-crest derived lineage easily driven to hepatoblast / hepatocytes and stellate cells once triggered with adequate differentiation factors.

Protocol 2

In contrast to protocol 1, protocol 2 was characterized by the absence of HGF in the very early phases of mesodermal induction being substituted by Activin A, a member of the TGFb superfamily well known for its ability to commit human embryonic stem cells to the endodermal lineage [214]. However, since at this early phase we did not observe a consistent biosynthesis

of hepatic markers like AFP and, later HNF-3β we conclude that Activin A is likely not necessary for thyroid stem cell induction to the hepatic lineage due to their endodermal origin, that does not require an endodermal shift from a totipotent condition.

A second feature of protocol 2 was the much higher concentration (more than two times) of HGF with respect to protocol 1, and its administration at slightly later times while keeping this dosage for the entire differentiation period. Since all morphological cellular changes resulted much weaker with this protocol than with protocol 1, especially at the end of the entire differentiation period we raise the hypothesis that the high dose of HGF could have paradoxically shutdown the initial shift to the hepatic lineage, as a consequence of a Met receptor saturation process, in a kind of tachyphylaxis. Possibly, later this induced a compensatory inhibition of progenitor replication, to restrain an excess of proliferation well known to interfere with any terminal differentiation process. This possibility seems confirmed by the very limited presence of glycogen and ALB in the last differentiation phase.

Finally, we cannot exclude that also the administration of EGF only at the end of the hepatoblast induction phase might have resulted in an insufficient activation of the initial hepatic differentiation program, leading to a disruption of the maturation steps of hepatoblasts into functional hepatocytes, as suggested by the presence of diffuse immature morphologies in the late cultures.

TSC/P mass spectrometry analysis revealed, as for protocol 1, a different protein expression between 3, 10 and 24 days, although in this case it was seen a lower change during differentiation process. The proteins amount maintained during all differentiation time was 14,9% (against 5,9% of protocol 1), about 2,5 times more than protocol 1. In addition, compared to protocol 1, we observed less protein changes from the beginning to the end of the differentiation. In particular, common proteins between treated and control cells at 3 days were

38,9%, while at 30 days they remained 37,5%, confirming the worse results obtained in immunocytochemistry with protocol 2 respect to protocol 1 (data not shown).

3. Hepatic differentiation of adult rat bone marrow – mesenchymal stem cells

It is well known the capacity of bone marrow – derived mesenchymal stromal cells to differentiate in cells derived from the three embryonic sheets (endoderm, mesoderm, neuroectoderm), making them a “gold standard” of *in vitro* differentiation and tissue bioengineering.

We choose rat MSCs of a well-known strain (Sprague-Dawley) at early culture passages (P4), in light of the recent evidence that rat MSCs exhibit a morphology and proliferation potential similar to human MSCs [215], more easily replicate at low seeding density than the human counterpart [216], may quickly reach at P2-P3 a stable immunophenotype, and their contamination by cells with haemopoietic features (e.g. CD45-positive) quickly disappears at early steps (P2-P3), although being variably dependent on the animal strain [138;217].

The bm-MSCs capacity to differentiate in hepatic cells is well known in literature [218;219;220]. In this sense, we tested the potential of adult rat bone marrow – derived mesenchymal stromal cells to reach hepatic features, under the influence of specific differentiation stimuli. For this purpose, the original protocols used are based on the sequential administration of growth factors, which are implicated in different phases of *in vivo* liver organogenesis, as mesoderm induction, hepatoblast differentiation and hepatocyte differentiation [3;49]. These original hepatic differentiation protocols are not provided of growth factors specific for cholangiocyte lineage [80;197], with the scope to restrict the study at only hepatocytes. Rat bm-MSCs

express, as mature hepatocytes, Met receptor for hepatocyte growth factor (HGF) [221;222]. This evidence suggested the importance of HGF as mitogenic factor to induce *in vitro* hepatic differentiation of bm-MSCs, as testified by the constant presence of this factor, although at variable concentrations, for both protocol 1 and 2 during differentiation period. Indeed, HGF is known for stimulate the growth, migration and morphological modifications in different endodermal and mesodermal (like bm-MSCs) cell types [194].

Protocol 1

In protocol 1, the main factor constantly present is HGF, which has different and also contrast influence on mesodermal and endodermal cells, as said before. The HGF action is combined with EGF function, epithelial tyrosine kinase – dependent growth factor, essential *in vivo* for hepatic regeneration after partial hepatectomy in rat model [223] and to direct hepatic stem cells to epatogenic differentiation during early stages of organ maturation (3 – 15 days), as well as to be a well-known mitogen for hepatocytes *in vitro*. However, because the EGF maturational action in liver organogenesis is based on epithelial intermediate filament development regulation (as cytokeratins), we deduce that EGF could not be a critical factor for bm-MSCs cytokeratins induction, as attested by the cytokeratin expression limited at the first 3 days of protocol 1 differentiation period.

Another growth factor constantly present in our protocol is bFGF, which is important for proliferative regulation, migration and differentiation in several cellular types. *In vivo*, it is released in large quantities by cardiac mesoderm during earlier stages of hepatic induction [3; 49] and, moreover, it is detectable at high concentration in the hepatic tissue after an hepatic damage [79], as mentioned before.

Last but not least, oncostatin M, a Jack – Stat intracellular transduction system activator, could have perform a role to stimulate the terminal differentiation to hepatocytes, because it is well-known to encourage *in vitro* an increase of albumin levels and glycogen accumulations, with consequent decrease of α-fetoprotein marker [204;205]. In addition, as specified before, oncostatin M is involved, *in vivo*, to make the hepatic endodermal foregut sensitive to the influence of the surrounding mesoderm (which will become the septum trasversum) and to specification signals [43; 44].

Based on these premises, we speculate that the positivity observed for all analysed hepatic markers has been partially related to the differentiation time *in vitro*. The early hepatic marker AFP, which was observed with remarkable positivity at 3 days of differentiation, decreasing progressively at 7 and 10 days (as expected for a typical in vitro hepatic differentiation), while HNF-3β, which showed weak positivity at 7 days, and cytokeratins, which were observed at 3 days, exhibited an expression timing compatible with an initial hepatic differentiation process, as report in literature. Also the late hepatic marker ALB highlighted an homogeneous immunoreactivity at 10 days, with few positive cells at the end of differentiation (30 days). At the end, the morphological changes study, evaluated through haematoxylin – eosin staining and scanning electron microscope analysis, showed some single cells (and few cells groups) with polygonal shape and round and central nuclei, typical features of mature hepatocytes, at the end of differentiation period. Moreover, glycogen storage analysis, performed using Periodic Schiff's Acid histochemical reaction, displayed a progressively increase in number of accumulations from 3 days to 15 and then 30 days, suggesting an activation of the glycogenic function.

Considering these results, we suggest the idea that adult rat bm-MSCs are able to initiate but not efficiently terminate the differentiation in hepatic lineage, using the growth factor mix specific

for hepatic induction, as report in literature [79;224]. Between the different cytokines administered in cell culture medium there is also dexamethasone [202;203], an important factor to promote the maturation from hepatoblast to hepatocyte [96]. However, it is plausible that has been HGF to perform a critic role in hepatic differentiation. In fact, some studies have demonstrated as c-Met receptor, which is expressed also by bm-MSCs, mediates the differentiation process through hepatic lineage, although it is involved also in the mesenchymal stromal cells' migration [221;225]. Furthermore, in order to explain the difficulty to reach a mature hepatocyte – like condition by bm-MSCs, we have to consider the HGF ability to inhibit their proliferation state, activating the cell cycle inhibitors (p53, p21 e p27) [222;226]. In addition, it is well-known as a 3D culture system of bm-MSCs during a differentiation protocol give rise to better results than a 2D standard culture method, as reported in literature [79;224;227;228;229;230].

Taking together, these hypotheses could explain why, although we observed the early hepatic features and also few of the late ones, the original hepatic differentiation protocol 1 displays better results on the beginning stages of differentiation, while it showed lower capacity to achieve the typical characteristics of mature hepatocytes.

To confirm the achievement of new features during differentiation process, is essential to check the presence of the specific markers for the new cell type, but it is equally important to observe the entire proteomic alteration due to the differentiation. In this sense, proteomic analysis demonstrates the presence of 32% of common proteins, which remains expressed during all differentiation phases. This result confirms the immunocytochemical evidences about incomplete expression of typical hepatic markers, and, moreover, it led to consider the protocol 1 not adequate for a proteome change of bm-MSCs toward an hepatic phenotype. In addition, comparing protocol 1 with protocol 2, we observed a delay to respond at the different stimuli

derived from the diverse growth factors used in the 2 protocols (as demonstrate by the 46,9% of shared protein between the 2 protocols at 3 days), despite at the end of the differentiation the bone marrow cells respond more differently then TSC/P to the diverse stimuli of the 2 protocols, as confirmed by the lower percentage of common protein at 30 days (15,9%) (data not shown).

Protocol 2

Differently in protocol 2, the absence of HGF in the early phase of mesodermal induction of differentiation process has been compensate by Activin A, a member of the TGFb superfamily important for committing human embryonic stem cells to the endodermal lineage [214]. However, since the immunoreactivity for AFP and HNF-3β was not compatible with an adequate hepatic induction effect, we speculate that Activin A is likely not enough for adult rat bone marrow – mesenchymal stromal cell induction to the hepatic lineage.

Another feature of protocol 2 was the much higher concentration (more than two times) of HGF respect to protocol 1, administered for the first time at 4 days and keep constant for all differentiation period. Since the expression of late markers (primarily ALB, which was observed at 15 days, i.e. during the transition phase from hepatoblasts to hepatocytes) resulted much weaker with this protocol than protocol 1, we raise the hypothesis that the high dose and the constant presence of HGF could have paradoxically saturated the Met receptor, slowing down and/or altering the switch from mesoderm to endoderm phenotype. This effect is compatible with the well – known capacity of HGF to inhibit the differentiation process of bm-MSCs [222;226]. Furthermore, it is possible that HGF has stimulate the mobilization of bm-MSCs, inducing an epithelial – mesenchymal transition state, interfering with their hepatoblast differentiation phase [194;221;225].

The tyrosine kinase – dependent factor EGF, instead, was administered only at the end of the hepatoblast phase, i.e. from day 11 of differentiation. As mentioned before, EGF is important to direct hepatic stem cells to hepatogenic differentiation during early stages of organ maturation (3 – 15 days), as well as to be a well-known mitogen for hepatocytes *in vitro*. In this sense, it is plausible that its presence only at late differentiation phase had reduced the differentiation passage from bm-MScs to hepatoblast, leading to a too immature phenotype for the consequent switch to hepatocyte. In fact, the presence of several cells with primitive morphology into the differentiation cultures at the end of differentiation period (24 days) confirm this hypothesis, as well as the premature interruption of max expression of cytokeratins at 15 days. During the *in vivo* organogenesis, the expression of intermediate filaments, as cytokeratins, depend to EGF. In our culture condition, the EGF was administered immediately before the cytokeratinic peak (starting from 11 days), too late respect to its physiological function during *in vivo* development.

Another important consideration is about the culture conditions. As said before, a 2D culture method (monolayer), although the use of rat tail collagen as biomaterial for substrate coating, is a limit for the differentiation capacity of bm-MSCs, considering that they prefer a tridimensional space to exhibit their differentiation potential [79;224;227;228;229;230]. In addition, the choice to use rat bone marrow cells at high passage (cell passage 4), in order to evaluate which growth factors performed a key role in maintaining the differentiated state in a low – responsive condition, could have negatively influenced the success of the differentiation. In fact, for a differentiation process using bm-MSCs was recommended a cell passage between 1 and 3 in literature, because they are suitable for express their best differentiation capacity [231;232;233]. Remarkably, we speculate about the idea that is the administration time of HGF

– EGF ratio to perform *in vitro* an essential hepatic differentiation action on adult male rat bm-MSCs.

Mass spectrometry analysis revealed for bm-MSCs an amount of only 10% of shared proteins during all differentiation time (data not shown). This result could find an explanation considering the importance for this source of cells of mesoderm induction with Activin A and bFGF. In fact, the mesoderm induction could be essential for bm-MSCs for a change in proteomic signature, despite it seems to be inadequate to induce the achievement of the typical hepatic markers and features, as seen in immunocytochemistry.

4. Characterization of human nasal chondrocytes

Thanks to the collaboration between the Laboratory of Regenerative Morphology and Bioartificial Structures of University of Parma, Italy (leaded by Prof. Toni) and the Laboratory of Tissue Engineering of University Hospital of Basel, Switzerland (leaded by Prof. Martin), an analysis to understand the embryological origin of adult stem cells present in the human nasal septum and used for the regenerative medicine of articular cartilage [234] These cells were taken following *in vivo* surgical sampling, and de-differentiated *in vitro* using a specific mix of growth factors.

Previous studies were carried out to evaluate the expression profile of Hox genes and other features that make nasal chondrocytes an excellent source for the repair of hyaline cartilage tissues, such as self-renewal and environmental plasticity, ability to grow and generate functional cartilaginous tissues, with a lower donor-related dependence [235], capacity to respond similarly to joint chondrocytes to physical forces that resemble joint load [163] and

capability to recover efficiently after exposure to inflammatory factors typical of a damaged joint [236].

Afterwards, a set of Hox genes were identified that capture the different ontogeny of nasal chondrocytes and articular chondrocytes, which form biochemically similar tissues but derive respectively from the neuroectoderm and the mesoderm [156].

Immunocytochemical investigations carried out both in Italy and Switzerland on the septal cartilage of human embryos (7th week) taken from the collection of the University Museum of Biomedicine - BIOMED (Scientific Director, Prof. Dott. Roberto Toni) in Parma (Embyo NC), the adult human septal cartilage (Native NC), and primary cultures of these cells (NC in culture) showed a pattern of markers of neuroectodermal and mesodermal lineages quite different in the three experimental models, whose only the primary mesodermal marker Brachyury (T) resulted consistently conserved in all the samples. Interestingly, neural crest markers, although quite different, are present in all sample source analyzed, suggesting not only the presence and preservation of this type of cells in human nasal cartilage from embryo phase, but also the importance of the specific part of nose biopsy used to achieve the primary culture of nasal chondrocytes.

On these premises, an evaluation about mesodermal and neuroectodermal / neural crest markers was carried out by flow cytometry on the primary cultures of adult septal cartilage, obtained by biopsy. Nasal chondrocytes were plated in culture well plate and expanded in complete medium supplemented with a specific combination of growth factors that was previously shown to enhance the proliferation of nasal chondrocytes [163], as well as their de-differentiation.

As determined by flow cytometry, the very wide (up to 80% of cells) co-expression of plasma membrane and intracellular markers of the mesodermal lineage (SSEA-4, FoxF1, Brachyury)

and neuroectodermal / neural crest lineage (P75, FoxD3, Dixdc1, Nestin) in nasal chondrocytes respect to controls (BM and P0) suggests that the majority of these cells are of ectomesenchymal origin and, thus arising from the neural crest lineage.

Since a minority of these cells (around 20%) express only markers of early mesodermal lineage (Brachyury), we speculate that they might belong to primary mesoderm, and may remain in the adult nasal septum as mesenchymal stem cells.

The expression of both mesodermal and neuroectodermal / neural crest markers suggests that the expansion and “dedifferentiation” culture medium used for nasal chondrocytes permits to these cells to be a very heterogeneous population with high plasticity of their phenotype (as expected by multipotent cells), in comparison to primary nasal chondrocytes (P0) and also to a well – known and used cell source like human bone marrow cells (BM). Thus, expanded nasal chondrocytes are able to increase their stemness pool under specific factor and cytokine stimuli, becoming more suitable to receive diverse differentiating stimuli, as confirm by different co-expression of the neuroectodermal and mesodermal markers between the NC cells and P0 cells (although they derive from the same donor, i.e. 101).

5. Proteomic signature of human nasal chondrocytes

In order to understand the complete protein expression profile and confirm the evidences about ectomesenchymal neural crest-derived state of human NC, a mass spectrometry analysis was performed. In a first step, we established the difference between expanded (NC176 and NC101) and differentiated (P0) nasal chondrocytes, and we evaluated also the different proteomic profile of 2 patients. The shared proteins between nasal chondrocytes derived from 2 donors and P0 resulted of 25 – 27%, confirming the changes occurred in these cells after

expansion. In contrast, 35,2% of protein resulted expressed by both NC176 and NC101, proving a greater similarity between the 2 sources of NC cells, despite the individual differences due to the interpatient variability make this percentage less than expected.

HeatMap and Hierarchical Clustering show a greater similarity between NC176 and NC101 than P0 cells. In fact, although the differences due to divers donor, expanded NC cells display analogous proteomic signature respect to differentiated chondrocytes (P0). In addition, for expanded nasal chondrocytes were observed similar down- and up-regulated proteins, respect to P0 cells. Specifically, considering NC176 and NC101 together, both down- and up-regulated proteins are involved in regulation, organization, development and morphogenesis mechanisms. In fact, it must be considered that NC cells derive from a primary tissue culture, which was expanded using specific factors, and then these expanded chondrocytes express proteins necessary for cellular changes towards a dedifferentiated phenotype. In the same way, differentiated P0 cells show the up-regulation of protein implicated in cellular organization and regulation because involved in a differentiation process. Nevertheless, in NCs up-regulated proteins was observe a decrease in catabolic / metabolic processes, expressing only mechanisms implied in protein folding and cell proliferation. In fact, the up-regulated T-complex protein 1 is important as molecular chaperone complex that assists the folding of proteins upon ATP hydrolysis [237], and in NCs could be essential to permit to reach the dedifferentiated state at the nasal chondrocytes in culture helping the folding of the new synthesized proteins. The Peroxiredoxin-1 (PRDX1) metabolic mechanism, another up-regulated process, has been reported to be important for proliferation, specifically in cancer cells. Indeed, it promotes cell proliferation and inhibits apoptosis of human gliomas via TNF-α/NF-κB pathway [238] and stimulates cell proliferation and metastasis through enhancing Akt/mTOR in human osteosarcoma cells [239]. In our nasal chondrocytes culture, the specific expansion medium

and the growth factors utilized could be induced a high proliferation state, consequently activating the expression of this protein.

Between down-regulated proteins there are also some DNA – associated Histone (H2A, H2B and H4), highly alkaline proteins found in eukaryotic cell nuclei that package and order the DNA into structural units called nucleosomes. In particular, two copies each of the core histone proteins H2A, H2B, H3, and H4 associate with DNA to form the octamer, which is wrapped by ~147 bp DNA about 1.75 rounds to form nucleosomes [240]. Constitutive expression of histones and accumulation of soluble histones outside S phase triggers chromosome aggregation or loss and are toxic to cells [241]. Thus, the synthesis and accumulation of these histones are tightly restricted to S phase to provide sufficient histones to assemble the replicated DNA into chromatin and prevent excess accumulation of histones at other cell cycle stages [242]. In NCs, the downregulation of histone proteins can be related to a more stable DNA state, feature highly pursued in the field of stem cells (greatly subjected to DNA damage), which in our situation may be due to the dedifferentiation process.

Furthermore, in NCs down-regulated protein (up-regulated in P0) there are proteins involved in glycolysis and ATP production mechanisms. These processes, which are down-regulated in NCs probably due to the shift toward a more dedifferentiated state, are important for chondrocytes in differentiation (like our P0 cells) because, as report in literature, ATP and ADP induced in chondrocytes an increase in intracellular Ca2+ concentration, and that calcium signaling is an important regulator of chondrogenesis [243]. In addition, it was demonstrated that chondrocyte pellet cultures treated with ATP produced more proteoglycans and collagen that enhanced their functional properties [244]. In particular, glycolysis was the principal pathway to supply ATP in the chondrocytes, and they utilize predominantly glycolytic metabolism to produce optimal ATP due to the surrounding avascular microenvironment,

yielding lactate as the end product [245;246]. In our P0 cells, the up-regulation of glycolytic enzymes L-lactate dehydrogenase, Phosphoglycerate kinase 1, Phosphoglycerate mutase 1, Glyceraldehyde-3-phosphate dehydrogenase, Fructose-bisphosphate aldolase A, Alpha-enolase and the oxidative phosphorylation enzyme ATP synthase (involved in the production of the energy storage molecule adenosine triphosphate (ATP)) could represent a proof that differentiation process was occurred. It is reasonable speculate that P0 cells, differentiated for 2 weeks using a chondrogenic medium, start to overexpress the glycolytic and oxidative phosphorylation enzymes in order to carry on and complete the differentiation process.

CONCLUSIONS

In summary, mass spectrometry data (LC-LIT-Orbitrap XL and LC-MS/MS SRM through in silico sequencing) have shown that our adult, male rat thyroid stem cells/progenitors () express an admixture of endodermal, mesodermal, neuroectodermal / neural crest, and epithelial - mesenchymal transition markers. Although we cannot exclude that part of our TSC/P are endodermal progenitors, however a large majority of them depict a protein profile consistent with an ectomesenchymal lineage and, thus of cells from the neural crest. This is in keeping with the recent evidence that in rodents the neural crest contributes to the development of the thyroid gland providing the cells of the stromal matrix. In addition, since our TSC/P were originally isolated from adult thyroids using a long-term starvation procedure (2-4 months in length), and have the remarkable property to remain stable in liquid nitrogen and for a long number of culture passages (more than 20) without any change, it is plausible that the procedure selected more than a single stem cells type, resistant for months to the starvation protocol. Therefore, I raise the possibility that our TSC/P are a mixed, adult stem cell population constituted by a minor fraction of pure endodermal stem cells and a major fraction of ectomesenchymal stem cells. The multipotential of our TSC/P is confirmed by their capacity to differentiate to hepatocytes in 2D culture, much better than bm-MSC currently believed a gold standard for hepatic differentiation in vitro. Clonogenic studies are in progress to determine whether our TSC/P are either an homogeneous or an heterogeneous population of adult stem cells, and to selectively establish the contribution of each possible cell type to the hepatic differentiation. Similar, studies in collaboration with Prof. Gabriella De Vita, from the

Department of Genetics at the University of Naples, in Italy are also in progress to induce the neural differentiation of our TSC/P and study whether it would involve all or only part of our supposedly heterogeneous adult stem cells population.

Finally, thanks to the collaboration with the group of Prof. Ivan Martin at the University of Basel a new source of neural crest-derived, adult ectomesenchymal stem cells has become available. Whether these cells may be really differentiated in vitro to human hepatocytes remains to be detemined. However, their marker profile and proteomic signature is consistent with a high phenotype plasticity. Therefore, collaborative trascriptomic studies are already planned with Prof. Filippo Rijli from the University of Basel, to identify relevant molecular convergences with our proteomic data and, based on their availability as viable cells other investigations can be conducted at UNIPR to induce their hepatic differentiation, with the intent to identify an innovative cell source for regenerative medicine and tissue engineering of the human liver.

REFERENCES

1. Douarin NM. An experimental analysis of liver development. Med. Biol. 1975; 53: 427–455.
2. Tremblay KD, and Zaret KS. Distinct populations of endoderm cells converge to generate the embryonic liver bud and ventral foregut tissues. Dev. Biol. 2005; 280: 87–99.
3. Karim Si-Tayeb, Frédéric P Lemaigre, and Stephen A Duncan. Organogenesis and Development of the Liver. Dev Cell 2010 Feb 16;18:175-89.
4. Gualdi R, Bossard P, Zheng M, Hamada Y, Coleman JR, Zaret KS. Hepatic specification of the gut endoderm in vitro: cell signaling and transcriptional control. Genes Dev 1996;10:1670–1682.
5. Jung J, Zheng M, Goldfarb M, Zaret KS. Initiation of mammalian liver development from endoderm by fibroblast growth factors. Science 1999;284:1998–2003.
6. Cirillo LA, Lin FR, Cuesta I, Friedman D, Jarnik M, Zaret KS. Opening of compacted chromatin by early developmental transcription factors HNF3 (FoxA) and GATA-4. Mol Cell 2002;9:279–289.
7. Serls AE, Doherty S, Parvatiyar P, Wells JM, Deutsch GH. Different thresholds of fibroblast growth factors pattern the ventral foregut into liver and lung. Development 2005;132:35–47.
8. McLin VA, Rankin SA, Zorn AM. Repression of Wnt/beta-catenin signaling in the anterior endoderm is essential for liver andpancreas development. Development 2007;134:2207–2217.

9. Finley KR, Tennessen J, Shawlot W. The mouse secreted frizzled- related protein 5 gene is expressed in the anterior visceral endoderm and foregut endoderm during early post-implantation development. Gene Expr Patterns 2003;3:681–684.
10. Bort R, Signore M, Tremblay K, Martinez Barbera JP, Zaret KS. Hex homeobox gene controls the transition of the endoderm to a pseudostratified, cell emergent epithelium for liver bud development. Dev Biol 2006;290:44–56.
11. Shiojiri N, Sugiyama Y. Immunolocalization of extracellular matrix components and integrins during mouse liver development. Hepatology 2004;40:346–355.
12. Martinez-Barbera JP, Clements M, Thomas P, Rodriguez T, Meloy D, Kioussis D, Beddington RS. The homeobox gene Hex is required in definitive endodermal tissues for normal forebrain, liver and thyroid formation. Development 2000;127:2433–2445.
13. Keng VW, Yagi H, Ikawa M, Nagano T, Myint Z, Yamada K, Tanaka T, Sato A, Muramatsu I, Okabe M, Sato M, Noguchi T. Homeobox gene Hex is essential for onset of mouse. Biochem Biophys Res Commun 2000;276:1155–1161.
14. Zhao R, Watt AJ, Li J, Luebke-Wheeler J, Morrisey EE, Duncan SA. GATA6 is essential for embryonic development of the liver but dispensable for early heart formation. Mol Cell Biol 2005;25:2622–2631.
15. Margagliotti S, Clotman F, Pierreux CE, Lemoine P, Rousseau GG, Henriet P, Lemaigre FP. Role of metalloproteinases at the onset of liver development. Dev Growth Differ 2008;50:331–338.
16. Zaret KS. Regulatory phases of early liver development: paradigms of organogenesis. Nat Rev Genet. 2002 Jul;3:499-512.
17. Tanimizu N, Miyajima A. Molecular mechanism of liver development and regeneration. Int Rev Cytol 2007;259:1–48.

18. Weinstein M, Monga SP, Liu Y, Brodie SG, Tang Y, Li C, Mishra L, Deng CX. Smad proteins and hepatocyte growth factor control parallel regulatory pathways that converge on beta1-integrin to promote normal liver development. Mol Cell Biol 2001;21:5122–5131.
19. Suksaweang S, Lin CM, Jiang TX, Hughes MW, Widelitz RB, Chuong CM. Morphogenesis of chicken liver: identification of localized growth zones and the role of beta-catenin/Wnt in size regulation. Dev Biol 2004;266: 109–122.
20. Doi TS, Marino MW, Takahashi T, Yoshida T, Sakakura T, Old LJ, Obata Y. Absence of tumor necrosis factor rescues RelA-deficient mice from embryonic lethality. Proc Natl Acad Sci U S A 1999;96:2994–2999.
21. Kamiya A, Kakinuma S, Onodera M, Miyajima A, Nakauchi H. Prospero-related homeobox 1 and liver receptor homolog 1 coordinately regulate long-term proliferation of murine fetal hepatoblasts. Hepatology 2008;48:252–264.
22. Krupczak-Hollis K, Wang X, Kalinichenko VV, Gusarova GA, Wang IC, Dennewitz MB, Yoder HM, Kiyokawa H, Kaestner KH, Costa RH. The mouse Forkhead Box m1 transcription factor is essential for hepatoblast mitosis and development of intrahepatic bile ducts and vessels during liver morphogenesis. Dev Biol 2004;276: 74–88.
23. Reimold AM, Etkin A, Clauss I, Perkins A, Friend DS, Zhang J, Horton HF, Scott A, Orkin SH, Byrne MC, Grusby MJ, Glimcher LH. An essential role in liver development for transcription factor XBP-1. Genes Dev 2000; 14:152–157.
24. Hentsch B, Lyons I, Li R, Hartley L, Lints TJ, Adams JM, Harvey RP. Hlx homeo box gene is essential for an inductive tissue interaction that drives expansion of embryonic liver and gut. Genes Dev 1996;10:70–9.
25. Giroux S, Charron J. Defective development of the embryonic liver in N-myc-deficient mice. Dev Biol 1998;195:16–28.

26. Li J, Ning G, Duncan SA. Mammalian hepatocyte differentiation requires the transcription factor HNF-4alpha. Genes Dev 2000; 14:464–474.
27. Antoniou A, Raynaud P, Cordi S, Zong Y, Tronche F, Stanger BZ, Jacquemin P, Pierreux CE, Clotman F, Lemaigre FP. Intrahepatic bile ducts develop according to a new mode of tubulogenesis regulated by the transcription factor SOX9. Gastroenterology 2009 Jun;136:2325-33.
28. Suzuki A, Iwama A, Miyashita H, Nakauchi H, Taniguchi H. Role for growth factors and extracellular matrix in controlling differentiation of prospectively isolated hepatic stem cells. Development 2003;130: 2513–2524.
29. Tanimizu N, Miyajima A. Notch signaling controls hepatoblast differentiation by altering the expression of liver-enriched transcription factors. J Cell Sci 2004;117:3165–3174.
30. Decaens T, Godard C, de Reyniès A, Rickman DS, Tronche F, Couty JP, Perret C, Colnot S. Stabilization of beta-catenin affects mouse embryonic liver growth and hepatoblast fate. Hepatology 2008;47:247–258.
31. Coffinier C, Gresh L, Fiette L, Tronche F, Schütz G, Babinet C, Pontoglio M, Yaniv M, Barra J. Bile system morphogenesis defects and liver dysfunction upon targeted deletion of HNF1beta. Development 2002;129:1829–1838.
32. Friedman JR, Kaestner KH. The Foxa family of transcription factors in development and metabolism. Cell Mol Life Sci 2006; 63:2317–2328.
33. Fayard E, Auwerx J, Schoonjans K. LRH-1: an orphan nuclear receptor involved in development, metabolism and steroidogenesis. Trends Cell Biol 2004;14:250–260.
34. Lee YK, Moore DD. Liver receptor homolog-1, an emerging metabolic modulator. Front Biosci 2008;13:5950–5958.

35. Lahuna O, Fernandez L, Karlsson H, Maiter D, Lemaigre FP, Rousseau GG, Gustafsson J, Mode A. Expression of hepatocyte nuclear factor 6 in rat liver is sex-dependent and regulated by growth hormone. Proc Natl Acad Sci U S A 1997;94: 12309–13.
36. Pierreux CE, Stafford J, Demonte D, Scott DK, Vandenhaute J, O'Brien RM, Granner DK, Rousseau GG, Lemaigre FP. Antiglucocorticoid activity of hepatocyte nuclear factor-6. Proc Natl Acad Sci U S A 1999;96:8961–8966.
37. Beaudry JB, Pierreux CE, Hayhurst GP, Plumb-Rudewiez N, Weiss MC, Rousseau GG, Lemaigre FP. Threshold levels of hepatocyte nuclear factor 6 (HNF-6) acting in synergy with HNF-4 and PGC-1alpha are required for time-specific gene expression during liver development. Mol Cell Biol 2006;26:6037–6046.
38. Lannoy VJ, Decaux JF, Pierreux CE, Lemaigre FP, Rousseau GG. Liver glucokinase gene expression is controlled by the onecut transcription factor hepatocyte nuclear factor-6. Diabetologia 2002;45:1136–1141.
39. Wang M, Tan Y, Costa RH, Holterman AX. In vivo regulation of murine CYP7A1 by HNF-6: a novel mechanism for diminished CYP7A1 expression in biliary obstruction. Hepatology 2004;40:600–608.
40. Tan Y, Yoshida Y, Hughes DE, Costa RH. Increased expression of hepatocyte nuclear factor 6 stimulates hepatocyte proliferation during mouse liver regeneration. Gastroenterology 2006;130: 1283–1300.
41. Battle MA, Konopka G, Parviz F, Gaggl AL, Yang C, Sladek FM, Duncan SA. Hepatocyte nuclear factor 4alpha orchestrates expression of cell adhesion proteins during the epithelial transformation of the developing liver. Proc Natl Acad Sci U S A 2006;103:8419–8424.
42. Luebke-Wheeler J, Zhang K, Battle M, Si-Tayeb K, Garrison W, Chhinder S, Li J, Kaufman RJ, Duncan SA. Hepatocyte nuclear factor 4alpha is implicated in endoplasmic reticulum

stressinduced acute phase response by regulating expression of cyclic adenosine monophosphate responsive element binding protein H. Hepatology 2008;48:1242–1250.

43. Kamiya A, Kinoshita T, Ito Y, Matsui T, Morikawa Y, Senba E, Nakashima K, Taga T, Yoshida K, Kishimoto T, Miyajima A. Fetal liver development requires a paracrine action of oncostatin M through the gp130 signal transducer. EMBO J 1999;18:2127–2136.
44. Ito Y, Matsui T, Kamiya A, Kinoshita T, Miyajima A. Retroviral gene transfer of signaling molecules into murine fetal hepatocytes defines distinct roles for the STAT3 and ras pathways during hepatic development. Hepatology 2000;32:1370–1376.
45. Matsumoto K, Miki R, Nakayama M, Tatsumi N, Yokouchi Y. Wnt9a secreted from the walls of hepatic sinusoids is essential for morphogenesis, proliferation, and glycogen accumulation of chick hepatic epithelium. Dev Biol 2008;319:234–247.
46. Katz N, Jungermann K. Autoregulatory shift from fructolysis to lactate gluconeogenisis in rat hepatocyte suspensions. The problem of metabolic zonation of liver parenchyma. Hoppe Seylers Z Physiol Chem 1976;357:359–375.
47. Jungermann K, Katz N. Functional specialization of different hepatocyte populations. Physiol Rev 1989;69:708–764.
48. Benhamouche S, Decaens T, Godard C, Chambrey R, Rickman DS, Moinard C, Vasseur-Cognet M, Kuo CJ, Kahn A, Perret C, Colnot S. Apc tumor suppressor gene is the ”zonation keeper” of mouse liver. Dev Cell 2006;10:759–770.
49. Lemaigre FP. Mechanisms of liver development: concepts for understanding liver disorders and design of novel therapies. Gastroenterology. 2009 Jul;137(1):62-79.
50. Clotman F, Lannoy VJ, Reber M, Cereghini S, Cassiman D, Jacquemin P, Roskams T, Rousseau GG, Lemaigre FP. The onecut transcription factor Hnf6 is required for normal development of the biliary tract. Development 2002;129:1819–1828.

51. Kalinichenko VV, Zhou Y, Bhattacharyya D, Kim W, Shin B, Bambal K, Costa RH. Haploinsufficiency of the mouse Forkhead Box f1 gene causes defects in gall bladder development. J Biol Chem 2002;277:12369– 12374.
52. Ito A, Nishikawa Y, Ohnuma K, Ohnuma I, Koma Y, Sato A, Enomoto K, Tsujimura T, Yokozaki H. SgIGSF is a novel biliaryepithelial cell adhesion molecule mediating duct/ductule development. Hepatology 2007;45:684–694.
53. Fabris L, Strazzabosco M, Crosby HA, Ballardini G, Hubscher SG, Kelly DA, Neuberger JM, Strain AJ, Joplin R. Characterization and isolation of ductular cells coexpressing neural cell adhesion molecule and Bcl-2 from primary cholangiopathies and ductal plate malformations. Am J Pathol 2000;156:1599–1612.
54. Yamasaki H, Sada A, Iwata T, Niwa T, Tomizawa M, Xanthopoulos KG, Koike T, Shiojiri N. Suppression of C/EBPα expression in periportal hepatoblasts may stimulate biliary cell differentiation through increased Hnf6 and Hnf1β expression. Development 2006;133:4233–4243.
55. Suzuki K, Tanaka M, Watanabe N, Saito S, Nonaka H, Miyajima A. p75 Neurotrophin receptor is a marker for precursors of stellate cells and portal fibroblasts in mouse fetal liver. Gastroenterology 2008;135: 270–281.
56. Lemaigre FP. Notch signaling in bile duct development: new insights raise new questions. Hepatology 2008;48:358–360.
57. Fabris L, Cadamuro M, Fiorotto R, Roskams T, Spirlì C, Melero S, Sonzogni A, Joplin RE, Okolicsanyi L, Strazzabosco M. Effects of angiogenic factor overexpression by human and rodent cholangiocytes in polycystic liver diseases. Hepatology 2006;43:1001–1012.

58. Sato Y, Harada K, Kizawa K, Sanzen T, Furubo S, Yasoshima M, Ozaki S, Ishibashi M, Nakanuma Y. Activation of the MEK5/ERK5 cascade is responsible for biliary dysgenesis in a rat model of Caroli's disease. Am J Pathol 2005;166:49–60.
59. Sato Y, Harada K, Furubo S, Kizawa K, Sanzen T, Yasoshima M, Ozaki S, Isse K, Sasaki M, Nakanuma Y. Inhibition of intrahepatic bile duct dilation of the polycystic kidney rat with a novel tyrosine kinase inhibitor gefitinib. Am J Pathol 2006;169:1238–1250.
60. Sherer GK. Tissue interaction in chick liver development: a reevaluation. I. Epithelial morphogenesis: the role of vascularity in mesenchymal specificity. Dev Biol. 1975 Oct;46:281-95.
61. Rossi JM, Dunn NR, Hogan BL, Zaret KS. Distinct mesodermal signals, including BMPs from the septum transversum mesenchyme, are required in combination for hepatogenesis from the endoderm. Genes Dev. 2001 Aug 1;15:1998-2009.
62. Sosa-Pineda B, Wigle JT, Oliver G. Hepatocyte migration during liver development requires Prox1. Nat Genet. 2000 Jul;25:254-5.
63. Zaret KS. Regulatory phases of early liver development: paradigms of organogenesis. Nat Rev Genet. 2002 Jul;3:499-512.
64. Matsumoto K, Yoshitomi H, Rossant J, Zaret KS. Liver organogenesis promoted by endothelial cells prior to vascular function. Science. 2001 Oct 19;294:559-63.
65. Widmann JJ, Fahimi HD. Proliferation of mononuclear phagocytes (Kupffer cells) and endothelial cells in regenerating rat liver. A light and electron microscopic cytochemical study. Am J Pathol. 1975 Sep;80:349-66.
66. Yamane A, Seetharam L, Yamaguchi S, Gotoh N, Takahashi T, Neufeld G, Shibuya M. A new communication system between hepatocytes and sinusoidal endothelial cells in liver

through vascular endothelial growth factor and Flt tyrosine kinase receptor family (Flt-1 and KDR/Flk-1). Oncogene. 1994 Sep;9:2683-90.

67. Ross MA, Sander CM, Kleeb TB, Watkins SC, Stolz DB. Spatiotemporal expression of angiogenesis growth factor receptors during the revascularization of regenerating rat liver. Hepatology. 2001 Dec;34:1135-48.
68. Marcus S, Katari R, Patel T, Peloso A, Mugweru J, Owusu K and Orlando G. Extracellular Matrix Scaffold Technology for Bioartificial Pancreas Engineering: State of the Art and Future Challenges. Journal of Diabetes Science and Technology 2014. 1;8:159-169.
69. Scadden DT. The stem-cell niche as an entity of action. Nature 2006; 44, pp. 1075-1079.
70. Burdick JA, Vunjak-Novakovic G. Engineered microenvironments for controlled stem cell differentiation. Tissue Eng. Part A. 2009; 15, pp. 205–219.
71. Lund AW, Yener B, Stegemann JP, Plopper GE. The natural and engineered 3D microenvironment as a regulatory cue during stem cell fate determination. Tissue Eng. Part B Rev. 2009; 15, pp. 371–380.
72. Edelman GM. Topobiology, an Introduction to Molecular Embryology, Basic Book Inc, New York (1988).
73. Engler AJ, Humbert P O, Wehrle-Haller B, Weaver V. M. Multiscale modeling of form and function. Science 2009; 324, 208–212.
74. Toni Roberto, Elena Bassi, Fulvio Barbaro, Nicoletta Zini, Alessandra Zamparelli, Marco Alfieri, Davide Dallatana, Salvatore Mosca, Claudia della Casa, Cecilia Gnocchi, Giuseppe Lippi, Giulia Spaletta, Elena Bassoli, Lucia Denti, Andrea Gatto, Francesca Ricci, Pier Luigi Tazzari, Annapaola Parrilli, Milena Fini, Monica Sandri, Simone Sprio, and Anna Tampieri. Bioartificial Endocrine Organs: At the Cutting Edge of Translational Research in

Endocrinology. Bio-Inspired Regenerative Medicine: Materials, Processes, and Clinical Applications, Pan Stanford 2016; Chapter 15: 357-388.

75. Takayama K, Inamura M, Kawabata K, Sugawara M, Kikuchi K, Higuchi M, Nagamoto Y, Watanabe H, Tashiro K, Sakurai F, Hayakawa T, Furue MK, Mizuguchi H. Generation of metabolically functioning hepatocytes from human pluripotent stem cells by FOXA2 and HNF1alpha transduction. J Hepatol 2012; 57: 628-636.
76. Wang ZM, Yuan XH, Shen H. BMP-4 induced proliferation and oriented differentiation of rat hepatic oval cells into hepatocytes. Asian Pac J Trop Med. 2015 May;8:412-6.
77. Lázaro CA, Rhim JA, Yamada Y, Fausto N. Generation of hepatocytes from oval cell precursors in culture. Cancer Res. 1998 Dec 1;58:5514-22.
78. Dunn, J., Yarmush. M.. Koebe, H.. and Tompkins, R. Hepatocytc function and extracellular matrix geometry: long-term culture in a sandwich configuration. FASEB J 1989 Feb;3:174-177.
79. Lin N, Lin J, Bo L, Weidong P, Chen S, Xu R. Differentiation of bone marrow-derived mesenchymal stem cells into hepatocyte-like cells in an alginate scaffold. Cell Prolif. 2010 Oct;43:427-34.
80. Ouyang J, Shao J, Zou H, Lou Y, Yu Y. Hepatic differentiation of rat mesenchymal stem cells by a small molecule. ChemMedChem. 2012 Aug;7:1447-52.
81. Sgodda M, Aurich H, Kleist S, Aurich I, König S, Dollinger MM, Fleig WE, Christ B. Hepatocyte differentiation of mesenchymal stem cells from rat peritoneal adipose tissue in vitro and in vivo. Exp Cell Res. 2007 Aug 1;313:2875-86.
82. Sarvandi SS, Joghataei MT, Parivar K, Khosravi M, Sarveazad A, Sanadgol N. In vitro differentiation of rat mesenchymal stem cells to hepatocyte lineage. Iran J Basic Med Sci. 2015 Jan;18:89-97.

83. Lange C, Bassler P, Lioznov MV, Bruns H, Kluth D, Zander AR, Fiegel HC. Hepatocytic gene expression in cultured rat mesenchymal stem cells. Transplant Proc. 2005 Jan-Feb;37:276-9.
84. Schwartz RE, Reyes M, Koodie L, Jiang Y, Blackstad M, Lund T, Lenvik T, Johnson S, Hu WS, Verfaillie CM. Multipotent adult progenitor cells from bone marrow differentiate into functional hepatocyte-like cells. J Clin Invest. 2002 May;109:1291-302.
85. Wells JM and Melton DA. Early mouse endoderm is patterned by soluble factors from adjacent germ layers. Development 2000; 127:1563–1572.
86. Oh SH, Miyazaki M, Kouchi H, Inoue Y, Sakaguchi M, Tsuji T, Shima N, Higashio K, Namba M. Hepatocyte growth factor induces differentiation of adult rat bone marrow cells into a hepatocyte lineage in vitro. Biochem. Biophys. Res. Commun. 2000; 279:500-504.
87. Yoon JH, Lee HV, Lee JS, Park JB and Kim CY. Development of a non-transformed human liver cell line with differentiatedhepatocyte and urea-synthetic functions: applicable for bioartificial liver. International Journal of Artificial Organs 1999; 22:769–777.
88. Hamamoto R, Kamihira M and Iijima S. Growth and differentiation of cultured fetal hepatocytes isolated various developmental stages. Biosci. Biotechnol. Biochem. 1999; 63:395–401.
89. Miyazaki M, Mars WM, Runge D, Kim TH, Bowen WC, Michalopoulos GK. Phenobarbital suppresses growth and accelerates restoration of differentiation markers of primary culture rat hepatocytes in the chemically defined hepatocyte growth medium containing hepatocyte growth factor and epidermal growth factor. Exp. Cell Res. 1998; 241:445–457.
90. Wang T, Chen T, Liang HY, Yan HT, Lin N, Liu LY, Luo H, Huang Z, Li NL, Liu WH, Tang LJ. Notch inhibition promotes fetal liver stem/progenitor cells differentiation into hepatocytes via the inhibition of HNF-1β. Cell Tissue Res. 2014 Jul;357:173-84.

91. Block GD, Locker J, Bowen WC, Petersen BE, Katyal S, Strom SC, Riley T, Howard TA, Michalopoulos GK. Population expansion, clonal growth, and specific differentiation patterns in primary cultures of hepatocytes induced by HGF/SF, EGF and TGF alpha in a chemically defined (HGM) medium. J Cell Biol. 1996 Mar;132:1133-49.
92. Kleinman, H.K., M.L. McGarvey, L.A. Liotta, P.G. Robey, K. Tryggvason, and G.R. Martin. Isolation and characterization of type IV procollagen, laminin, and heparan sulfate proteoglycan from the EHS sarcoma. Biochemistry 1982 Nov 23;21:6188-93.
93. Nishiofuku M, Yoshikawa M, Ouji Y, Saito K, Moriya K, Ishizaka S, Nishimura F, Matsuda R, Yamada S, Fukui H. Modulated differentiation of embryonic stem cells into hepatocyte-like cells by coculture with hepatic stellate cells. J Biosci Bioeng. 2011 Jan;111:71-7.
94. Ruhnke M, Ungefroren H, Zehle G, Bader M, Kremer B, Fändrich F. Long-term culture and differentiation of rat embryonic stem cell-like cells into neuronal, glial, endothelial, and hepatic lineages. Stem Cells. 2003;21:428-36.
95. Marongiu F, Gramignoli R, Dorko K, Miki T, Ranade AR, Paola Serra M, Doratiotto S, Sini M, Sharma S, Mitamura K, Sellaro TL, Tahan V, Skvorak KJ, Ellis EC, Badylak SF, Davila JC, Hines R, Laconi E, Strom SC. Hepatic differentiation of amniotic epithelial cells. Hepatology. 2011 May;53:1719-29.
96. Sun C, Hu JJ, Pan Q, Cao Y, Fan JG, Li GM. Hepatic differentiation of rat induced pluripotent stem cells in vitro. World J Gastroenterol. 2015 Oct 21; 21:11118-26.
97. Dumont JE, Lamy F, Roger P, Maenhaut C. Physiological and pathological regulation of thyroid cell proliferation and differentiation by thyrotropin and other factors. Physiol Rev. 1992 Jul;72:667-97.
98. Coclet J, Foureau F, Ketelbant P, Galand P, Dumont JE. Cell population kinetics in dog and human adult thyroid. Clin Endocrinol (Oxf). 1989 Dec;31:655-65.

99. Hoshi N, Kusakabe T, Taylor BJ, Kimura S. Side population cells in the mouse thyroid exhibit stem/progenitor cell-like characteristics. Endocrinology. 2007 Sep;148:4251-8.

100. Umemoto T, Yamato M, Nishida K, Yang J, Tano Y, Okano T. Limbal epithelial side-population cells have stem cell-like properties, including quiescent state. Stem Cells 2006; 24:86-94.

101. De Paiva CS, Pflugfelder SC, Li DQ. Cell size correlates with phenotype and proliferative capacity in human corneal epithelial cells. Stem Cells 2006; 24: 368–375.

102. Kehler J, Tolkunova E, Koschorz B, Pesce M, Gentile L,Boiani M, Lomeli H, Nagy A, McLaughlin KJ, Scholer HR, Tomilin A. Oct4 is required for primordial germ cell survival. EMBO Rep 2004; 5:1078–1083.

103. Tai MH, Chang CC, Kiupel M, Webster JD, Olson LK, Trosko JE. Oct4 expression in adult human stem cells: Evidence in support of the stem cell theory of carcinogenesis. Carcinogenesis 2005; 26:495–502.

104. Tsai RY and McKayRD. A nucleolar mechanism controlling cell proliferation in stem cells and cancer cells. Genes Dev 2002; 16:2991–3003.

105. Niwa H, Miyazaki J, Smith AG. Quantitative expression of Oct-3/4 defines differentiation, dedifferentiation or self-renewal of ES cells. Nat Genet 2000; 24:372–376.

106. Pesce M, Scholer HR. Oct-4: gatekeeper in the beginnings of mammalian development. Stem Cells 2001; 19:271–278.

107. De Felice M, Di Lauro R. Thyroid development and its disorders: genetics and molecular mechanisms. Endocr Rev 2004; 25:722–746.

108. Barbaro F, Zamparelli A, Zini N, Dallatana D, Bassi E, Mosca S, Parrilli A, Fini M, Giardino R and Toni R. Adult stem/progenitor cells of the rat thyroid: side population

distribution, intermediate filament expression, and long-term in vitro expansion. IJAE, 2013; Vol. 118 n°2 (Supplement).

109. Strusi V, Zini N, Mastrogiacomo S, Zamparelli A, Barbaro F, Dallatana D, Parrilli A, Giardino R and Toni R. Identification of putative adult stem cells in the rat thyroid and their use in ex situ bioengineering. IJAE 2012; Vol. 117 n°2 (Supplement): 184.

110. Bassi E, Barbaro F, Zamparelli A, Zini N, Cattini L, Dallatana D, Gnocchi C, Lippi G, Mosca S, Parrilli A, Fini M, Giardino R, Toni R. Thyrogenic, adipogenic, and osteogenic differentiation of adult rat, thyroid stem cells enriched by long-term adherent subculture. IJAE, 2014; Vol. 119 n°1 (Supplement):15.

111. Bassi E, Barbaro F, Zamparelli A, Zini N, Spaletta G, Ricci F, Velati C, Dallatana D, Gnocchi C, Lippi G, Alfieri M, Mosca S, Della Casa C, Crafa P, Parrilli A, Fini M, Toni R. Multipotent Adult Rat, Thyroid Stem Cells Can Be Differentiated To Follicular Thyrocyte, And Hepatocyte- Like Cells In 2D And 3D Culture Systems. IJAE 2015; Vol. 120 n°1 (Supplement):87.

112. Lehmann WD. "All proteins all the time"- a comment on visions, claims, and wording in mass spectrometry-based proteomics. Anal Bioanal Chem. 2015 407:2659-2663.

113. Aebersold R, Mann M. Mass spectrometry-based proteomics. Nature. 2003 422:198-207.

114. Mehmood S, Allison TM, Robinson CV. Mass spectrometry of protein complexes: from origins to applications. Annu Rev Phys Chem. 2015 66:453-474.

115. Zhang Y, Fonslow BR, Shan B, Baek MC, Yates JR 3rd. Protein analysis by shotgun/bottom-up proteomics. Chem Rev. 2013 113:2343-2394.

116. Calloni R, Cordero EA, Henriques JA, Bonatto D. Reviewing and updating the major molecular markers for stem cells. Stem Cells Dev. 2013 22:1455-1476.

117. Lv FJ, Tuan RS, Cheung KM, Leung VY. Concise review: the surface markers and identity of human mesenchymal stem cells. Stem Cells. 2014 32:1408-1419.

118. Zhang L, Hong TP, Hu J, Liu YN, Wu YH, Li LS. Nestin-positive progenitor cells isolated from human fetal pancreas have phenotypic markers identical to mesenchymal stem cells. World J. Gastroenterol. 2005 11:2906-2911.

119. Wong A, Ghassemi E, Yellowley CE. Nestin expression in mesenchymal stromal cells: regulation by hypoxia and osteogenesis. BMC Vet. Res. 2014 10:173.

120. Zulewski H, Abraham EJ, Gerlach MJ, Daniel PB, Moritz W, Müller B, Vallejo M, Thomas MK, Habener JF. Multipotential nestin-positive stem cells isolated from adult pancreatic islets differentiate ex vivo into pancreatic endocrine, exocrine, and hepatic phenotypes. Diabetes. 2001 50:521-533.

121. Neradil J, Veselska R. Nestin as a marker of cancer stem cells. Cancer Sci. 2015 106:803-811.

122. Krebsbach PH, Villa-Diaz LG. The Role of Integrin α6 (CD49f) in Stem Cells: More than a Conserved Biomarker. Stem Cells Dev. 2017 26:1090-1099.

123. Sanchez-ramos J, Song S, Cardozo-pelaez F, Hazzi C, Stedeford T, Willing A, Freeman TB, Saporta S, Janssen W, Patel N, Cooper DR, Sanberg PR. Adult bone marrow stromal cells differentiate into neural cells in vitro. Exp Neurol 2000; 164: 247-256.

124. Petersen BE, Bowen WC, Patrene KD et al. Bone marrow as a potential source of hepatic oval cells. Science 1999;284:1168.

125. Friedenstein AJ, Petrakova KV, Kurolesova AI and Frolova GP. Heterotopic of bone marrow. Analysis of precursor cells for osteogenic and hematopoietic tissues. Transplantation 1968; 6, 230–247.

126. Friedenstein AJ, Chailakhjan RK and Lalykina KS. The development of fibroblast colonies in monolayer cultures of guinea-pig bone marrow and spleen cells. Cell Tissue Kinet 1970; 3, 393–403.

127. Friedenstein AJ, Gorskaja JF and Kulagina NN. Fibroblast precursors in normal and irradiated mouse hematopoietic organs. Exp. Hematol. 1976; 4, 267–274.

128. Dexter TM, Allen TD and Lajtha LG. Conditions controlling the proliferation of haemopoietic stem cells in vitro. J. Cell. Physiol. 1977, 91, 335–344.

129. Weiss L. The hematopoietic microenvironment of the bone marrow: an ultrastructural study of the stroma in rats. Anat. Rec. 1976, 186, 161–184.

130. Bianco P. Minireview: The Stem Cell Next Door: Skeletal and Hematopoietic Stem Cell “Niches” in Bone Endocrinology, August 2011, 152:2957–2962.

131. Sacchetti B, Funari A, Michienzi S, Di Cesare S, Piersanti S, Saggio I, Tagliafico E, Ferrari S, Robey PG, Riminucci M and Bianco P. Self-Renewing Osteoprogenitors in Bone Marrow Sinusoids Can Organize a Hematopoietic Microenvironment, Cell 2007; 131, 324–336.

132. Caplan AI. Mesenchymal stem cells. J. Orthop. Res. 1991; 9, 641–650.

133. Horwitz EM, Le Blanc K, Dominici M, Mueller I, Slaper-Cortenbach I, Marini FC, Deans RJ, Krause DS and Keating A. Clarification of the nomenclature for MSC: The International Society for Cellular Therapy position statement. Cytotherapy 2005; 7, 393–395.

134. Dominici M, Le Blanc K, Mueller I, Slaper-Cortenbach I, Marini FC, Krause DS, Deans RJ, Keating A, Prockop DJ and Horwitz EM. Minimal criteria for defining multipotent mesenchymal stromal cells. Cytotherapy 2006; 8, 315–317.

135. Conget PA and Minguell JJ. Phenotypical and functional properties of human bone marrow mesenchymal progenitor cells. J Cell Physiol,1999; 181,67-73.

136. Le Blanc K, Tammik C, Rosendahl K, Zetterberg E and Ringdén O. HLA expression and immunologic properties of differentiated and undifferentiated mesenchymal stem cells. Exp Hematol, 2003; 31,890-896.

137. Peister A, Mellad JA, Larson BL, Hall BM, Gibson LF, Prockop DJ. Adult stem cells from bone marrow (MSCs) isolated from different strains of inbred mice vary in surface epitopes, rates of proliferation, and differentiation potential. Blood. 2004 Mar 1;103:1662-8.

138. Harting MT, Jimenez F, Pati S, Baumgartner J and Cox CS. Immunophenotype characterization of rat mesenchymal stromal cells. Cytotherapy, 2008; Vol. 10, No. 3, 243-253.

139. Gronthos S, Simmons PJ, Graves SE and Robey PG. Integrin mediated interactions between human bone marrow stromal precursor cells and the extracellular matrix. Bone, 2001; 28,174-181.

140. Zuk, P.A., Zhu, M., Ashjian, P., De Ugarte, D.A., Huang, J.I., Mizuno, H., Alfonso, Z.C., Fraser, J.K., Benhaim, P., and Hedrick, M.H. (2002). Human adipose tissue is a source of multipotent stem cells. Mol. Biol. Cell 13, 4279–4295.

141. Wang, H.S., Hung, S.C., Peng, S.T., Huang, C.C., Wei, H.M., Guo, Y.J., Fu, Y.S., Lai, M.C., and Chen, C.C. (2004). Mesenchymal stem cells in the Wharton's jelly of the human umbilical cord. Stem Cells 22, 1330–1337.

142. Gronthos, S., Mankani, M., Brahim, J., Robey, P.G., and Shi, S. (2000). Postnatal human dental pulp stem cells (DPSCs) in vitro and in vivo. Proc. Natl. Acad. Sci. USA 97, 13625–13630.

143. Erices, A., Conget, P., and Minguell, J.J. (2000). Mesenchymal progenitor cells in human umbilical cord blood. Br. J. Haematol. 109, 235–242.

144. Jaiswal N, Haynesworth SE, Caplan AI, Bruder SP. Osteogenic differentiation of purified, culture-expanded human mesenchymal stem cells in vitro. J Cell Biochem 1997; 64:295-312.

145. Dennis JE, Haynesworth SE, Young RG, Caplan AI. Osteogenesis in marrow-derived mesenchymal cells porous ceramic composites transplanted subcutaneously: Effect of fibronectin and laminin on cell retention and rate of osteogenic expression. Cell Transplant 1992; 1:23-32.

146. Bar-Or D, Thomas GW, Rael LT, Gersch ED, Rubinstein P, Brody E. Low molecular weight fraction of commercial human serum albumin induces morphologic and transcriptional changes of bone marrow-derived mesenchymal stem cells. Stem Cells Transl. Med. 2015; 4, 945–955.

147. Saulnier N, Lattanzi W, Puglisi MA, Pani G, Barba M, Piscaglia AC, Giachelia M, Alfieri S, Neri G, Gasbarrini G, Gasbarrini A. Mesenchymal stromal cells multipotency and plasticity: induction toward the hepatic lineage, European Review for Medical and Pharmacological Sciences 2009; 13(Suppl 1): 71-78.

148. Manea CM, Rusu MC, Constantin D, Mănoiu VM, Moldovan L, Jianu AM. Ultrastructural features of human adipose-derived multipotent mesenchymal stromal cells. Rom J Morphol Embryol 2014, 55:1363–1369.

149. Shunji Kumabe, Michiko Nakatsuka, Rie Iwai, Katsura Ueda, Yoshifumi Matsuda, Shosuke Morita, Yasutomo Iwai. A fine structure study on osteogenesis of mesenchymal stem cells cultured with a 3D collagen scaffold. Integrative Molecular Medicine, 2015.

150. Hnia K, Ramspacher C, Vermot J, Laporte J. Desmin in muscle and associated diseases: beyond the structural function. Cell Tissue Res, 2015, 360:591–608.

151. Karaoz E, Aksoy A, Ayhan S, Sariboyaci AE, Kaymaz F, Kasap M. Characterization of mesenchymal stem cells from rat bone marrow: ultrastructural properties, differentiation potential and immunophenotypic markers. Histochem Cell Biol, 2009,132:533–546.

152. Karaöz E, Okçu A, Gacar G, Sağlam O, Yürüker S, Kenar H. A Comprehensive Characterization Study of Human Bone Marrow MSCs with an Emphasis on Molecular and Ultrastructural Properties. J Cell Physiol. 2011 May;226:1367-82.

153. O'Rahilly R and Müller F. The Development of the Neural Crest in the Human. J Anat. 2007 Sep; 211: 335–351.

154. Müller F and O'Rahilly R. Olfactory Structures in Staged Human Embryos. Cells Tissues Organs. 2004;178:93-116.

155. Schwanzel-Fukuda M, Crossin K L, Pfaff D W, Bouloux P M, Hardelin J P, And Petit C. Migration of Luteinizing Hormone-Releasing Hormone (Lhrh) Neurons in Early Human Embryos. J Comp Neurol. 1996 Mar 11;366:547-57.

156. Pelttari K, Pippenger B, Mumme M, Feliciano S, Scotti C, Mainil-Varlet P, Procino A, Von Rechenberg B, Schwamborn T, Jakob M, Cillo C, Barbero A, And Martin I. Adult Human Neural Crest-Derived Cells for Articular Cartilage Repair. Sci Transl Med, 2014, 6:251ra119.

157. Leucht P, Kim J-B, Amasha R, James A W, Girod S, And Helms J A. Embryonic Origin and Hox Status Determine Progenitor Cell Fate During Adult Bone Regeneration. Development, 2008, 135:2845.

158. Pelttari K, Mumme M, Barbero A, And Martin I. Nasal Chondrocytes as a Neural Crest-Derived Cell Source for Regenerative Medicine. Curr Opin Biotechnol, 2017, 47:1-6.

159. Mumme M, Steinitz A, Nuss K M, Klein K, Feliciano S, Kronen P, Jakob M, Von Rechenberg B, Martin I, Barbero A, And Pelttari K. Regenerative Potential of Tissue-

Engineered Nasal Chondrocytes in Goat Articular Cartilage Defects. Tissue Eng Part A, 2016, 22:1286-1295.

160. Toni R, Zini N, Barbaro F, Zamparelli A, Dallatana D, Bassi E, Mosca S, Lippi G, Spaletta G, Bassoli E, Denti L, Gatto A, Parilli A, Fini M, Giardino R, Ceglia I, Sandri M, Sprio S, Tampieri A. Bioartificial Endocrin Organs: a translational perspective in regenerative endocrinology. MiMe: Materials in Medecine. International Conference 1st Edition, Faenza, Italy, 2013.

161. Zamparelli A, Zini N, Cattini L, Spaletta G, Dallatana D, Bassi E, Barbaro F, Iafisco M, Mosca S, Parrilli A, Fini M, Giardino R, Sandri M, Sprio S, Tampieri A, Maraldi NM, Toni R. Growth on poly(L-lactic acid) porous scaffold preserves CD73 and CD90 immunophenotype markers of rat bone marrow mesenchymal stromal cells. J Mater Sci Mater Med. 2014 Oct;25:2421-36.

162. Chen Y, Wang F, Xu F, Yang T. Mass Spectrometry-Based Protein Quantification. Adv Exp Med Biol. 2016 919:255-279; Manes NP, Nita-Lazar A. Application of targeted mass spectrometry in bottom-up proteomics for systems biology research. J Proteomics. 2018 1874-3919:30057-5.

163. Candrian C, Vonwil D, Barbero A, Bonacina E, Miot S, Farhadi J, Wirz D, Dickinson S, Hollander A, Jakob M, Li Z, Alini M, Heberer M, and Martin I. Engineered Cartilage Generated by Nasal Chondrocytes Is Responsive to Physical Forces Resembling Joint Loading. Arthritis Rheum. 2008 Jan;58:197-208.

164. Frank O, Heim M, Jakob M, Barbero A, Schafer D, Bendik I, Dick W, Heberer M, And Martin I. Real-Time Quantitative Rt-Pcr Analysis of Human Bone Marrow Stromal Cells During Osteogenic Differentiation in Vitro. J Cell Biochem. 2002;85:737-46.

165. Nilsson M and Fagman H. Development of the thyroid gland. Development. 2017 Jun 15;144:2123-2140.

166. Duncan SA, Manova K, Chen WS, Hoodless P, Weinstein DC, Bachvarova RF, Darnell JE, Jr. Expression of transcription factor HNF-4 in the extraembryonic endoderm, gut, and nephrogenic tissue of the developing mouse embryo: HNF-4 is a marker for primary endoderm in the implanting blastocyst. Proc Natl Acad Sci USA, 1994. 91:7598–7602.

167. Di Palma T, Nitsch R, Mascia A, Nitsch L, Di Lauro R, Zannini M. The paired domain-containing factor Pax8 and the homeodomain-containing factor TTF-1 directly interact and synergistically activate transcription. J Biol Chem, 2003. 278:3395–3402.

168. Thomas T, Nowka K, Lan L, Derwahl M. Expression of endoderm stem cell markers: evidence for the presence of adult stem cells in human thyroid glands. Thyroid, 2006. 16:537–544.

169. Arceci RJ, King AA, Simon MC, Orkin SH, Wilson DB. Mouse GATA-4: A retinoic acid-inducible GATA-binding transcription factor expressed in endodermally derived tissues and heart. Mol Cell Biol, 1993. 13:2235–2246.

170. Rodewald HR. Thymus organogenesis. Annu. Rev. Immunol., 2008. 26:355–388.

171. Peters H, Neubüser A, Kratochwil K and Balling R. Pax9-deficient mice lack pharyngeal pouch derivatives and teeth and exhibit craniofacial and limb abnormalities. Genes Dev., 1998. 12:2735–2747.

172. Couly G, Grapin-Botton A, Coltey P, Ruhin B, Le Douarin NM. Determination of the identity of the derivatives of the cephalic neural crest: incompatibility between Hox gene expression and lower jaw development. Development. 1998 Sep;125:3445-59.

173. Gendron-Maguire M, Mallo M, Zhang M and Gridley T. Hoxa- 2 mutant mice exhibit homeotic transformation of skeletal elements derived from cranial neural crest. Cell 75, 1993. 1317-1331.

174. Rijli FM, Mark M, Lakkaraju S, Dierich A, Dollé P and Chambon P. A homeotic transformation is generated in the rostral branchial region of the head by disruption of Hoxa-2, which acts as a selector gene. Cell 75, 1993. 1333-1349.

175. Kanzler B, Kuschert SJ, Liu YH and Mallo M. Hoxa-2 restricts the chondrogenic domain and inhibits bone formation during development of the branchial area. Development 125, 1998. 2587-2597.

176. Ohnemus S, Bobola N, Kanzler B and Mallo M. Different levels of Hoxa2 are required for particular developmental processes. Mech. Dev., 2001. 108:135-147.

177. Lee TI, Jenner RG, Boyer LA, Guenther MG, Levine SS, Kumar RM, Chevalier B, Johnstone SE, Cole MF, Isono K, Koseki H, Fuchikami T, Abe K, Murray HL, Zucker JP, Yuan B, Bell GW, Herbolsheimer E, Hannett NM, Sun K, Odom DT, Otte AP, Volkert TL, Bartel DP, Melton DA, Gifford DK, Jaenisch R, Young RA. Control of developmental regulators by Polycomb in human embryonic stem cells. Cell. 2006 Apr 21;125:301-13.

178. Liedtke S, Buchheiser A, Bosch J, Bosse F, Kruse F, Zhao X, Santourlidis S, Kögler G. The HOX Code as a "biological fingerprint" to distinguish functionally distinct stem cell populations derived from cord blood. Stem Cell Res. 2010 Jul;5:40-50.

179. Francis R, Xu X, Park H, Wei CJ, Chang S, Chatterjee B, Lo C. Connexin43 modulates cell polarity and directional cell migration by regulating microtubule dynamics. PLoS One. 2011;6:e26379.

180. Moore R, Theveneau E, Pozzi S, Alexandre P, Richardson J, Merks A, Parsons M, Kashef J, Linker C, Mayor R. Par3 controls neural crest migration by promoting microtubule catastrophe during contact inhibition of locomotion. Development. 2013 Dec;140:4763-75.

181. Lee MK, Tuttle JB, Rebhun LI, Cleveland DW, Frankfurter A. The expression and posttranslational modification of a neuron-specific beta-tubulin isotype during chick embryogenesis. Cell Motil Cytoskeleton. 1990;17:118-32.

182. Lee VM and Pixley SK. Age and differentiation-related differences in neuron-specific tubulin immunostaining of olfactory sensory neurons. Brain Res Dev Brain Res. 1994 Dec 16;83:209-15.

183. Menezes JR and Luskin MB. Expression of neuron-specific tubulin defines a novel population in the proliferative layers of the developing telencephalon. J Neurosci. 1994 Sep;14:5399-416.

184. Chacon J and Rogers CD. Early expression of Tubulin Beta-III in avian cranial neural crest cells. Gene Expr Patterns. 2019 Jul 29;34:119067.

185. Barrallo-Gimeno A and Nieto MA. The Snail genes as inducers of cell movement and survival: implications in development and cancer. Development. 2005 Jul;132:3151-61.

186. Zeisberg M and Neilson EG. Biomarkers for epithelial-mesenchymal transitions. J Clin Invest. 2009 Jun;119:1429-37.

187. Yu W, Kamara H and Svoboda KK. The role of twist during palate development. Dev Dyn. 2008 Oct;237:2716-25.

188. Castanon I and Baylies MK. A Twist in fate: evolutionary comparison of Twist structure and function. Gene. 2002 Apr 3;287:11-22.

189. Venkov CD, Link AJ, Jennings JL, Plieth D, Inoue T, Nagai K, Xu C, Dimitrova YN, Rauscher FJ and Neilson EG. A proximal activator of transcription in epithelial-mesenchymal transition. J Clin Invest. 2007 Feb;117:482-91.

190. Kida Y, Asahina K, Teraoka H, Gitelman I, Sato T. Twist relates to tubular epithelial-mesenchymal transition and interstitial fibrogenesis in the obstructed kidney. J Histochem Cytochem. 2007 Jul;55:661-73.

191. Yang MH, Wu MZ, Chiou SH, Chen PM, Chang SY, Liu CJ, Teng SC, Wu KJ. Direct regulation of TWIST by HIF-1alpha promotes metastasis. Nat Cell Biol. 2008 Mar;10:295-305.

192. Yang J, Mani SA, Donaher JL, Ramaswamy S, Itzykson RA, Come C, Savagner P, Gitelman I, Richardson A, Weinberg RA. Twist, a master regulator of morphogenesis, plays an essential role in tumor metastasis. Cell. 2004 Jun 25;117:927-39.

193. Yang Z, Zhang X, Gang H, Li X, Li Z, Wang T, Han J, Luo T, Wen F, Wu X. Up-regulation of gastric cancer cell invasion by Twist is accompanied by N-cadherin and fibronectin expression. Biochem Biophys Res Commun. 2007 Jul 6;358:925-30.

194. Furlong RA. The biology of Hepatocyte growth factor/Scatter factor. Bioessays 1992; 14:613–617.

195. Dremier S, Taton M, Coulonval K, Nakamura T, Matsumoto K, Dumont JE. Mitogenic, dedifferentiating, and scattering effects of hepatocyte growth factor on dog thyroid cells. Endocrinology 1994; 135:135–140.

196. Eccles N, Ivan M, Wynford-Thomas D. Mitogenic stimulation of normal and oncogene-transformed human thyroid epithelial cells by hepatocyte growth factor. Mol Cell Endocrinol 1996; 117:247–251.

197. Lee JS, Shin J, Park HM, Kim YG, Kim BG, Oh JW, Cho SW. Liver extracellular matrix providing dual functions of two-dimensional substrate coating and three-dimensional injectable hydrogel platform for liver tissue engineering. Biomacromolecules. 2014 Jan 13; 15:206-18.

198. Michalopoulos GK. Liver regeneration: molecular mechanisms of growth control. FASEB J. 1990; 4:176-87.

199. Paine A, Williams LJ, and Legg RF. Apparent maintenance of cytochrome P 450 by nicotinamide in primary cultures of rat hepatocytes. Life Sci. 1979; 24:2185-2191.

200. Inoue C, Yamamoto H, Nakamura T, Ichihara A, and Okamoto H. Nicotinamide prolongs survival of primary cultured hepatocytes without involving loss of hepatocyte-specific functions. J. Biol. Chem. 1989; 264:4747-4750.

201. Mitaka T, Saltier CA, Sattler GL, Sargent LM, and Pitot HC. Multiple cell cycles occur in rat hepatocytes cultured in the presence of nicotinamide and epidermal growth factor. Hepatology 1991; 13:21-30.

202. Wang H, Pang B, Li Y, Zhu D, Pang T, Liu Y. Dexamethasone has variable effects on mesenchymal stromal cells. Cytotherapy 2012; 14:424–430.

203. Langenbach F, Handschel J. Effects of dexamethasone, ascorbic acid and β-glycerophosphate on the osteogenic differentiation of stem cells in vitro. Stem Cell Res Ther. 2013; 4:117.

204. Snykers S, De Kock J, Rogiers V, Vanhaecke T. In vitro differentiation of embryonic and adult stem cells into hepatocytes: state of the art. Stem Cells 2009; 27: 577-605.

205. Zhang W, Li W, Liu B, Wang P, Zhang H. Efficient generation of functional hepatocyte-like cells from human fetal hepatic progenitor cells in vitro. J Cell Physiol 2012; 227:2051–2058.

206. Shyh-Chang N and Ng HH. The metabolic programming of stem cells. Genes Dev. 2017 Feb 15;31:336-346.

207. Vander Heiden MG, Cantley LC, Thompson CB. Understanding the Warburg effect: the metabolic requirements of cell proliferation. Science. 2009 May 22;324:1029-33.

208. Petkov PM, Zavadil J, Goetz D, Chu T, Carver R, Rogler CE, Bottinger EP, Shafritz DA, Dabeva MD. Gene expression pattern in hepatic stem/progenitor cells during rat fetal development using complementary DNA microarrays. Hepatology. 2004 Mar;39:617-27.

209. Donato R, Cannon BR, Sorci G, Riuzzi F, Hsu K, Weber DJ, Geczy CL. Functions of S100 proteins. Curr Mol Med. 2013 Jan;13:24-57.

210. Kristensen DB, Kawada N, Imamura K, Miyamoto Y, Tateno C, Seki S, Kuroki T, Yoshizato K. Proteome analysis of rat hepatic stellate cells. Hepatology. 2000 Aug;32:268-77.

211. Duan L, Wu R2, Zou Z, Wang H, Ye L, Li H, Yuan S, Li X, Zha H, Sun H, Zhang Y, Chen X, Zhou L. S100A6 stimulates proliferation and migration of colorectal carcinoma cells through activation of the MAPK pathways. Int J Oncol. 2014 Mar;44:781-90.

212. Xia P, He H, Kristine MS, Guan W, Gao J, Wang Z, Hu J, Han L, Li J, Han W, Yu Y. Therapeutic effects of recombinant human S100A6 and soluble receptor for advanced glycation end products(sRAGE) on CCl4-induced liver fibrosis in mice. Eur J Pharmacol. 2018 Aug 15;833:86-93.

213. Norifumi Kawada. Molecular mechanism of stellate cell activation and therapeutic strategy for liver fibrosis. Comp Hepatol. 2004; 3(Suppl 1): S3.

214. Borowiak M, Maehr R, Chen S, Chen AE, Tang W, Fox JL, Schreiber SL, Melton DA. Small molecules efficiently direct endodermal differentiation of mouse and human embryonic stem cells. Cell Stem Cell 2009; 4:348 –358.

215. Ayatollahi M, Salmani MK, Geramizadeh B, Tabei SZ, Soleimani M, Sanati MH. Conditions to improve expansion of human mesenchymal stem cells based on rat samples. World J Stem Cells. 2012;4:1-8.

216. Javazon EH, Colter DC, Schwarz EJ, Prockop DJ. Rat marrow stromal cells are more sensitive to plating density and expand more rapidly from single-cell-derived colonies than human marrow stromal cell. Stem Cells. 2001;19:219-25.

217. Barzilay R, Sadan O, Melamed E, Offen D. Comparative characterization of bone marrow-derived mesenchymal stromal cells from four different rat strains. Cytotherapy. 2009;11:435-42.

218. Kang XQ, Zang WJ, Song TS, Xu XL, Yu XJ, Li DL, Meng KW, Wu SL, Zhao ZY. Rat bone marrow mesenchymal stem cells differentiate into hepatocytes in vitro. World J Gastroenterol 2005;11:3479-3484.

219. Lin N, Lin J, Bo L, Weidong P, Chen S, Xu R. Differentiation of bone marrow-derived mesenchymal stem cells into hepatocyte-like cells in an alginate scaffold. Cell Prolif., 2010;Oct;43:427-34.

220. Subramanian K, Owens DJ, O'Brien TD, Verfaillie CM, Hu WS. Enhanced Differentiation of Adult Bone Marrow-Derived Stem Cells to Liver Lineage in Aggregate Culture. Tissue Eng Part A. 2011 Sep;17:2331-41.

221. Neuss S, Becher E, Wöltje M, Tietze L, Jahnen-Dechent W. Functional expression of HGF and HGF receptor/c-met in adult human mesenchymal stem cells suggests a role in cell mobilization, tissue repair, and wound healing. Stem Cells. 2004;22:405-14.

222. Forte G, Minieri M, Cossa P, Antenucci D, Sala M, Gnocchi V, Fiaccavento R, Carotenuto F, De Vito P, Baldini PM, Prat M, Di Nardo P. Hepatocyte growth factor effects on

mesenchymal stem cells: proliferation, migration, and differentiation. Stem Cells. 2006 Jan;24:23-33.

223. Skov Olsen P, Boesby S, Kirkegaard P, Therkelsen K, Almdal T, Poulsen SS, Nexø E. Influence of epidermal growth factor on liver regeneration after partial hepatectomy in rats. Hepatology 1988.

224. Bao J, Wu Q, Wang Y, Li Y, Li L, Chen F, Wu X, Xie M, Bu H. Enhanced hepatic differentiation of rat bone marrow-derived mesenchymal stem cells in spheroidal aggregate culture on a decellularized liver scaffold. Int J Mol Med. 2016 Aug; 38:457–465.

225. Valente S, Ciavarella C, Pasanisi E, Ricci F, Stella A, Pasquinelli G. Hepatocyte Growth Factor Effects on Mesenchymal Stem Cells Derived from Human Arteries: A Novel Strategy to Accelerate Vascular Ulcer Wound Healing. Stem Cells Int. 2016; 1-11.

226. Chen K, Perez-Stable C, D'Ippolito G, Schiller PC, Roos BA, and Howard GA. Human bone marrow-derived stem cell proliferation is inhibited by hepatocyte growth factor via increasing the cell cycle inhibitors p53, p21 and p27. Bone. 2011, vol. 49, no. 6, pp. 1194–1204.

227. Hao-Wei Han, Shigetaka Asano and Shan-hui Hsu. Cellular Spheroids of Mesenchymal Stem Cells and Their Perspectives in Future Healthcare. Appl. Sci. 2019, 9:627.

228. Bae YJ, Kwon YR, Kim HJ, Lee S, Kim YJ. Enhanced differentiation of mesenchymal stromal cells by three-dimensional culture and azacitidine. Blood Res. 2017 Mar; 52:18–24.

229. Talaei-Khozani T, Borhani-Haghighi M, Ayatollahi M, Vojdani Z. An in vitro model for hepatocyte-like cell differentiation from Wharton's jelly derived-mesenchymal stem cells by cell-base aggregates. Gastroenterol Hepatol Bed Bench. 2015 Summer;8:188-99.

230. Wu Q, Tang J, Li Y, Li L, Wang Y, Bao J, Bu H. Hepatic differentiation of mouse bone marrow-derived mesenchymal stem cells using a novel 3D culture system. Mol Med Rep. 2017 Dec;16:9473-9479.

231. Yang YK, Ogando CR, Wang See C, Chang TY, Barabino GA. Changes in phenotype and differentiation potential of human mesenchymal stem cells aging in vitro. Stem Cell Res Ther. 2018 May 11;9:131.

232. Shall G, Menosky M, Decker S, Nethala P, Welchko R, Leveque X, Lu M, Sandstrom M, Hochgeschwender U, Rossignol J, Dunbar G. Effects of Passage Number and Differentiation Protocol on the Generation of Dopaminergic Neurons from Rat Bone Marrow-Derived Mesenchymal Stem Cells. Int J Mol Sci. 2018 Mar 2;19.

233. Jiang T, Xu G, Wang Q, Yang L, Zheng L, Zhao J, Zhang X. In vitro expansion impaired the stemness of early passage mesenchymal stem cells for treatment of cartilage defects. Cell Death Dis. 2017 Jun 1;8:e2851.

234. Mumme M, Barbero A, Miot S, Wixmerten A, Feliciano S, Wolf F, Asnaghi A M, Baumhoer D, Bieri O, Kretzschmar M, Pagenstert G, Haug M, Schaefer D J, Martin I, and Jakob M. Nasal Chondrocyte-Based Engineered Autologous Cartilage Tissue for Repair of Articular Cartilage Defects: An Observational First-in-Human Trial. Lancet, 2016. 388, pp. 1985-1994.

235. Tay A G, Farhadi J, Suetterlin R, Pierer G, Heberer M, And Martin I. Cell Yield, Proliferation, and Postexpansion Differentiation Capacity of Human Ear, Nasal, and Rib Chondrocytes. Tissue Eng, 2004, 10:762-70.

236. Scotti C, Osmokrovic A, Wolf F, Miot S, Peretti G M, Barbero A, And Martin I. Response of Human Engineered Cartilage Based on Articular or Nasal Chondrocytes to Interleukin-1beta and Low Oxygen. Tissue Eng Part A, 2012, 18:362-72.

237. Seo S, Baye LM, Schulz NP, Beck JS, Zhang Q, Slusarski DC, Sheffield VC. BBS6, BBS10, and BBS12 form a complex with CCT/TRiC family chaperonins and mediate BBSome assembly. Proc Natl Acad Sci U S A. 2010 Jan 26;107:1488-93.

238. Jin-Ge Liu, Ke-Bin Zhang, Jin-Liang Tang, Ya-Li Wang, Sheng-Qing Lv, Jian-Ping Xu. PRDX-1 promotes cell proliferation and inhibits apoptosis of human gliomas via TNF-α/NF-κB pathway. Int J Clin Exp Pathol 2016;9:3152-3160.

239. An-Lie Cai, Wei Zeng, Wei-Liang Cai, Jing-Ling Liu, Xue-Wen Zheng, Ying Liu, Xiang-Cheng Yang, Yi Long, and Jie Li. Peroxiredoxin-1 promotes cell proliferation and metastasis through enhancing Akt/mTOR in human osteosarcoma cells. Oncotarget. 2018 Feb 2; 9: 8290–8302.

240. Luger K, Mader AW, Richmond RK, Sargent DF, Richmond TJ. Crystal structure of the nucleosome core particle at 2.8A resolution. Nature. 1997; 389:251-260.

241. Singh RK, Kabbaj MH, Paik J, Gunjan A. Histone levels are regulated by phosphorylation and ubiquitylation-dependent proteolysis. Nature cell biology. 2009; 11:925-933.

242. Qianyun Mei, Junhua Huang, Wanping Chen, Jie Tang, Chen Xu, Qi Yu, Ying Cheng, Lixin Ma, Xilan Yu, and Shanshan Li. Regulation of DNA replication-coupled histone gene expression. Oncotarget. 2017 Nov 7; 8:95005–95022.

243. Bulman WA, Iannotti JP, Glowacki K, Bleuit J, Clark CC. Serum fractions and related agonists with calcium-mobilizing activity in the bovine growth plate chondrocyte. J Orthop Res. 1995, 13:220–229.

244. Croucher LJ, Crawford A, Hatton PV, Russel RG, Buttle DJ. Extracellular ATP and UTP stimulate cartilage proteoglycan and collagen accumulation in bovine articular chondrocyte pellet cultures. Biochim Biophys Acta. 2000, 1502:297–306.

245. Meredith D, Bell P, McClure B, Wilkins R. Functional andmolecular characterization of lactic acid transport in bovine articular chondrocytes. Cell Physiol Biochem 2002; 12:227e34.24.

246. Heywood HK, Lee DA. Low oxygen reduces the modulation to an oxidative phenotype in monolayer-expanded chon-drocytes. J Cell Physiol 2010; 222:248e53.